BROOD: Bilevel and Robust Optimization and Outlier Detection for Efficient Tuning of High-Energy Physics Event Generators

Wenjing Wang[1], Mohan Krishnamoorthy[2], Juliane Müller[1*], Stephen Mrenna[3*], Holger Schulz[4], Xiangyang Ju[1], Sven Leyffer[2], Zachary Marshall[1]

1 Lawrence Berkeley National Laboratory, Berkeley, CA 94720
2 Argonne National Laboratory, Lemont, IL 60439
3 Fermi National Accelerator Laboratory, Batavia, IL 60510
4 Department of Computer Science, Durham University, South Road, Durham DH1 3LE, UK
* julianemueller@lbl.gov mrenna@fnal.gov

September 1, 2021

1 Abstract

The parameters in Monte Carlo (MC) event generators are tuned on experimental measurements by evaluating the goodness of fit between the data and the MC predictions. The relative importance of each measurement is adjusted manually in an often time-consuming, iterative process to meet different experimental needs. In this work, we introduce several optimization formulations and algorithms with new decision criteria for streamlining and automating this process. These algorithms are designed for two formulations: bilevel optimization and robust optimization. Both formulations are applied to the datasets used in the ATLAS A14 tune and to the dedicated hadronization datasets generated by the SHERPA generator, respectively. The corresponding tuned generator parameters are compared using three metrics. We compare the quality of our automatic tunes to the published ATLAS A14 tune. Moreover, we analyze the impact of a pre-processing step that excludes data that cannot be described by the physics models used in the MC event generators.

---

1 Introduction and Motivation

Monte Carlo (MC) event generators are simulation tools that predict the properties of high-energy particle collisions. Event generators are built from theoretical formulae and models that describe the probabilities for various sub-event phenomena that occur in a high-energy collision. They are developed by physicists as a bridge between particle physics perturbation theory, which is defined at very high energy scales, and the observed sub-atomic particles, which are low-energy states of the strongly-interacting full theory. This bridge is essential for interpreting event collision data in terms of the fundamental quantities of the underlying theory. See [1] for an overview of the event generators used for physics analysis at the Large Hadron Collider (LHC).

The description of particle collisions requires an understanding of phenomena at many different energy scales. At high energy scales (much larger than the masses of the sub-atomic particles), first principle predictions can be made in a perturbative framework based on a few universal parameters. At intermediate energy scales, an approximate perturbation theory can be established that introduces less universal parameters. At low energy, motivated, but subjective, models are introduced to describe sub-atomic particle production. These low-energy models introduce a large number of narrowly defined parameters. To make predictions or inferences, one must have a handle on the preferred models and the values of the parameters needed to describe the data. This process of adjusting the parameters of the MC simulations to match data is called *tuning*.

This tuning task is complicated by the fact that the phenomenological models cannot claim to be complete or scale-invariant. When compared to a large set of collider data collected in different energy regimes, the MC-models do not describe the full range of event properties equally well. Typically, the physicists demand a tune that describes a subset of the data very well, another subset moderately well, and a remainder that must only be described qualitatively. This distribution of subsets may well vary from one group of physicists to another and has led to the education of experts who subjectively select and weigh data to achieve some physics goal. Two such exercises are the Monash tune [2] and the A14 tune [3], though others exist in the literature. Both of these tunes are successful, in the sense that they have been useful in understanding a wide range of phenomena observed at particle colliders. However, the current approach to tuning remains inefficient and

biased and, given the nature of the problem with physicists having different tuning objectives, mathematical rigor is lacking.

This work introduces a framework that, once agreed upon, greatly reduces the subjective element of the tuning process and replaces it with an automated way to select the data for parameter tuning.

1.1 Notation and terminology

The data used in the tuning process are in the form of observables, denoted by $\mathcal{O}$, and the set of observables is denoted by $\mathcal{S}_\mathcal{O}$. Observables are quantities constructed from the (directly or indirectly) measured sub-atomic particles produced in an event. In this case, each observable is presented as a *histogram* that shows the frequency that the observable is measured over a range of possible values (see Figure 8 for example histograms). The range can be one or many divisions of the interval from the minimum to the maximum value that the observable can obtain. These divisions are called *bins*. In practice, the size of a bin is set by how well an observable can be measured. The number of bins of an observable $\mathcal{O}$ is denoted as $|\mathcal{O}|$. We use $\mathcal{R}$ to denote the reference data in the histograms, a subscript b to denote a bin, $\mathcal{R}_b$ to denote the data value in a bin, and $\Delta\mathcal{R}_b$ to denote the corresponding 1-σ measurement uncertainty which is interpreted as the standard deviation of a Gaussian random variable.

The MC-model has parameters $\mathbf{p}$, a d-dimensional vector in the space Ω, $\mathbf{p} \in \Omega \subset \mathbb{R}^d$. The MC-based simulations are denoted by $\mathrm{MC}(\mathbf{p})$ to emphasize that they depend on the physics parameters $\mathbf{p}$. The histograms computed from the MC simulation have the same structure as the histograms obtained from the measurement data $\mathcal{R}$, with a prediction per bin $\mathrm{MC}_b(\mathbf{p})$ and an uncertainty associated with each bin $\Delta\mathrm{MC}_b(\mathbf{p})$. The uncertainty on the MC simulation is the numerical precision of the prediction, which typically scales as the inverse of the square root of the number of simulated events in a particular bin. Theoretical and model uncertainties are not currently included, but are discussed later.

1.2 Mathematical formulation of the tuning problem

Our goal is to find a set of physics parameters, $\mathbf{p}^*$, that minimizes the difference between the experimental data and the simulated data from an MC event generator. This difference is defined as follows:

$$\chi^2_{\mathrm{MC}}(\mathbf{p}, \mathbf{w}) = \sum_{\mathcal{O} \in \mathcal{S}_\mathcal{O}} w_\mathcal{O} \sum_{b \in \mathcal{O}} \frac{(\mathrm{MC}(\mathbf{p}) - \mathcal{R}_b)^2}{\Delta\mathrm{MC}_b(\mathbf{p})^2 + \Delta\mathcal{R}_b^2}, \tag{1}$$

where $w_\mathcal{O}$ is the weight for an observable $\mathcal{O}$ and $\mathbf{w}$ is a vector of weights, $\mathbf{w} = [w_1, \ldots, w_{|\mathcal{S}_\mathcal{O}|}]^T$. In general, the number of bins can be different for different observables. The weights $w_\mathcal{O} \geq 0$ reflect

142 how much an observable contributes to the tune, i.e., if $w_{\mathcal{O}} = 0$ for some $\mathcal{O}$, then this observable will
143 not influence the tuning of **p**. Since (1) is likely multimodal, several local optima exist (see [4, page
144 13] for the definition of local optimality) and our goal with using numerical optimization is to find
145 at least a locally optimal solution, which is not guaranteed to be found by hand-tuning methods.
146 Note that (1) treats the observables independently without correlations. Currently, the majority of
147 collider data available for tuning are provided without these correlations. When such information
148 becomes readily available, (1) will need to be modified in a non-trivial way to include them.

149   The MC simulation is computationally expensive (the generation of 1 million events for a given
150 set of parameters consumes about 800 CPU minutes on a typical computing cluster), severely
151 limiting the number of parameter choices **p** that can be used in the tuning. To overcome these issues,
152 we construct a parameterization of the MC simulation following the work in [5] and advancing the
153 method to new approximation models. Our new implementation, named APPRENTICE, is available
154 at `https://github.com/HEPonHPC/apprentice`. The function in Eq. (1) is not minimized directly.
155 Instead, during the optimization over **p**, the MC simulation is replaced by a surrogate model (here,
156 a polynomial (see [5]) or a rational approximation to a number of MC simulations). For each bin b
157 of each histogram, the central value and the corresponding uncertainty of the model prediction are
158 parameterized independently as functions of the model parameters **p** yielding analytic expressions
159 $f_b(\mathbf{p})$ and $\Delta f_b(\mathbf{p})$, respectively, that can be evaluated in milliseconds. Thus, instead of Eq. (1), we
160 minimize

$$\chi^2(\mathbf{p}, \mathbf{w}) = \sum_{\mathcal{O} \in \mathcal{S}_{\mathcal{O}}} w_{\mathcal{O}} \sum_{b \in \mathcal{O}} \frac{(f_b(\mathbf{p}) - \mathcal{R}_b)^2}{\Delta f_b(\mathbf{p})^2 + \Delta \mathcal{R}_b^2}. \tag{2}$$

161 which can be done efficiently using numerical methods. Eq. (2) implicitly assumes that each bin b
162 is completely independent of all other bins. Note that the choice of surrogate model introduces an
163 uncertainty whose quantification is outside of the scope of this paper.

164   In practice, the weights $w_{\mathcal{O}}$ in Eq. (2) are adjusted manually, based on experience and physics
165 intuition. The selection of weights is time-consuming and different experts may have different
166 opinions about how well each observable is approximated by the model. Our goal is to automate the
167 weight adjustment, yielding a less subjective and less time-consuming process to find the optimal
168 physics parameters **p** that will then be used in the actual MC simulation. This problem was
169 also considered in [6], where weights are assigned based on correlations between parameters and
170 observables without any reference to measured data values. Also related to this work is that of
171 [7], which treats tuning as a black-box optimization problem within the framework of Bayesian
172 optimization, but with no weighting of data.

173   For convenience, we summarize our notation in Table 1.

Table 1: Notation.

Notation	Definition
$\mathcal{O}$	observables that are constructed from data and MC-based simulations in the form of histograms
$|\mathcal{O}|$	the number of bins in an observable $\mathcal{O}$
$\mathcal{S}_\mathcal{O}$	the set of observables used in the tune
$|\mathcal{S}_\mathcal{O}|$	the number of observables
$\mathcal{R}$	the data in the histograms
b	a bin of a histogram $\mathcal{O}$
$\mathcal{R}_b$	the data value in a bin
$\Delta\mathcal{R}_b$	data uncertainty corresponding to the data value in a bin
$\mathbf{p}$	a d-dimensional vector of real-valued parameters
$\mathrm{MC}(\mathbf{p})$	an MC simulation that depends on the physics parameters $\mathbf{p}$
$\mathrm{MC}_b(\mathbf{p})$	the MC simulation in a bin b
$\Delta\mathrm{MC}_b(\mathbf{p})$	an uncertainty associated with the MC simulation in a bin b
$f_b(\mathbf{p})$	central value of the model prediction parameterized independently as a function of the model parameters $\mathbf{p}$
$\Delta f_b(\mathbf{p})$	the uncertainty of the model prediction parameterized independently as a function of the model parameters $\mathbf{p}$
$r_b(\mathbf{p})$	the variance associated with bin b as a function of model parameter $\mathbf{p}$
$\mathbf{w}$	an $|\mathcal{S}_\mathcal{O}|$-dimensional vector of real-valued weights
$w_\mathcal{O}$	the weight given to a histogram in constructing a tune (if $w_\mathcal{O} = 0$ for some $\mathcal{O}$, then this observable will not influence the tuning of $\mathbf{p}$).
$\widehat{\mathbf{p}}_\mathbf{w}$	optimal physics parameters for a given choice for the weights
$\mathbf{w}^*$	an optimal set of weights for the observables
$\widehat{\mathbf{p}}_{\mathbf{w}^*}$	the optimal set of simulation parameters corresponding to an optimal set of weights $\mathbf{w}^*$ for the observables
g	the outer objective function of $\mathbb{R}^{|\mathcal{S}_\mathcal{O}|\times d} \mapsto \mathbb{R}$ used in the bilevel optimization
μ	a hyperparameter that specifies the percentage of the observables used in the robust optimization
$\chi^2_\mathcal{O}(\mathbf{p})$	the per-observable error averaged over all bins in the observable $\mathcal{O}$
$\mathbf{p}^\mathcal{O}_{\mathrm{ideal}}$	the *ideal* tune for an observable $\mathcal{O}$, i.e., the parameters that minimize Eq. (12) when using only observable $\mathcal{O}$ for the tune

2   Finding the Optimal Weights for Each Observable

In this section, we describe two mathematical formulations for finding the optimal weights in Eq. (2) namely   bilevel and robust optimization.

2.1   Bilevel optimization formulation

We formulate a bilevel optimization problem as follows:

$$\min_{\mathbf{w}\in[0,1]^{|\mathcal{S}_{\mathcal{O}}|},\hat{\mathbf{p}}_{\mathbf{w}}\in\Omega} g(\mathbf{w},\widehat{\mathbf{p}}_{\mathbf{w}}) \tag{3a}$$

$$\text{subject to } \sum_{\mathcal{O}\in\mathcal{S}_{\mathcal{O}}} w_{\mathcal{O}} = 1 \tag{3b}$$

$$\widehat{\mathbf{p}}_{\mathbf{w}} \in \arg\min_{\mathbf{p}\in\Omega} \chi^2(\mathbf{p},\mathbf{w}) \tag{3c}$$

where the upper-level function $g : \mathbb{R}^{|\mathcal{S}_{\mathcal{O}}|\times d} \mapsto \mathbb{R}$ describes a merit function to determine the goodness of weights (see below for the definitions we use in this work). The lower-level Eq. (3c) (same as Eq. (2)) corresponds to finding optimal parameters $\widehat{\mathbf{p}}_{\mathbf{w}}$ for a given set of weights $\mathbf{w}$ (note that, in general, multiple local minimizers may exist). The weights are normalized to sum to unity, see Eq. (3b), in order to prevent the trivial solution where all weights are 0. Bilevel optimization problems have been studied extensively in the literature, see, e.g., [8–12].

In the following, we discuss two definitions of the outer objective function $g(\mathbf{w},\widehat{\mathbf{p}}_{\mathbf{w}})$. Other formulations are possible and our selection is driven by the goal to achieve reasonably good agreement between the simulated and the observed data for all observables (rather than fitting a few observables extremely well and others poorly).

2.1.1   Formulation 1: Portfolio to balance mean and variance of errors

The portfolio objective function is motivated by portfolio optimization in finance [13], where the goal is to maximize the expected return while minimizing the risk. Translated to our problem, we want to minimize the expected error over all observables while also minimizing the variance over these errors.

For a given set of weights $\mathbf{w}$, we obtain the "$\mathbf{w}$-optimal" parameters $\widehat{\mathbf{p}}_{\mathbf{w}} = \hat{\mathbf{p}}(\mathbf{w})$. For each observable $\mathcal{O}$, an error term is averaged over the number of bins in the observable ($|\mathcal{O}|$):

$$e_{\mathcal{O}}(\widehat{\mathbf{p}}_{\mathbf{w}}) = \frac{1}{|\mathcal{O}|} \sum_{b\in\mathcal{O}} \frac{(f_b(\widehat{\mathbf{p}}_{\mathbf{w}}) - \mathcal{R}_b)^2}{\Delta f_b(\widehat{\mathbf{p}}_{\mathbf{w}})^2 + \Delta\mathcal{R}_b^2}, \ \mathcal{O} \in \mathcal{S}_{\mathcal{O}}, \tag{4}$$

where the error $e_{\mathcal{O}}(\widehat{\mathbf{p}}_{\mathbf{w}})$ for each observable depends on the choice of the weights $\mathbf{w}$. Thus, we obtain a set of $|\mathcal{S}_{\mathcal{O}}|$ average error values from which we compute the following statistics:

$$\mu(\hat{\mathbf{p}}(\mathbf{w})) = \mu(\widehat{\mathbf{p}}_{\mathbf{w}}) = \frac{1}{|\mathcal{S}_{\mathcal{O}}|} \sum_{\mathcal{O} \in \mathcal{S}_{\mathcal{O}}} e_{\mathcal{O}}(\widehat{\mathbf{p}}_{\mathbf{w}}): \text{ average error over all observables,} \tag{5a}$$

$$\sigma^2(\hat{\mathbf{p}}(\mathbf{w})) = \sigma^2(\widehat{\mathbf{p}}_{\mathbf{w}}) = \frac{1}{|\mathcal{S}_{\mathcal{O}}|} \sum_{\mathcal{O} \in \mathcal{S}_{\mathcal{O}}} [e_{\mathcal{O}}(\widehat{\mathbf{p}}_{\mathbf{w}}) - \mu(\widehat{\mathbf{p}}_{\mathbf{w}})]^2 : \text{ empirical variance of errors over all observables.}$$

$$\tag{5b}$$

The portfolio objective function for the outer optimization then becomes

$$g(\mathbf{w}, \widehat{\mathbf{p}}_{\mathbf{w}}) = \mu(\widehat{\mathbf{p}}_{\mathbf{w}}) + \sigma^2(\widehat{\mathbf{p}}_{\mathbf{w}}), \tag{6}$$

which aims at simultaneously minimizing the expected error *and* the variance of the errors of all observables. Thus, instead of minimizing only an expected value and potentially obtaining a solution that allows for some observables having large errors and others small errors, we aim to find a solution that provides a good tradeoff between both metrics. For problems in which minimizing the variance is of higher priority, one can introduce a multiplier λ before the variance term that reflects "risk aversion". In that case, if λ is large, we are more risk-averse, since reducing the variance associated with the errors will drive the minimization. If λ is small, we are less risk-averse, and minimizing the mean of the errors is emphasized.

2.1.2   Formulation 2: Scoring of model fit and data uncertainty

We consider a second outer objective function formulation based on scoring schemes ([14, Eq. (27)]). The performance of a generic predictive model P at a point x is defined by a scoring rule, $S(P, x) = -\left(\frac{x - \mu_P}{\sigma_P}\right)^2 - \log \sigma_P^2$, where P has mean performance μ_P and variance σ_P^2. A larger value for $S(P, x)$ signifies better model performance. Thus, we minimize the negative of $S(P, x)$:

$$s(P, x) = -S(P, x) = \left(\frac{x - \mu_P}{\sigma_P}\right)^2 + \log \sigma_P^2. \tag{7}$$

The intuition behind this scoring scheme is that it takes both the model fit and data uncertainty into consideration. For our application, x corresponds to the simulation prediction $f_b(\mathbf{p})$, μ_P to our observation data $\mathcal{R}_b$, and the variance σ_P^2 to our data uncertainty $\Delta \mathcal{R}_b$. For each bin b in an observable, we calculate the score based on Eq. (7). Then, we compute the median (and mean) of the scores over all bins to obtain the median (average) performance for each observable. In order to form the upper-level objective function, we sum up the median (mean) scores over all observables:

- Outer objective based on median score

$$g(\mathbf{w}, \widehat{\mathbf{p}}_{\mathbf{w}}) = \sum_{\mathcal{O} \in \mathcal{S}_{\mathcal{O}}} \tilde{s}_{\mathcal{O}}(\widehat{\mathbf{p}}_{\mathbf{w}}), \tag{8a}$$

$$\tilde{s}_{\mathcal{O}}(\widehat{\mathbf{p}}_{\mathbf{w}}) = \text{median of } \left\{ \left(\frac{f_b(\widehat{\mathbf{p}}_{\mathbf{w}}) - \mathcal{R}_b}{\Delta \mathcal{R}_b} \right)^2 + \log(\Delta \mathcal{R}_b^2), \forall b \in \mathcal{O} \right\}. \tag{8b}$$

- Outer objective based on mean score

$$g(\mathbf{w}, \widehat{\mathbf{p}}_{\mathbf{w}}) = \sum_{\mathcal{O} \in \mathcal{S}_{\mathcal{O}}} \bar{s}_{\mathcal{O}}(\widehat{\mathbf{p}}_{\mathbf{w}}), \tag{9a}$$

$$\bar{s}_{\mathcal{O}}(\widehat{\mathbf{p}}_{\mathbf{w}}) = \frac{1}{|\mathcal{O}|} \sum_{b \in \mathcal{O}} \left\{ \left(\frac{f_b(\widehat{\mathbf{p}}_{\mathbf{w}}) - \mathcal{R}_b}{\Delta \mathcal{R}_b} \right)^2 + \log(\Delta \mathcal{R}_b^2) \right\}. \tag{9b}$$

Both the median and the mean score outer objective functions take into account the deviation of the prediction of $f_b(\widehat{\mathbf{p}}_{\mathbf{w}})$ from $\mathcal{R}_b$ and the uncertainty in the data $\Delta \mathcal{R}_b$. Thus, if an observable has large uncertainties in the data or the model $f_b(\widehat{\mathbf{p}}_{\mathbf{w}})$ does not approximate the data $\mathcal{R}_b$ well, the score for this observable deteriorates. Ideally, both terms $\left(\frac{f_b(\widehat{\mathbf{p}}_{\mathbf{w}}) - \mathcal{R}_b}{\Delta \mathcal{R}_b} \right)^2$ and $\log(\Delta \mathcal{R}_b^2)$ will be small.

2.1.3 Solving the bilevel optimization problem using surrogate models

Solving the inner optimization problem (3c) for each weight vector $\mathbf{w}$ is generally computationally non-trivial and its computational demand increases with the number of physics parameters $\mathbf{p}$ that have to be optimized and the number of observables present. Here, we use APPRENTICE to obtain a set of optimal physics parameters $\widehat{\mathbf{p}}_{\mathbf{w}}$. The goal is to try as few weights $\mathbf{w}$ as possible. We interpret the solution of the inner optimization problem as a black-box function evaluation of $g(\mathbf{w}, \hat{\mathbf{p}}_{\mathbf{w}})$ for $\mathbf{w}$. Given an initial set of input-output data pairs $\{(\mathbf{w}_i, g(\mathbf{w}_i, \hat{\mathbf{p}}_{\mathbf{w}_i})\}_{i=1}^I$, we fit a surrogate model[1] (here a radial basis function [15]) that allows us to predict the values of $g(\mathbf{w}, \hat{\mathbf{p}}_{\mathbf{w}})$ at untried $\mathbf{w}$. In each iteration of the optimization algorithm, these predictions are used to select the most promising weight vector for which the inner optimization problem should be solved next. Promising weight vectors have either low predicted values of $g(\cdot)$ or are far away from already evaluated points [16,17]. Each time a new weight vector has been evaluated, the surrogate model is updated. This iterative

---

[1]This surrogate model for the weights is independent of the one used to evaluate the MC-based predictions.

244 process repeats until a stopping criterion has been met, e.g., a maximal number of weight vectors
245 has been evaluated or a maximal CPU time has been reached. Details about the surrogate model
246 algorithm are given in the online supplement Section 8.1.

247 Note that the surrogate model based optimizer balances local and global searches in order to
248 enable an escape from local optima. However, our algorithm cannot guarantee to converge to the
249 globally optimal solution because the optimization problem is highly multi-modal and blackbox.

2.2 Robust optimization formulation

251 As an alternative to the bilevel formulation, we developed a single-level robust optimization formu-
252 lation for finding the optimal weights for Eq. (2). Robust optimization estimates the parameters $\mathbf{p}$
253 that minimize the largest deviation $(f_b(\mathbf{p}) - \mathcal{R}_b)^2$ over all bins in an uncertainty set $\mathcal{U}_b$ of bin b:

$$\underset{\mathbf{w} \in [0,1], \mathbf{p} \in \Omega}{\text{minimize}} \sum_{\mathcal{O} \in \mathcal{S}_{\mathcal{O}}} \frac{w_{\mathcal{O}}}{|\mathcal{O}|} \sum_{b \in \mathcal{O}} \underset{\mathcal{R}_b \in \mathcal{U}_b}{\text{maximize}} \left(f_b(\mathbf{p}) - \mathcal{R}_b \right)^2. \tag{10}$$

254 The uncertainty set $\mathcal{U}_b$ contains uncertain data and the goal of the optimization is to choose the
255 best (most robust) solution among candidates that remain feasible for all realizations of the data
256 in $\mathcal{U}_b$. Furthermore, $\mathcal{U}_b$ is not a probability distribution since it is a bound set and we only consider
257 feasible data within the set. Assuming that the experiment and the MC simulation are described
258 using independent random variables with mean $\mathcal{R}_b$, the uncertainty set $\mathcal{U}_b$ for each bin b is described
259 by the interval $[\mathcal{R}_b - \Delta\mathcal{R}_b - \Delta f_b(\mathbf{p}), \mathcal{R}_b + \Delta\mathcal{R}_b + \Delta f_b(\mathbf{p})]$.

260 Introducing slack variables $\boldsymbol{t} = \left[t_1, t_2, \ldots, t_{|\mathcal{O}|}\right]$, we rewrite (10) as:

$$\underset{\boldsymbol{t}, \mathbf{w} \in [0,1], \mathbf{p} \in \Omega}{\text{minimize}} \sum_{\mathcal{O} \in \mathcal{S}_{\mathcal{O}}} \frac{w_{\mathcal{O}}}{|\mathcal{O}|} \sum_{b \in \mathcal{O}} t_b \tag{11a}$$

subject to

$$t_b \geq \left(f_b(\mathbf{p}) - (\mathcal{R}_b - \Delta\mathcal{R}_b - \Delta f_b(\mathbf{p})) \right)^2 \quad \forall b \in \mathcal{O}, \forall \mathcal{O} \in \mathcal{S}_{\mathcal{O}} \tag{11b}$$

$$t_b \geq \left(f_b(\mathbf{p}) - (\mathcal{R}_b + \Delta\mathcal{R}_b + \Delta f_b(\mathbf{p})) \right)^2 \quad \forall b \in \mathcal{O}, \forall \mathcal{O} \in \mathcal{S}_{\mathcal{O}}$$

$$\sum_{\mathcal{O} \in \mathcal{S}_{\mathcal{O}}} \frac{w_{\mathcal{O}}}{|\mathcal{O}|} \geq \frac{\mu}{100} \sum_{\mathcal{O} \in \mathcal{S}_{\mathcal{O}}} \frac{1}{|\mathcal{O}|} \tag{11c}$$

261 where the constraint (11c) is enforced to avoid the trivial solution of all weights being zero. In this
262 constraint, we bound the sum of the weights away from zero by a hyperparameter μ that specifies
263 the percentage of the observables that should be used in the optimization. Problem (11) is attractive
264 because it formulates the problem of finding optimal weights as a single-level optimization problem,
265 which is easier to solve than the bilevel problem Eq. (3). However, like the bilevel algorithms,

266 this approach cannot guarantee to converge to the globally optimal solution due to the nonlinear
267 constraints (11b).

268 Selecting the best μ among all the 100 runs of robust optimization is determined using a cumu-
269 lative density curve of the number of observables satisfying $\dfrac{\chi^2_{\mathcal{O}}(\mathbf{p}^*, \mathbf{w})}{|\mathcal{O}|} \leq \tau$, where $\mathbf{p}^*$ is the optimal
270 parameter obtained from the robust optimization run, $\mathbf{w} = \mathbf{1}$, $\tau \in \mathbb{R}^+$ and $\mathcal{O} \in \mathcal{S}_{\mathcal{O}}$. Hence, in the
271 plot of this curve (e.g., see Figure 11), the number of observables on the y-axis is monotonically
272 increasing as τ increases on the x-axis. Then, the area between the cumulative density curve for
273 each robust optimization run and the ideal cumulative density curve is computed. To build the
274 ideal cumulative density curve, the $\mathbf{p}^*$ in $\dfrac{\chi^2_{\mathcal{O}}(\mathbf{p}^*, \mathbf{w})}{|\mathcal{O}|} \leq \tau$ is obtained by considering only observable
275 $\mathcal{O}$ in Eq. (2). The best run is then chosen to be the one whose area to the ideal cumulative density
276 curve is the smallest. An example plot of the cumulative density curve and an illustration of the
277 procedure to find the best run is included in Section 8.4 of the online supplement.

3 Data Pre-processing: Filtering Observables or Bins

279 We also investigate the question of how to detect and exclude observables or bins whose data $\mathcal{R}_b$
280 cannot be explained by the MC simulation model. This is driven by a significant discrepancy
281 between the simulation and data. Such discrepancies can arise for at least two reasons: (1) a
282 mistake has been made in the experimental analysis; and/or (2) the observable is out of the domain
283 of predictions that can be made reliably with the simulation. For our studies, we assume that
284 the source of discrepancies is from (2). Because the simulation is a metamodel constructed from
285 many smaller models, it is difficult to make *a priori* statements about the domain of its predictions.
286 If the intrinsic theoretical uncertainty on our models were known quantitatively, then it could be
287 incorporated into the fitting procedure. However, such uncertainties are not known currently except
288 by the brute-force method of choosing extreme values of the input parameters. Important physics
289 may be missing from the metamodel and/or a model can describe the mean behavior but not the
290 rarer fluctuations around the mean. The simulation should be able to describe the physics, but the
291 inclusion of some observables worsen the description. Thus, it is quite reasonable to exclude these
292 observables. [Reviewer comment iii:] Our goal is therefore to find a good model fit in regions where it
293 is valid. The methods described below for excluding data ("filtering") may have two outcomes. First,
294 the removed data lies in regions that cannot be explained by the model. Second, data is removed
295 from regions where the model is valid, which may impact the resulting parameter uncertainties.

296 This is however not of major concern as illustrated in the eigentune analysis in Section 5.

297 In our discussion to this point, we have assumed that each *observable* has a given weight.
298 However, in those situations where the model can describe the mean behavior, it can be beneficial
299 to filter out individual bins b of the observable. In the observables considered in this study, and
300 typical of the high energy physics phenomenon, the models can have difficulties in describing the
301 complete distribution.

3.1 Filtering of observables by outlier detection

303 Using the surrogate model $f_b(\mathbf{p})$ to approximate the expensive MC simulation, we can efficiently
304 minimize the per-observable-χ^2 function:

$$\chi_{\mathcal{O}}^2(\mathbf{p}) = \frac{1}{|\mathcal{O}|} \sum_{b \in \mathcal{O}} \frac{(f_b(\mathbf{p}) - \mathcal{R}_b)^2}{\Delta f_b(\mathbf{p})^2 + \Delta \mathcal{R}_b^2}, \mathcal{O} \in \mathcal{S}_{\mathcal{O}} \tag{12}$$

305 for each observable $\mathcal{O} \in \mathcal{S}_{\mathcal{O}}$ separately. $\chi_{\mathcal{O}}^2(\mathbf{p})$ represents the average per-bin error for the observable
306 and the best possible fit of the model for this single observable. If we used only one observable
307 for the tune, the parameters $\mathbf{p}_{\text{ideal}}^{\mathcal{O}}$ that minimize Eq. (12) would represent the *ideal* tune. The
308 corresponding ideal objective function value $\chi_{\mathcal{O}}^2(\mathbf{p}_{\text{ideal}}^{\mathcal{O}})$ is the best possible result for each individual
309 observable $\mathcal{O}$. Because the ideal parameter values will be different for each observable, we will not
310 be able to obtain one parameter set that minimizes Eq. (12) for all observables simultaneously.
311 Therefore, we obtain a set $\mathcal{X}$ of length $|\mathcal{S}_{\mathcal{O}}|$ of ideal objective function values of Eq. (12): $\mathcal{X} :=$
312 $\{\chi_1^2(\mathbf{p}_{\text{ideal}}^1), \chi_2^2(\mathbf{p}_{\text{ideal}}^2), \ldots, \chi_{|\mathcal{S}_{\mathcal{O}}|}^2(\mathbf{p}_{\text{ideal}}^{|\mathcal{S}_{\mathcal{O}}|})\} = \{\chi_i\}_{i=1}^{|\mathcal{S}_{\mathcal{O}}|}$. If the ideal error is large for some observables,
313 it means that the model is not able to fit the data of these observables well at all. Therefore, the
314 inclusion of these data in optimizing Eq. (2) may negatively impact the overall optimization because
315 large errors might bias the optimization.[2]

316 To address this issue, we use the distribution of the values in $\mathcal{X}$ to identify outliers (observables
317 with values for Eq. (12) "that deviate so much from other observations as to arouse suspicions
318 that it was generated by a different mechanism." [18]). We exclude the outlier observables from the
319 optimization of Eq. (2) by setting their corresponding weights to zero, $w_{\mathcal{O}} = 0$.

320 Multiple methods can be used for outlier detection, such as scatter plots [19], Z-score [19, Section
321 1.3.5.17], interquartile range [20], generalized extreme studentized deviate [21], Grubb's test [22,23],
322 Dixon's Q test [24], Thompson tau test [25], Pierce's Criterion [26], and Tietjen-Moore test [27],
323 to name a few. We obtained reasonable results using the Z-score. For the set $\mathcal{X} = \{\chi_i\}_{i=1}^{|\mathcal{S}_{\mathcal{O}}|}$, the
324 Z-score of an observation χ_i is defined as $z_i = (\chi_i - m)/s$ where m is the mean of the observation set

---

[2]We address later the fidelity of the surrogate model.

325 $\mathcal{X}$ and s is the standard deviation. We calculate the Z-score for each data point i in $\mathcal{X}$ and define
326 an outlier as $z_i \geq 3$. In other words, any ideal fit with a residual outside of 3 standard deviations
327 is classified as an outlier. The value 3 was chosen based on the rule of thumb for outlier detection
328 in which almost all of the data (99.7%) should be within three standard deviations from the mean.
329 The benefit of performing the outlier detection is that the computational cost of minimizing Eq. (2)
330 is reduced.

3.2 Filtering of bins by [reviewer comment e:]null-hypothesis testing

332 We explore a second and more refined approach that allows us to identify and exclude bin data
333 that cannot be approximated well by the MC simulator model from the optimization of Eq. (2)
334 instead of eliminating whole observables. The observables themselves are typically chosen to test
335 theoretical or phenomenological models, and the binning is chosen so that it represents the detector
336 resolution. The motivation of excluding bins is that physics models often fail near the boundaries
337 of observables, such as the turn on or tail of a particle production spectrum.

338 To this end, we use the χ^2 test, which is a [reviewer comment e:]null-hypothesis test performed
339 when the test statistic is χ^2-distributed under the null hypothesis [28]. Note that the χ^2 test
340 statistic is different from the $\chi^2(\mathbf{p}, \mathbf{w})$ objective function introduced earlier. We first compute the
341 χ^2 test statistic for a subset $\mathcal{B}$ of the bins in an observable $\mathcal{O}$ using the computationally cheap
342 approximation model $f_b(\mathbf{p})$:

$$\chi^2_{\mathcal{B}}(\mathbf{p}) = \frac{1}{|\mathcal{B}|} \sum_{b \in \mathcal{B} \subset \mathcal{O}} \frac{(f_b(\mathbf{p}) - \mathcal{R}_b)^2}{\Delta f_b(\mathbf{p})^2 + \Delta \mathcal{R}_b^2}. \tag{13}$$

343 Since, this test statistic is calculated per bin and then summed over a subset of bins $\mathcal{B}$ to get the
344 total test statistic, we believe that the χ^2 [reviewer comment e:]null-hypothesis test is appropriate.
345 For this statistic, we hypothesize that:

346   Null hypothesis H_0: $f_b(\mathbf{p}) = \mathcal{R}_b$

347   Alternate hypothesis H_1: H_0 is rejected, i.e., $f_b(\mathbf{p}) \neq \mathcal{R}_b$

348 In (13), we have a sample of size $|\mathcal{B}|$ based on which we compute the χ^2 test statistic. However,
349 the degrees of freedom of the χ^2 distribution is not $|\mathcal{B}|$ because the samples $f_b(\mathbf{p}), b \in \mathcal{B} \subset \mathcal{O}$ are not
350 independent and they are related to each other through the parameters $\mathbf{p}$. Due to this relationship,
351 the number of degrees of freedom is reduced (see [29] for a similar argument). Hence the resulting
352 degrees of freedom of the χ^2 distribution for the set $\mathcal{B}$ is given by

$$\rho_{\mathcal{B}} = |\mathcal{B}| - d, \tag{14}$$

353   where d is the dimension of $\mathbf{p}$.

354   We now choose a value for the significance level α. In general, α is chosen by the user and
355   commonly used values are 0.01, 0.05, or 0.1. For the results discussed in Section 4.5, we use 0.05.
356   From a χ^2 distribution table, we then obtain the critical value $\chi^2_{c,\mathcal{B}}$ for bins in $\mathcal{B}$ as a function of
357   the significance level α and degrees of freedom $\rho_{\mathcal{B}}$. More formally, we say that if the probability
358    $P_{H_0}(T \leq \chi^2_{c,\mathcal{B}}) = \alpha$, then under $H_0 : T \sim \chi^2(\rho_{\mathcal{B}})$. Let us assume a random variable $Z \sim \chi^2(\rho_{\mathcal{B}})$,
359   then $P(Z \leq \chi^2_{c,\mathcal{B}}) = \alpha$. Thus, to find $\chi^2_{c,\mathcal{B}}$, we need to compute the inverse of the cumulative
360   distribution function (CDF) of the χ^2 distribution with $\rho_{\mathcal{B}}$ degrees of freedom and at level α. Then
361   we compare the test statistic with the critical value to decide whether H_0 is accepted or not, i.e., if
362    $\chi^2_{\mathcal{B}} \leq \chi^2_{c,\mathcal{B}}$, we keep the bin subset $\mathcal{B}$; otherwise, we cannot keep this bin subset.

363   We mainly intend to exclude bins at the extremes of the observables, and hence we require that
364   the bins we keep are contiguous. For some observables all bins may pass the χ^2 test, for others, all
365   bins may be excluded, or a subset of contiguous bins is kept.

366   The problem is then to find the largest contiguous subset of bins $\mathcal{B}$ such that $\chi^2_{\mathcal{B}} \leq \chi^2_{c,\mathcal{B}}$. This
367   is equivalent to solving the mixed-integer program

$$\max_{s,e \in \{1,2,\ldots,|\mathcal{O}|\}} \quad e - s$$
$$\text{s.t. } \chi^2_{\mathcal{B}} \leq \chi^2_{c,\mathcal{B}}, \quad \mathcal{B} = \{s,\ldots,e\}, \tag{15}$$

368   where s and e are the start and end indices of contiguous bins in observable $\mathcal{O}$. We want to note
369   here that this optimization problem assumes that the constraint can be evaluated for all subsets $\mathcal{B}$
370   of the observable $\mathcal{O}$. Thus, the view of the hypothesis test from an optimization standpoint is the
371   data required to check the satisfaction of the constraint, which will either lead to the rejection of the
372   null hypothesis or the failure to reject the null hypothesis for each subset $\mathcal{B}$. Additionally, before
373   starting the optimization, we would need to evaluate the $\chi^2_{\mathcal{B}}$ and $\chi^2_{c,\mathcal{B}}$ for all subsets $\mathcal{B}$ of observable
374    $\mathcal{O}$. This can become tedious especially for observables with a large number of bins. To avoid this,
375   we also propose a polynomial-time algorithm based on the maximum sub-array problem [30]. This
376   algorithm is described in Section 8.2 in the online supplement. In some cases, the bins to keep
377   may not be unique, i.e., there may be multiple ranges of $\{s,\ldots,e\}$ that are of the same maximum
378   length and satisfy the null hypothesis (or satisfy the constraint in Eq. (15)). In practice, this is not
379   a problem, since selecting any one of these bin subsets does not change the outcome of the filtering
380   or the optimization in Eq. (2).

4 Numerical Experiments and Comparison of Different Tunes

In this section, we describe the setup of our numerical experiments, the datasets we use in our study, and the results. A comparison of the computation times required by the different optimizers is provided in Section 4.9. More details can be found in the online supplement.

4.1 Setup of the numerical experiments

Table 2: Optimization methods used in this study.

Name	Methodology	Reference
"Bilevel-portfolio"	bilevel optimization with portfolio outer objective function	Section 2.1.1.
"Bilevel-medianscore"	bilevel optimization with median score outer objective function	Section 2.1.2.
"Bilevel-meanscore"	bilevel optimization with mean score outer objective function	Section 2.1.2.
"Robust optimization"	single level robust optimization approach	Section 2.2.
"Expert"	weight adjustment done by the expert (only for the A14 dataset, see Section 4.3)	[3]
"All-weights-equal"	no optimization is used and all observable weights are set to 1	

We compare the results of using the methods shown in Table 2 for adjusting the weights of the observables in our datasets. The performance of each method is evaluated with and without data pre-processing (observable-filtering and bin-filtering approaches, see Sections 3.1 and 3.2), and when using a cubic polynomial (results presented in the online supplement) versus a rational approximation for $f_b(\mathbf{p})$ in APPRENTICE. We found relatively good performance using the degrees 3 and 1 for the numerator and denominator polynomial, respectively, for the rational approximation.

For the bilevel optimization formulation (see Eq. (3)), we made the following choices: The initial experimental design for the outer optimization has $|\mathcal{S}_\mathcal{O}| + 1$ points, where $|\mathcal{S}_\mathcal{O}|$ is the number of observables (number of weights to be adjusted). The total number of allowed outer objective function evaluations (number of weight vectors tried) is 1000. Because the inner optimization function is multimodal, we use 100 multi-starts with APPRENTICE to solve it. The bilevel optimization with each method (portfolio, meanscore, medianscore) is repeated three times with different random seeds and we report the results of the best run.

For the robust optimization formulation (Eq. (11)), a total of 100 random values of $\mu \in (0, 100]$ are used when evaluating Eq. (11c) and, for each μ, the algorithm is run once. The best run amongst these is returned as the best μ for the robust optimization. The procedure to select the best μ is described in Section 2.2.

4.2 Comparison metrics and optimal tuning parameters

There are many ways to assess the quality of a tune. In many cases, the domain experts visually inspect a potentially large number of histograms to make a judgment. As an objective measure, we propose three metrics, each represented as a single number that can be used to compare the quality of the model fits obtained by the different methods:

1. *Weighted χ^2*: the sum over all χ^2 at the best $\widehat{\mathbf{p}}_{\mathbf{w}^*}$,

$$\sum_{\mathcal{O} \in \mathcal{S}_{\mathcal{O}}} w_{\mathcal{O}}^* \sum_{b \in \mathcal{O}} \frac{(f_b(\widehat{\mathbf{p}}_{\mathbf{w}^*}) - \mathcal{R}_b)^2}{\Delta f_b(\widehat{\mathbf{p}}_{\mathbf{w}^*})^2 + \Delta \mathcal{R}_b^2}$$

.

2. *A-optimality*:

$$\mathrm{Tr}\left(\mathbf{\Gamma}_{\mathrm{post}}(\widehat{\mathbf{p}}_{\mathbf{w}^*}, \mathbf{w}^*)\right) = \sum_{i=1}^{d} \lambda_i$$

3. log *D-optimality*:

$$\log \det \left(\mathbf{\Gamma}_{\mathrm{post}}\left(\widehat{\mathbf{p}}_{\mathbf{w}^*}, \mathbf{w}^*\right)\right) = \sum_{i=1}^{d} \log \lambda_i,$$

where λ_i are the eigenvalues of $\mathbf{\Gamma}_{\mathrm{post}}$, $\mathbf{\Gamma}_{\mathrm{post}}$ is the weighted posterior covariance matrix in the Bayesian formulation of the inverse problem, d is the dimension of $\widehat{\mathbf{p}}_{\mathbf{w}^*}$. To find $\mathbf{\Gamma}_{\mathrm{post}}$, we compute the optimal parameter point $\widehat{\mathbf{p}}_{\mathbf{w}^*}$, which is also referred to as the maximum a posteriori probability estimate in the context of Bayesian inverse problems [31]. Given the optimal parameters, we can find a linearization of the model as

$$\mathbf{F}_{\mathcal{O}}(\widehat{\mathbf{p}}_{\mathbf{w}^*}) = \left[\frac{\partial f_1\left(\widehat{\mathbf{p}}_{\mathbf{w}^*}\right)}{\partial \mathbf{p}}, \frac{\partial f_2\left(\widehat{\mathbf{p}}_{\mathbf{w}^*}\right)}{\partial \mathbf{p}}, \ldots, \frac{\partial f_{|\mathcal{O}|}\left(\widehat{\mathbf{p}}_{\mathbf{w}^*}\right)}{\partial \mathbf{p}} \right]^{\top}$$

for each observable $\mathcal{O}$. Then the weighted posterior can be approximated by a Gaussian $\mathcal{N}\left(\widehat{\mathbf{p}}_{\mathbf{w}^*}, \mathbf{\Gamma}_{\mathrm{post}}\right)$. Here

$$\mathbf{\Gamma}_{\mathrm{post}}(\widehat{\mathbf{p}}_{\mathbf{w}^*}, \mathbf{w}^*) = \left(\sum_{\mathcal{O} \in \mathcal{S}_{\mathcal{O}}} w_{\mathcal{O}}^* \mathbf{F}_{\mathcal{O}}^{\top}(\widehat{\mathbf{p}}_{\mathbf{w}^*}) \mathbf{\Gamma}_{\mathrm{noise}}^{-1} \mathbf{F}_{\mathcal{O}}(\widehat{\mathbf{p}}_{\mathbf{w}^*}) \right)^{-1} \tag{16}$$

where $\mathbf{\Gamma}_{\mathrm{noise}}[\mathcal{O}] = \mathrm{diag}\left(\Delta f_1(\widehat{\mathbf{p}}_{\mathbf{w}^*})^2 + \Delta \mathcal{R}_1^2, \Delta f_2(\widehat{\mathbf{p}}_{\mathbf{w}^*})^2 + \Delta \mathcal{R}_2^2, \ldots, \Delta f_{|\mathcal{O}|}(\widehat{\mathbf{p}}_{\mathbf{w}^*})^2 + \Delta \mathcal{R}_{|\mathcal{O}|}^2\right)$. In the computation of all three metrics $w_{\mathcal{O}}^*$ is the weight of observable $\mathcal{O}$ obtained from the methods and is scaled such that $w_{\mathcal{O}}^* \in [0, 1]$ and $\sum_{\mathcal{O} \in \mathcal{S}_{\mathcal{O}}} w_{\mathcal{O}}^* = 1$.

422   The $\mathbf{\Gamma}_{\text{post}}(\widehat{\mathbf{p}}_{\mathbf{w}^*}, \mathbf{w}^*)$ calculated at the optimal parameters and the optimal weights in (16) are
423 used here to describe the confidence region around the tuned parameters $\widehat{\mathbf{p}}_{\mathbf{w}^*}$. In order to summarize
424 the multidimensional nature of $\mathbf{\Gamma}_{\text{post}}$ into a scalar quantity, we use the A- and log D-optimality
425 criteria. A graphical representation of the optimality criteria is shown in Figure 5.1 of [32]. The
426 A-optimality criterion computes the trace of $\mathbf{\Gamma}_{\text{post}}$, which is equivalent to the sum of its eigenvalues.
427 This metric is proportional to the sum of the semiaxis lengths of the confidence ellipsoid of the
428 parameters (lower is better), which corresponds to the average sum of the variances of the estimated
429 parameters for the model [33]. The log D-optimality criterion computes the log of the determinant
430 of $\mathbf{\Gamma}_{\text{post}}$, which is equivalent to the sum of the log of the eigenvalues of $\mathbf{\Gamma}_{\text{post}}$. This metric is
431 proportional to the log volume of the confidence ellipsoid of the parameters (lower is better) [34].
432 It can be interpreted in terms of Shannon information. Note that since the weighted posterior
433 is approximated as a Gaussian, a Gaussianity test should reveal that the posterior is normally
434 distributed.

4.3   The A14 dataset

436 We chose the A14 tune [3] of the PYTHIA[3] event generator [35] as one benchmark for developing
437 and testing the methods proposed in this work. This tune has been widely used for Large Hadron
438 Collider (LHC) simulations, and is thus relevant to the particle physics community.

439   The A14 dataset contains 406 observables (thus, 406 weights to optimize) and there are 10
440 tunable physics parameters $\mathbf{p}$. The parameters are primarily related to the production of additional
441 jets in the collisions, the distribution of energy within those jets, and the kinematics (angles and
442 momenta) of the jets. They also relate to the sharing and spread of energy in the soft portion of
443 the event, the portion that is less dependent on the hard process (e.g., top-quark production or
444 Z-boson production). Further explanation of the generator parameters and settings are available
445 in Sections 8.3 and 8.16, respectively. The bounds over which we optimize the parameters were
446 carefully chosen such that the polynomial parameterizations are valid within the bounds and to
447 give a physically meaningful coverage such that the experimentally observed data was "covered" by
448 the range of predictions. We use the RIVET [36] package to compare our predictions to data. The
449 motivation for and selection of observables and parameters is explained in the A14 tune paper.

450   Because the coefficients of the cubic interpolation used in [3] were not available to us, we start by
451 reproducing the hand-tuned parameter values published in [3, Table 3], which we refer to as *NNPDF*.
452 In particular, we use the weights given in [3, Table 2], use their optimal parameter values as a starting
453 point for the χ^2 minimization, and apply our optimizer to Eq. (2). The resulting parameter values

---

[3]To match the original study, we used version v8.186.

are reassuringly close to the values reported in [3] as shown in Table 3 where we label the original parameters as NNPDF, and the re-optimized parameter values as *Expert*. We observe that most of the NNPDF parameter values lie within the confidence interval derived from eigentunes (see Section 5) for the re-optimized Expert values. Additionally, to check whether the parameters $\mathbf{p}$ reported in [3] are within the confidence ellipsoid centered on the parameters $\widehat{\mathbf{p}}_{\mathbf{w}}$ obtained from the χ^2 minimization (i.e., Expert parameter values), we calculate $s \equiv \left\| \mathbf{L}^T (\mathbf{p} - \widehat{\mathbf{p}}_{\mathbf{w}}) \right\|_2$, where $\mathbf{L}$ is the Cholesky factor of $\mathbf{\Gamma}_{\text{post}}(\widehat{\mathbf{p}}_{\mathbf{w}}, \mathbf{w})$ from Eq. (16) with weights $\mathbf{w}$ given in [3]. Since $s = 2.73 \times 10^{-3}$ is less than one, we say that the parameter $\mathbf{p}$ is covered within the confidence ellipsoid centered on $\widehat{\mathbf{p}}_{\mathbf{w}}$ [37].

In the remainder of this paper, we use the Expert parameter values for comparison. This provides a fairer comparison because we found that the original NNPDF parameter values did not correspond to a minimizer of the χ^2 optimization, Eq. (2). The main reason for this discrepancy is the fact that we use an improved optimization routine (APPRENTICE) that takes advantage of exact gradient and Hessian information and that requires significantly less time than the previous optimizer, and thus allows for an efficient multistart local optimization that increases the possibility to find better optima.

Table 3: Parameter values for A14 published tune (left), and A14 corrected expert tune and corresponding eigentune 68% confidence intervals (right).

Parameter name	A14 published expert tune	A14 corrected expert tune		
	NNPDF	Expert	min	max
SigmaProcess:alphaSvalue	0.140	0.143	0.075	0.193
BeamRemnants:primordialKThard	1.88	1.904	1.903	1.906
SpaceShower:pT0Ref	1.56	1.643	1.636	1.653
SpaceShower:pTmaxFudge	0.91	0.908	0.905	0.912
SpaceShower:pTdampFudge	1.05	1.046	1.044	1.048
SpaceShower:alphaSvalue	0.127	0.123	0.121	0.124
TimeShower:alphaSvalue	0.127	0.128	0.043	0.197
MultipartonInteractions:pT0Ref	2.09	2.149	1.665	2.543
MultipartonInteractions:alphaSvalue	0.126	0.128	0.068	0.177
BeamRemnants:reconnectRange	1.71	1.792	1.788	1.795

The A14 observables are measurements of properties of proton-proton collisions at $\sqrt{s} = 7$ TeV performed by the ATLAS collaboration. These include event properties (e.g., the Z-boson transverse momentum, or the opening angles between the highest transverse momentum jets in the event) and

properties of jets (e.g., the spread of energy within a jet, or the momentum of particles within a jet). In [3], the 406 observables are categorized into 10 groups (see Table 7), namely *Track jet properties* (200 observables) [38], *Jet shapes* (59 observables) [39], *Dijet decorr* (9 observables) [40], *Multijets* (8 observables) [41], p_T^Z (fit range < 50GeV, 20 observables) [42, 43], *Substructure* (36 observables) [44], $t\bar{t}$ *gap* (4 observables) [45], $t\bar{t}$ *jet shapes* (20 observables) [46], *Track-jet UE* (8 observables) [47, 48], and *Jet UE* (42 observables) [49, 50]. The highest weights in [3] are assigned to observables that relate to the production of additional high-momentum partons (the ratios of 3-jet to 2-jet events, and the fraction of top-quark production events that do not have an additional central jet). On the other hand, low weights are assigned to observables that measure the same physical phenomenon in several kinematic regimes. The weighting of these observables ensures that the additional radiation and soft part of the events are consistent and well-modeled for all hard processes. In addition, these parameters are difficult or impossible to constrain using data from e^+e^- collision events, and they must be tuned using data from the LHC.

4.4 The SHERPA dataset

As a second benchmark, we tune a set of parameters for the SHERPA event generator [51]. To our knowledge, the default parameters were not optimized by weighting data, and thus serve as an unbiased cross-check of our results. The data are confined to observables at e^+e^- colliders and they include event shapes and charged particle inclusive spectra from Z-boson decays, differential and integrated jet rates, measurements of B-hadron fragmentation, and the multiplicity of various hadrons [52–55]. Accordingly, the parameters are limited to those of the SHERPA hadronization model.

The SHERPA dataset contains 88 observables, hence 88 weights to optimize. This is significantly less than the set of observables available in the RIVET analyses (126) for the following reasons. First, we reduce the number of observables to 114 by removing those that measure more than 3 jets, since this is beyond the scope of the physics simulation. Then, we apply a pre-filter step that removes distributions where *none* of the data bins fall within the envelope of predictions from our surrogate model. These all correspond to single-bin particle counts (such as the number of f_0 mesons) that the SHERPA hadronization model either grossly under- or over-estimates. There are 13 tunable physics parameters whose definition and ranges are shown in Table 16 in Section 8.3 of the online supplement. These parameters are all part of the cluster model that produces physical particles from quarks and gluons. The reason for including this dataset in our study is to show the general applicability of our optimizers and to try them out on a dataset for which an expert tune is not provided.

4.5 Data pre-processing: filtering out observables and bins

In this subsection, we present the results of applying the filtering methods. First, we consider the outlier detection method described in Section 3.1. We find that the filtering results differ based on the choice of surrogate function (cubic polynomial versus a rational approximation). Based on the comparison of surrogate function predictions to the full MC simulations, we believe that the rational approximation yields a more faithful representation. Therefore, we present our main results using only the rational approximation. The names of the outlier observables in the A14 and the SHERPA dataset using a cubic polynomial and a rational approximation, respectively, are shown in the online supplement in Sections 8.5 and 8.6. Table 4 shows a distribution of the $\chi^2_{\mathcal{O}}$ values obtained for each observable $\mathcal{O}$ from Eq. (12) for A14 (left) and SHERPA (right) when using the rational approximation. We find that the per-observable ideal parameters yield mostly small $\chi^2_{\mathcal{O}}$ values (in $[0, 1)$), but outliers are present in both datasets. Using the rational approximation, 9 and 3 outlier observables are filtered from the A14 and SHERPA datasets, respectively.

Table 4: Distribution of the $\chi^2_{\mathcal{O}}$ values for A14 (left) and SHERPA (right). 2.0438 and 2.0177 correspond to the values where the Z-score equals 3 (see Section 3.1). The observables with $\chi^2_{\mathcal{O}} \geq$ 2.0438 for A14 and $\chi^2_{\mathcal{O}} \geq 2.0177$ for SHERPA are the outliers. There are 9 outliers (6+2+1) in A14 and 3 outliers (1+2+0) in SHERPA.

A14		SHERPA	
$\chi^2_{\mathcal{O}}$ range	Number of observables	$\chi^2_{\mathcal{O}}$ range	Number of observables
$[0, 1)$	367	$[0, 1)$	82
$[1, 2.0438)$	30	$[1, 2.0177)$	3
$[2.0438, 3)$	**6**	$[2.0177, 3)$	**1**
$[3, 4)$	**2**	$[3, 4)$	**2**
$[4, 5)$	**1**	$[4, 5)$	**0**

Figure 1 shows the outcomes of the bin-filtering approach described in Section 3.2 for each observable $\mathcal{O}$ in A14 (top) and SHERPA (bottom) when using the rational approximation. In both datasets, multiple bins are removed. More specifically, most bins are removed in the *Track jet properties* and p_T^Z groups of the A14 dataset. The patterns in the A14 plot result from the partitioning of the data. For *Tracked jet properties* (labeled A), the observables are replicated for two values of jet cone size ($R = 0.4, 0.6$), explaining the similarities between bins (1, 100) and (101, 200). Furthermore, 4 types of observables are considered, and each is sliced into different ranges of transverse momentum and rapidity.

In the SHERPA dataset, all bins are removed from some observables whereas from two observables, we remove only two and five bins (see observables in bold font in Table 22). Additionally, since the number of degrees of freedom of the χ^2 distribution is reduced by the number of parameters that the bins share in each observable (see Eq. (14)), the bin filter is not applied to any observable with fewer than 10 and 13 bins in the A14 and the SHERPA datasets, respectively. The names of the observables from which the bins have been filtered and their χ^2 test statistic and critical χ^2 values are given in Sections 8.7 and 8.8 of the online supplement. The single bin observables correspond to counts of a particular type of particle.
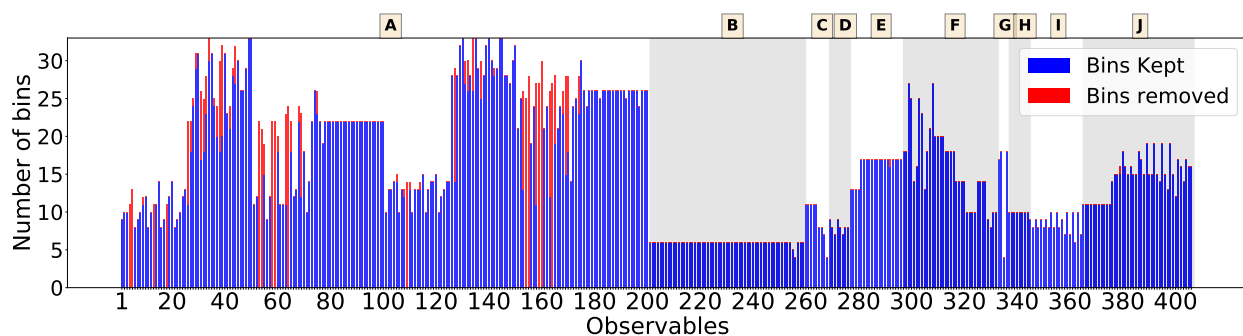
(a) Bins kept and removed by the bin filter in all A14 observables organized by the observable group. Group A is *Track jet properties*, group B is *Jet shapes*, group C is *Dijet decorr*, group D is *Multijets*, group E is p_T^Z, group F is *Substructure*, group G is $t\bar{t}$ *gap*, group H is *Track-jet UE*, group I is $t\bar{t}$ *jet shapes*, and group J is *Jet UE*.
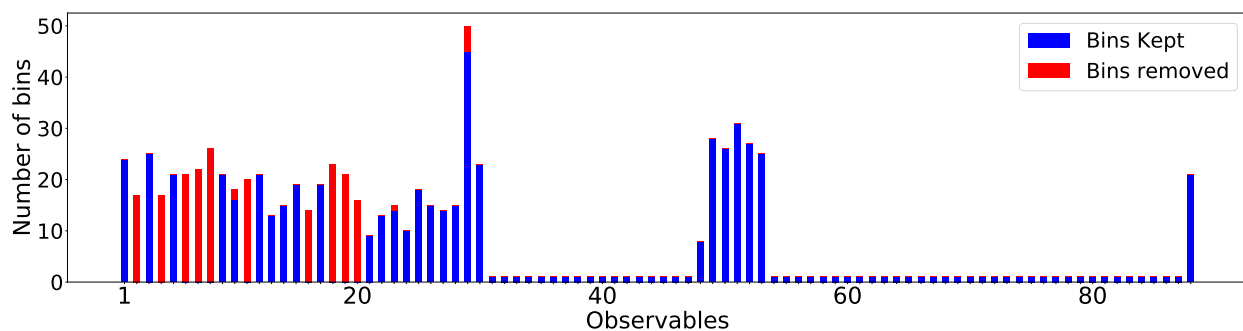
(b) Bins kept and removed by the bin filter in all SHERPA observables.

Figure 1: Illustration of the bin filtering results.

4.6   Results for the A14 dataset

In this section, we present a detailed analysis of our results with the A14 dataset.

4.6.1   Comparison metric outcomes for the A14 dataset

In this section, we consider the three metrics introduced in Section 4.2 to compare various tunes. For the A14 dataset, Table 5 shows the results when using the rational approximation for the full data, the observable-filtered data, and the bin-filtered data, respectively. The results when using the cubic polynomial approximation are shown in the online supplement in Section 8.12.1. Note that smaller numbers indicate better performance.

Based on these results we can see that no method performs the best for all metrics in all cases. In fact, for the full dataset, the *Expert* tune has the best score for two of our three metrics. The robust optimization consistently achieves the best performance under the Weighted χ^2 criterion.

The Bilevel-portfolio method performs the best under the A-optimality criteria, and the *Expert* tune performs the best under the D-optimality criteria for the observable-filtered datasets. The Bilevel-portfolio method performs the best under the A- and D-optimality criteria for the bin-filtered datasets. In comparison to the results obtained with the cubic polynomial approximation (see Section 8.12.1 of the online supplement), the rational approximation yields better results for all methods under the Weighted χ^2 criterion.

When comparing across Table 5, we see that in most cases, results with the observable-filtered data and bin-filtered data provide smaller values compared with those using the full dataset. We observe that by filtering out the observables and bins that cannot be well explained by the model, there is an improvement in the best values (in bold) of the metrics. This is an expected result because the excluded bins and observables no longer "distract" the optimizer by yielding large errors and thereby dominating the optimization. The selection of the best optimization method depends on the goals and preferences of the user as there is no one method that performs best for all metrics (no free lunch). However, we note here that lower A- log D-optimality values in the observable- and bin-filtered case indicate more confidence in the parameter predictions. We show in Section 8.9 that by excluding the filtered bins and observables from the fitting process, the quality of the model does not deteriorate.

4.6.2   Comparison of the cumulative distribution of bins at different variance levels

In this section, we introduce a new summarized graphical comparison of the results. We study the distribution of the χ^2 values per bin obtained using different tuning approaches. For each

Table 5: A14 results with the *full dataset, observable-filtered dataset* and *bin-filtered dataset* when using the *rational* approximation. Lower numbers are better. The best results are in bold. In each dataset, W-χ^2 refers to the Weighted χ^2 metric, A-o refers to the A-opt metric, and l-D-o refers to the log D-opt metric.

Data	Full dataset			Observable-filtered dataset			Bin-filtered dataset		
Method	W-χ^2	A-o	l-D-o	W-χ^2	A-o	l-D-o	W-χ^2	A-o	l-D-o
Meanscore	0.1119	0.8513	-63.6805	0.0671	0.6793	-65.1939	0.0923	0.7738	-64.8949
Medscore	0.1320	0.7673	-63.3846	0.0823	0.7008	-64.3410	0.1175	0.7734	-64.0170
Portfolio	0.1224	0.9425	-61.1694	0.1372	**0.5130**	-68.0382	0.1652	**0.4788**	**-68.8998**
Expert	0.0965	**0.5705**	**-68.4091**	0.0781	0.5765	**-68.4674**	0.0947	0.5868	-68.3093
Equal-weights	0.0815	0.7673	-64.0008	0.0563	0.7179	-64.5198	0.0640	0.7384	-65.2606
Robust opt	**0.0402**	1.0526	-65.7547	**0.0388**	1.1086	-65.7182	**0.0485**	0.8445	-67.3645

566 parameter set, we compute the ratio $r_b(\mathbf{p}) = \dfrac{(f_b(\mathbf{p}) - \mathcal{R}_b)^2}{\Delta f_b(\mathbf{p})^2 + \Delta \mathcal{R}_b^2}$ of the residual between the data and
567 the prediction divided by the variance per bin. The r_b values are sorted from the smallest to largest,
568 and the cumulative distribution is formed.

569   The cumulative distribution plot for all bins in the A14 dataset is shown in Figure 2 and for
570 the bins in each category in Figure 3. The more bins that reside on the bands of variance levels
571 less than 1 the better, as this indicates smaller deviations of the model from the experimental data.
572 Note that even though all the category plots have a scale between 0 and 1 on the y-axis, the number
573 of bins in the individual categories of A14 are very different, e.g., more than 50% of all bins in
574 the A14 dataset belong to *Track Jet Properties*. Note, however, that we can see from the optimal
575 weights assigned to each observable category (see Table 7, Section 4.6.4), the robust optimization
576 approach is able to recognize the redundancy in the data and gives the observables in three of four
577 subcategories little to no weight. On the other hand, the goal of the bilevel approaches is to fit each
578 observable approximately equally well and the optimal weights mimic the expert's hand-tuning.

579   It can be seen from Figure 2 that there is only a small difference among the approaches when all
580 A14 bins are considered. Near the variance boundary, the difference between the approaches is even
581 smaller and all approaches perform better than the *Expert* tune. For sample data x distributed
582 normally as $\mathcal{N}(\mu, \sigma)$, the χ^2 distribution with one degree of freedom is a distribution of the squared
583 standard normal deviate given by $((x - \mu)/\sigma)^2$ [56]. Hence, for a normally distributed sample, the
584 CDF of the bins with variance values $r_b(\mathbf{p})$ should theoretically follow a χ^2 distribution with one
585 degree of freedom. We compare the CDF of the bins against the CDF of this theoretical distribution
586 in Figure 2. We observe that the CDF of the bins obtained from the different methods does not

match the CDF of the theoretical distribution. In particular, we observe that bins whose residuals are $10^{-1} < r_b(\mathbf{p}) \le 10^{1.5}$ arise from samples that are not normally distributed.

Figure 3 shows that these differences become more prominent for individual categories of the A14 data. For instance, robust optimization performs well for *Jet shapes* and *Track-jet UE*. Near the variance boundary, the parameters obtained from the *Expert* tune perform better for *Multijets* and $t\bar{t}$ *gap* whereas the other approaches perform better for *Substructure*. These plots also show that there is a trade-off in fitting among the different approaches, which enables the physicist to use these results as guidance for selecting the most appropriate tuning method depending on the categories that are of greater significance.
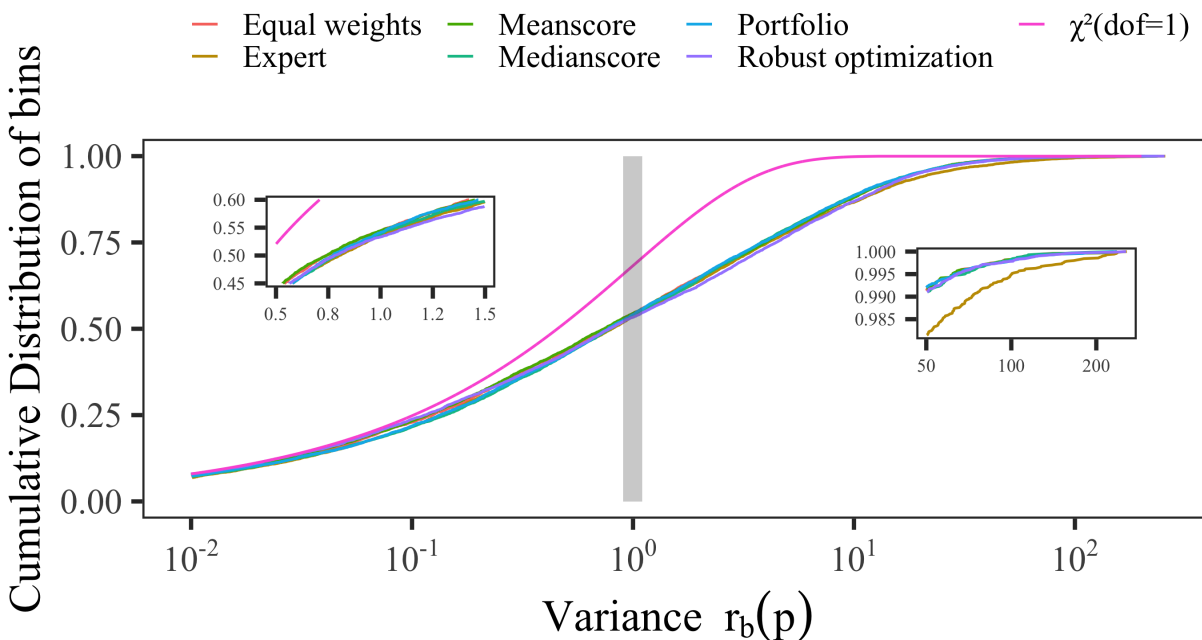
Figure 2: Cumulative distribution function (CDF) of all bins (y-axis) in the A14 dataset at different bands of variance levels (x-axis) given by $r_b(\mathbf{p}) = \frac{(f_b(\mathbf{p}) - \mathcal{R}_b)^2}{\Delta f_b(\mathbf{p})^2 + \Delta \mathcal{R}_b^2}$ and the theoretical χ^2 distribution with one degree of freedom.

4.6.3 Optimal parameter values for the A14 dataset with rational approximation

The optimal parameter values for the A14 dataset when using the full dataset, the outlier-filtered dataset, and the bin-filtered dataset are shown in Table 6. For a better visual comparison of the
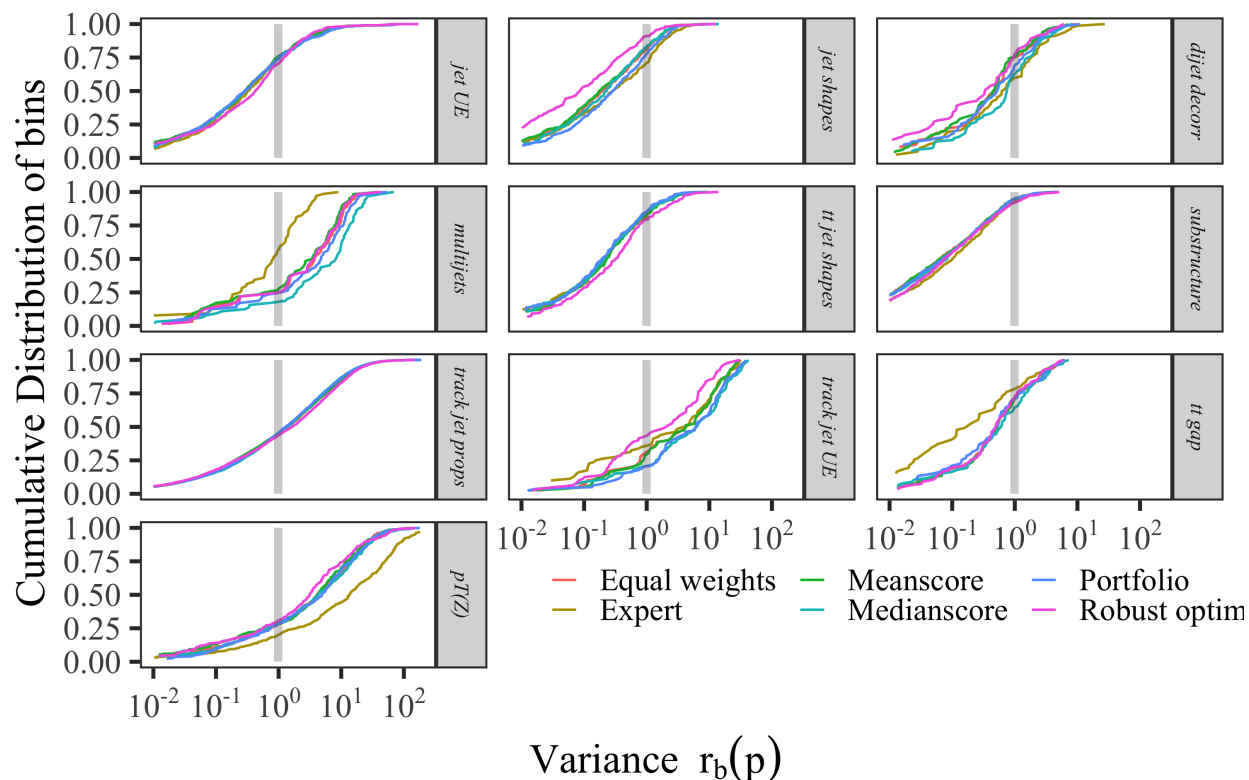
Figure 3: Cumulative distribution of bins (y-axis) in each category of the A14 dataset at different bands of variance levels (x-axis) given by $r_b(\mathbf{p}) = \frac{(f_b(\mathbf{p}) - \mathcal{R}_b)^2}{\Delta f_b(\mathbf{p})^2 + \Delta \mathcal{R}_b^2}$.

different solutions obtained with our methods, we illustrate the [0,1]-scaled optimal values in the online supplement Section 8.11. We have also computed the Euclidean distance between the *Expert* tune and our tunes after normalizing the parameter values to [0,1].

In Table 6, we can see that there are differences between the optimal parameters obtained with different methods and when using different filtering approaches. In particular, the results of the Bilevel-meanscore method tend to be approximately equally far from the expert solution no matter the filtering approach. This indicates that the bilevel-meanscore method is less sensitive to the data used in the optimization. The other methods show a larger variability of the optimal parameter values depending on the filtering approach. The eigentune results corresponding to the solutions in Table 6 are discussed in Section 5.

Table 6: Optimal parameter values for the A14 dataset when using the rational approximation in the optimization. Euclidean distances are calculated based on the normalized parameter values.

	ID	Parameter name	Expert	Meanscore	Medianscore	Portfolio	Robust opt	Equal-weights
All observables	1	SigmaProcess:alphaSvalue	0.143	0.138	0.133	0.136	0.139	0.137
	2	BeamRemnants:primordialKThard	1.904	1.855	1.723	1.796	1.883	1.851
	3	SpaceShower:pT0Ref	1.643	1.532	1.184	1.322	1.588	1.493
	4	SpaceShower:pTmaxFudge	0.908	1.014	1.083	1.041	1.025	1.026
	5	SpaceShower:pTdampFudge	1.046	1.071	1.084	1.061	1.084	1.067
	6	SpaceShower:alphaSvalue	0.123	0.128	0.129	0.128	0.127	0.128
	7	TimeShower:alphaSvalue	0.128	0.130	0.129	0.128	0.132	0.129
	8	MultipartonInteractions:pT0Ref	2.149	2.033	1.883	1.937	2.052	2.076
	9	MultipartonInteractions:alphaSvalue	0.128	0.124	0.118	0.120	0.126	0.125
	10	BeamRemnants:reconnectRange	1.792	2.082	1.914	1.987	2.602	1.980
		Euclidean distance from the expert solution		0.290	0.664	0.475	0.268	0.301
Observable-filtered	1	SigmaProcess:alphaSvalue	0.143	0.140	0.138	0.141	0.138	0.139
	2	BeamRemnants:primordialKThard	1.904	1.865	1.839	1.861	1.879	1.843
	3	SpaceShower:pT0Ref	1.643	1.574	1.603	1.593	1.614	1.550
	4	SpaceShower:pTmaxFudge	0.908	0.953	0.906	0.984	1.006	0.950
	5	SpaceShower:pTdampFudge	1.046	1.076	1.081	1.060	1.075	1.062
	6	SpaceShower:alphaSvalue	0.123	0.128	0.128	0.129	0.128	0.127
	7	TimeShower:alphaSvalue	0.128	0.123	0.123	0.118	0.132	0.124
	8	MultipartonInteractions:pT0Ref	2.149	2.064	2.017	2.095	2.022	2.039
	9	MultipartonInteractions:alphaSvalue	0.128	0.126	0.125	0.129	0.125	0.126
	10	BeamRemnants:reconnectRange	1.792	1.852	1.903	1.801	2.719	1.937
		Euclidean distance from the expert solution		0.227	0.293	0.273	0.291	0.254
Bin-filtered	1	SigmaProcess:alphaSvalue	0.143	0.139	0.140	0.131	0.137	0.140
	2	BeamRemnants:primordialKThard	1.904	1.877	1.885	1.811	1.822	1.876
	3	SpaceShower:pT0Ref	1.643	1.572	1.561	2.227	1.426	1.627
	4	SpaceShower:pTmaxFudge	0.908	0.964	0.968	0.869	0.948	0.943
	5	SpaceShower:pTdampFudge	1.046	1.056	1.053	1.481	1.053	1.068
	6	SpaceShower:alphaSvalue	0.123	0.128	0.128	0.136	0.128	0.128
	7	TimeShower:alphaSvalue	0.128	0.128	0.129	0.126	0.136	0.130
	8	MultipartonInteractions:pT0Ref	2.149	2.028	2.175	2.338	1.931	2.080
	9	MultipartonInteractions:alphaSvalue	0.128	0.124	0.128	0.135	0.120	0.126
	10	BeamRemnants:reconnectRange	1.792	2.047	1.854	1.820	2.404	2.001
		Euclidean distance from the expert solution		0.232	0.179	1.076	0.426	0.194

4.6.4   Comparison of optimal weights for the A14 dataset with rational approximation

We compare the optimal weights obtained by the different tuning methods in Table 7. We normalize the weights obtained to match the scale of weights assigned by *Expert* published in [3]. In each group, we report the average weight of observables in that group. The *Expert* tune assigned the highest weights to the categories *Multijets* and $t\bar{t}$ *gap*, which result in better fits as illustrated in the corresponding plots in Figure 5. The weights for the robust optimization approach are almost all either 0 or 17.85, which corresponds to unscaled $0 - 1$ weights that we would expect from this approach. We note that the weights for the four *Track-jet properties* classes are similar for the expert and the bilevel approaches (approx. 10), while the robust approach returns weights of $(17.85, 0, 1.62, 0)$. We believe that these weights indicate that the corresponding observables are nearly dependent resulting in redundant components of least-square residuals. We observe in Figure 3 that setting these weights to zero does not degrade the residuals of these observables, confirming that redundant information is present. This observation indicates that even though *Track jet properties* dominates the tune in terms of the number of observables, the inherent redundancy in the data does not dominate the final fit, and can be detected by the robust optimization approach.

4.6.5   Impact of data pre-processing by filtering on optimal results

In Table 8, we show the number of filtered and unfiltered bins in the A14 and SHERPA datasets that lie within a one σ variance level. A large number of bins within a one σ level indicates smaller deviations of the model from the experimental data. The cumulative distribution plot with the parameters obtained from the robust optimization approach for filtered and unfiltered data for the different categories is shown in Figure 4 (the plots for the other methods are shown in Section 8.9 of the online supplement).

From these results, we observe that there is no significant difference in the number of bins within the one σ variance level between the optimal parameters $\mathbf{p}_a^*$ obtained when all bins were used for tuning and the optimal parameters $\mathbf{p}_b^*$ and $\mathbf{p}_o^*$ obtained when only the bin filtered and observable filtered bins are used for tuning, respectively. Additionally, when comparing across Table 5, we see that in most cases, the results with the observable-filtered data and bin-filtered data provide smaller values in the proposed criteria compared with those using the full dataset. These observations indicate that the MC generator cannot explain the removed bins and that the information contained in these bins does not add significant information to the tune.

Table 7: Comparison of the optimal weights obtained by each method using the rational approximation. The observable grouping corresponds to the same grouping as in [3].

	Expert	Bilevel-meanscore	Bilevel-medianscore	Bilevel-portfolio	Robust opt
Track jet properties					
Charged jet multiplicity (50 distributions)	10	11.41	11.92	11.43	17.85
Charged jet z (50 distributions)	10	11.01	10.00	10.28	0.00
Charged jet p_T^{rel} (50 distributions)	10	9.47	10.20	13.11	1.62
Charged jet $\rho_{ch}(r)$ (50 distributions)	10	10.63	12.72	12.19	0.00
Jet shapes					
Jet shape ρ (59 distributions)	10	12.46	8.49	9.69	17.85
Dijet decorr					
Decorrelation $\Delta\phi$ (Fit range: $\Delta\phi > 0.75$) (9 distributions)	20	18.82	10.32	18.50	15.87
Multijets					
3-to-2 jet ratios (8 distributions)	100	15.06	11.18	11.06	17.85
$\boldsymbol{p_T^Z}$ (Fit range: $p_T^Z < 50\text{GeV}$)					
Z-boson p_T (20 distributions)	10	12.16	11.85	9.25	17.85
Substructure					
Jet mass, $\sqrt{d_{12}}, \sqrt{d_{23}}, \tau_{21}, \tau_{23}$ (36 distributions)	5	10.71	12.75	14.23	17.85
$\boldsymbol{t\bar{t}}$ **gap**					
Gap fraction vs Q_0, Q_{sum} for $|y| < 0.8$	100	24.56	5.05	1.97	17.85
Gap fraction vs Q_0, Q_{sum} for $0.8 < |y| < 1.5$	80	23.73	47.01	4.01	17.85
Gap fraction vs Q_0, Q_{sum} for $1.5 < |y| < 2.1$	40	2.39	14.20	7.35	17.85
Gap fraction vs Q_0, Q_{sum} for $|y| < 2.1$	10	5.47	19.00	12.82	17.85
Track-jet UE					
Transverse region N_{ch} profiles (5 distributions)	10	13.01	24.18	7.46	17.85
Transverse region mean p_T profiles for $R = 0.2, 0.4, 0.6$ (3 distributions)	10	7.91	16.89	9.68	17.85
$\boldsymbol{t\bar{t}}$ **jet shapes**					
Jet shapes $\rho(r), \psi(r)$ (20 distributions)	5	10.44	11.47	10.29	15.17
Jet UE					
Transverse, trans-max, trans-min sum p_T incl. profiles (3 distributions)	20	12.11	5.32	10.51	17.85
Transverse, trans-max, trans-min N_{ch} incl. profiles (3 distributions)	20	6.16	14.42	6.56	17.85
Transverse sum E_T incl. profiles (2 distributions)	20	5.11	2.71	7.72	17.85
Transverse sum ET/sum p_T ratio incl., excl. profiles (2 distributions)	5	11.94	10.81	11.65	17.85
Transverse mean p_T incl. profiles (2 distributions)	10	12.47	7.28	10.45	17.85
Transverse, trans-max, trans-min sum p_T incl. distributions (15 distributions)	1	10.54	14.44	8.27	17.85
Transverse, trans-max, trans-min sum N_{ch} incl. distributions (15 distributions)	1	11.62	10.33	11.48	17.85

Table 8: Number of bins in the A14 and Sherpa datasets within the one σ variance level. Larger numbers are better. The variance level for each bin is calculated as $r_b(\mathbf{p}) = \frac{(f_b(\mathbf{p}) - \mathcal{R}_b)^2}{\Delta f_b(\mathbf{p})^2 + \Delta \mathcal{R}_b^2}$. *Test data type* specifies the data over which $r_b(\mathbf{p})$ is calculated, where *All* means that all bins are used, *Not Filtered* refers to only the bins that remain after filtering, and *Filtered* refers to the bins that were filtered out by the respective filter specified in the *Filtering Method* as well as the envelope filter. For each data type, the number of bins in the corresponding dataset is also specified. *Parameters* specify the type of optimal parameters used in $r_b(\mathbf{p})$ where $\mathbf{p}_a^*$ are the parameters obtained when all bins were used during tuning whereas $\mathbf{p}_b^*$ and $\mathbf{p}_o^*$ are the parameters obtained when only the bin filtered and observable filtered date are used, respectively.

Dataset	Filtering method	Test data type	Parameters	Robust optimization	Bilevel-meanscore	Bilevel-medianscore	Bilevel-portfolio
A14	Bin Filtered	All (# 7010)	$\mathbf{p}_a^*$	3730	3724	3687	3693
			$\mathbf{p}_b^*$	3625	3775	3765	3573
		Not filtered (# 5199)	$\mathbf{p}_a^*$	3350	3317	3265	3273
			$\mathbf{p}_b^*$	3248	3365	3342	3185
		Filtered (# 1811)	$\mathbf{p}_a^*$	380	407	422	420
			$\mathbf{p}_b^*$	377	410	423	388
	Observable Filtered	All (# 7010)	$\mathbf{p}_a^*$	3730	3724	3687	3693
			$\mathbf{p}_o^*$	3732	3734	3695	3509
		Not filtered (# 6707)	$\mathbf{p}_a^*$	3675	3660	3624	3630
			$\mathbf{p}_o^*$	3679	3672	3629	3444
		Filtered (# 303)	$\mathbf{p}_a^*$	55	64	63	63
			$\mathbf{p}_o^*$	53	62	66	65
Sherpa	Bin Filtered	All (# 792)	$\mathbf{p}_a^*$	320	337	371	256
			$\mathbf{p}_b^*$	343	328	345	243
		Not filtered (# 588)	$\mathbf{p}_a^*$	272	283	317	214
			$\mathbf{p}_b^*$	282	270	292	200
		Filtered (# 204)	$\mathbf{p}_a^*$	48	54	54	42
			$\mathbf{p}_b^*$	61	58	53	43
	Observable Filtered	All (# 792)	$\mathbf{p}_a^*$	320	337	371	256
			$\mathbf{p}_o^*$	286	348	386	252
		Not filtered (# 727)	$\mathbf{p}_a^*$	304	319	355	237
			$\mathbf{p}_o^*$	271	331	370	235
		Filtered (# 65)	$\mathbf{p}_a^*$	16	18	16	19
			$\mathbf{p}_o^*$	15	17	16	17
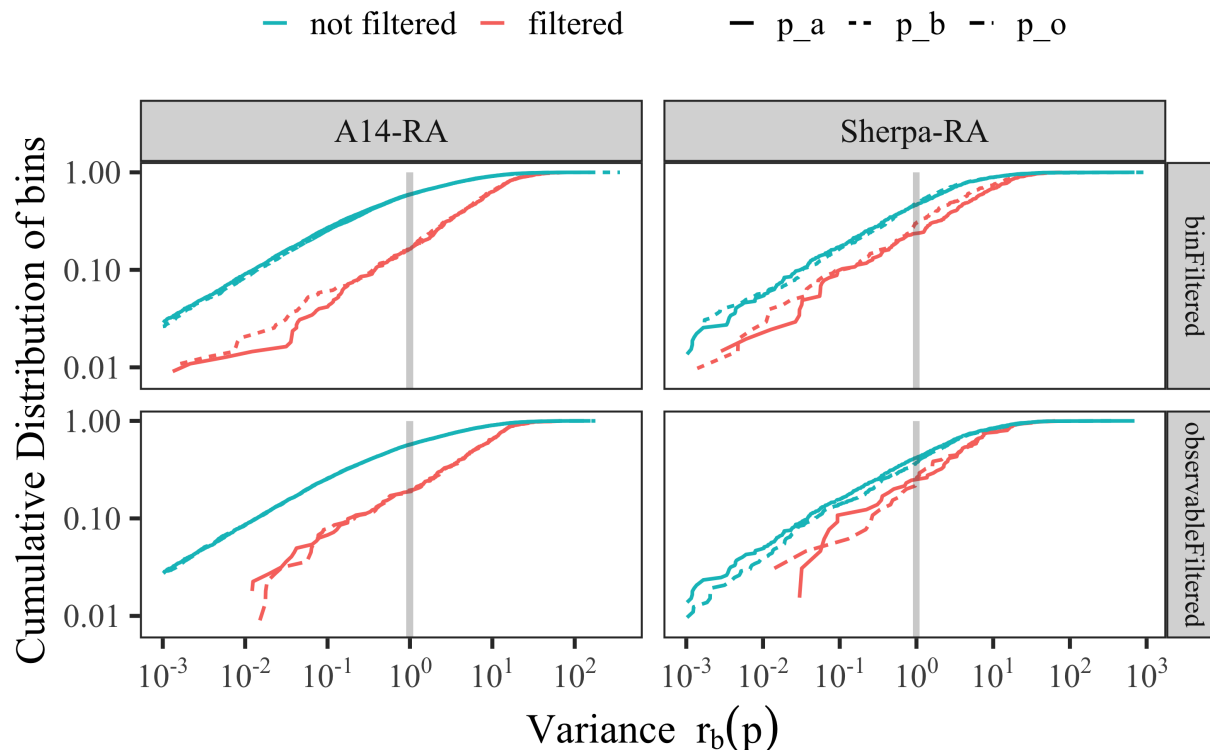
Figure 4: Cumulative distribution of bins remaining after filtering (*not filtered*) and of those filtered out (*filtered*) on the y-axis at different bands of variance levels on the x-axis. The variance level for each bin is calculated as $r_b(\mathbf{p}) = \frac{(f_b(\mathbf{p})-\mathcal{R}_b)^2}{\Delta f_b(\mathbf{p})^2 + \Delta\mathcal{R}_b^2}$ with parameters $\mathbf{p}_a^*$, which is obtained when all bins were used, and parameters $\mathbf{p}_b^*$ and $\mathbf{p}_o^*$, which are obtained when only the bin filtered and observable filtered data are used, respectively.

4.6.6 Comparison of rational approximation and the MC simulator

Similar to the analysis conducted in Section 4.6.2, we compare the cumulative distribution of bins at different bands of variance levels computed using the approximation model as $r_b(\mathbf{p}) = \frac{(f_b(\mathbf{p})-\mathcal{R}_b)^2}{\Delta f_b(\mathbf{p})^2 + \Delta\mathcal{R}_b^2}$ and the MC generator model as $\widetilde{r_b(\mathbf{p})} = \frac{(MC_b(\mathbf{p})-\mathcal{R}_b)^2}{\Delta MC_b(\mathbf{p})^2 + \Delta\mathcal{R}_b^2}$, where $\mathbf{p}$ are the parameters obtained from the tuning approaches. The more bins that are on the bands of variance levels less than one, the better. Figure 5 shows the plot of this comparison for bins in each category of the A14 dataset.[4] To avoid making the plot too busy, we show the results using the parameters from three

---

[4]The *Jet UE* comparison is missing from this figure because the internal ATLAS analysis is not available to us.

approaches. A similar plot showing the results with parameters from the remaining approaches is given in Section 8.10 in the online supplement.

We observe in Figure 5 that the *Dijet decorr*, *Jet shapes*, p_T^Z, *Track-jet UE*, and $t\bar{t}$ *gap* categories show differences in the performance between $r_b(\mathbf{p})$ and $\widetilde{r_b(\mathbf{p})}$ for each approach. Additionally, for the *robust optimization* and *Bilevel-meanscore* approaches, this difference in the performance is not as wide as that of the *Expert* (for e.g., see p_T^Z, *Track-jet UE* categories). This suggests that (a) there are categories where the approximations are not able to capture the MC generator perfectly, and (b) in general, the rational approximation is a better surrogate for the MC generator than the polynomial approximation.
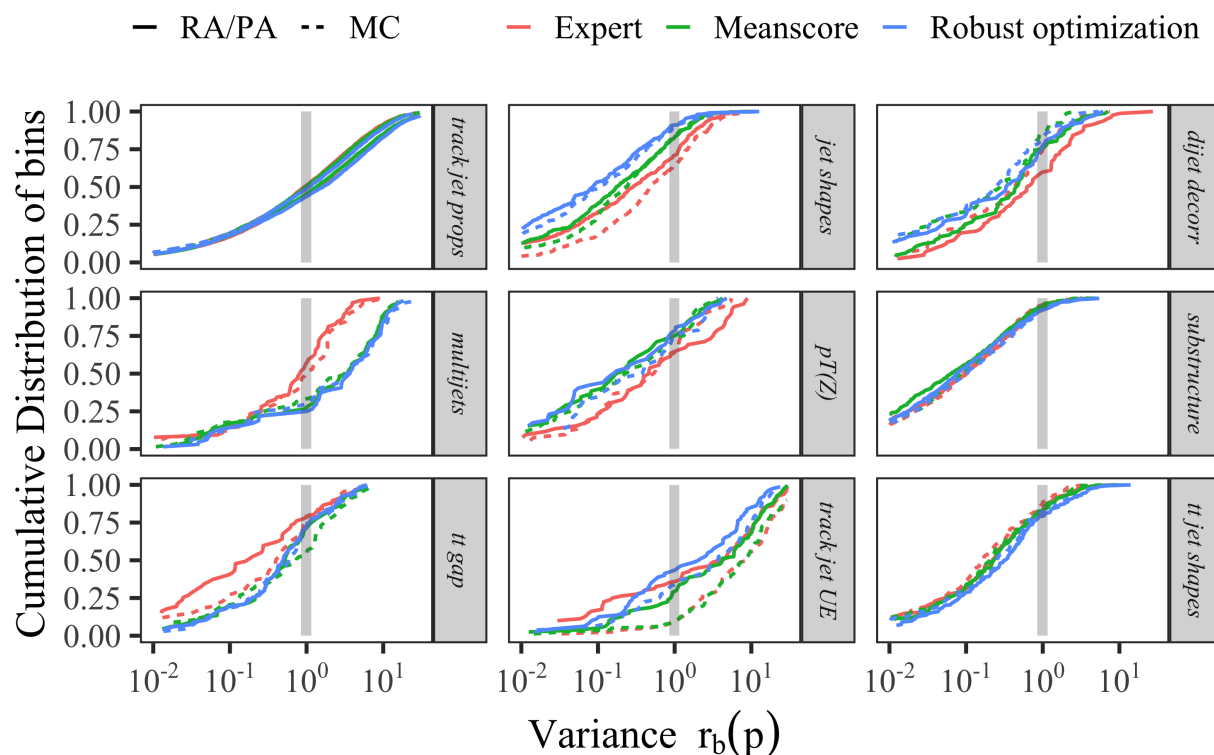
Figure 5: Cumulative distribution of bins (y-axis) in each category of the A14 dataset at different bands of variance levels (x-axis) computed with cubic polynomial approximation (PA) or rational approximation (RA) and the MC simulation.

4.7 Results for the SHERPA dataset

In this section, we present the detailed results for the SHERPA dataset.

4.7.1 Comparison metric outcomes for the SHERPA dataset

Table 9 shows the results when using the rational approximation (results for the cubic polynomial approximation are in the online supplement Section 8.12.6). Smaller numbers indicate better performance. The smallest number of each metric is bold for better visualization. Similar to A14, we find that the robust optimization approach achieves the best performance in terms of the Weighted χ^2 criterion. Assigning equal weights to all observables yields the best results in terms of A- and D-optimality for the full and the bin-filtered dataset. The portfolio approach yields the best A- and D-optimality values when using the observable-filtered dataset.

Compared with the results of A14, we see that the magnitudes of all metrics are much larger. The large A- and D-optimality values reflect that we have larger regions of uncertainty associated with the optimal parameters, and thus we have less confidence in the validity of the results obtained for the SHERPA dataset than for the A14 dataset.

Table 9: Results for the comparison metrics for the full, observable-filtered, and bin-filtered SHERPA dataset using the rational approximation. The best results are in bold. In each dataset, W-χ^2 refers to the Weighted χ^2 metric, A-o refers to the A-opt metric, and l-D-o refers to the log D-opt metric.

Data	Full dataset			Observable-filtered dataset			Bin-filtered dataset		
Method	W-χ^2	A-o	l-D-o	W-χ^2	A-o	l-D-o	W-χ^2	A-o	l-D-o
Meanscore	0.2201	9.0147	-39.3957	0.3621	11.1570	-36.5249	0.1490	17.9602	-33.5825
Medscore	0.2249	43.2031	-25.7164	0.2315	13.0679	-35.3498	0.2136	21.9361	-31.4329
Portfolio	0.1510	11.9869	-35.7488	0.4728	**8.5578**	**-38.6042**	0.1239	16.8518	-35.2237
Equal-weights	0.2794	**6.8428**	**-42.0325**	0.3930	59.9885	-18.8193	0.1753	**11.5372**	**-36.0252**
Robust opt	**0.0603**	55.8079	-22.0884	**0.0509**	32.9470	-30.5536	**0.0919**	17.9858	-33.6522

4.7.2 Comparison of the cumulative distribution of bins at different variance levels

Similar to the analysis conducted in Section 4.6.2, we compare the cumulative distribution of bins at different bands of variance level computed using the optimal parameters $\mathbf{p}$ obtained from the tuning approaches (see Figure 6). The results show that fewer bins lie within the variance boundary

673 of one when using the parameters of the bilevel-portfolio approach. On the other hand, the bilevel-
674 medianscore approach finds parameters that yield the most bins at lower bands of variance levels.
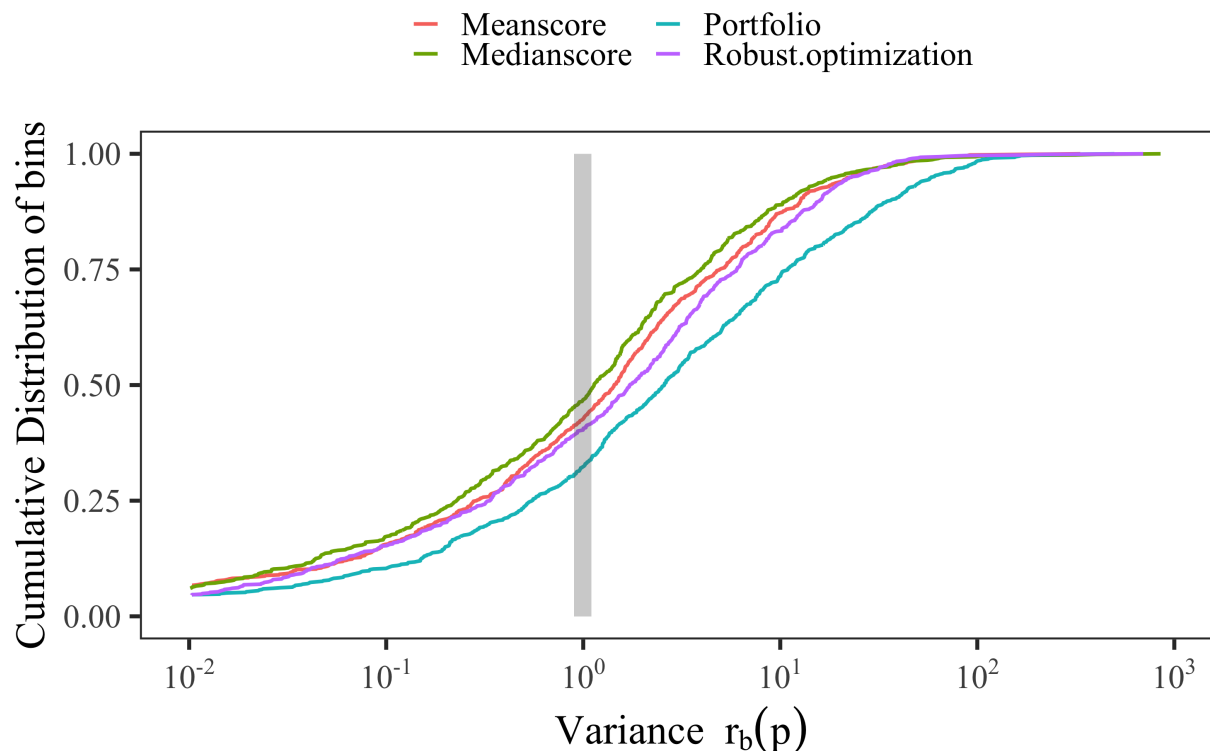
Figure 6: Cumulative distribution function (CDF) of all bins (y-axis) in the SHERPA dataset at different bands of variance levels (x-axis) given by $r_b(\mathbf{p}) = \frac{(f_b(\mathbf{p}) - \mathcal{R}_b)^2}{\Delta f_b(\mathbf{p})^2 + \Delta \mathcal{R}_b^2}$. This function is a normal CDF with mean 1 and a different standard deviation for each method.

4.7.3 Optimal parameter values for the SHERPA dataset with rational approximation

676 The optimal parameter values for the SHERPA dataset when no filtering, observable-filtering, and
677 bin-filtering were applied, respectively, are shown in Table 10. For a visualization of the different
678 solutions obtained with our methods, we illustrate the [0,1]-scaled optimal parameters in the online
679 supplement Section 8.12.4. We see that many of the parameters lie on the boundary of the parameter
680 space (shown in the table in bold), indicating that we might need to change the size of the parameter
681 domain to avoid model extrapolation.

682   Note that for the SHERPA dataset, we do not have an "expert" solution for benchmark compar-
683   ison. Instead, we compare the solutions to the chosen reasonable default setting. The parameter
684   range is constructed by multiplying the default value by 0.5 and 1.5 to obtain the lower and the
685   upper bound, respectively, i.e., the default values lie in the middle of the parameter range. We see
686   that there are differences between the optimal parameters obtained with the different methods, in
687   particular, bilevel-medianscore gives a very similar solution to the default setting when no filtering
688   is applied.

689   The distribution of weights from the different methods has a similar pattern as for the tunes
690   based on the A14 dataset. These patterns are displayed in Fig. 19 in the online supplement. Robust
691   optimization selects only one of the event shape observables as relevant, while applying the same
692   equal weight to most of the particle multiplicity (one bin) distributions. The other methods have
693   weights that are more widely distributed among the observables with a small number of weights far
694   from the average.

4.8   Closure test

696   In order to show that our proposed optimization methods are able to find the "correct" solutions,
697   we construct a simple toy model with linear approximations that has two parameters and four
698   observables. Each observable has five bins. The approximation $f_b(\mathbf{p})$ for each bin b is a linear
699   function of the form $\mathbf{a}^T\mathbf{p} + c$. The coefficients of the linear function are given in Section 8.14. The
700   deviation $\Delta f_b(\mathbf{p})$ is 0 for all bins. The experimental data is made up of standard deviation $\Delta \mathcal{R}_b$ and
701   mean values $\mathcal{R}_b$ for each bin b. The standard deviation is a constant of 0.005 for all bins. The mean
702   values of the bins are obtained by evaluating the linear function at known parameter values. For
703   the bins in the first three observables, the parameter value of $\overline{\mathbf{p}} = (-0.7778, 0.2729)$ is used whereas
704   for the bins in the fourth observable, the parameter value of $\widehat{\mathbf{p}} = (-0.0448, -0.3878)$ is used. We
705   expect that the combined weight of the first three observables is larger than the weight of the fourth
706   observable (with optimal tune $\overline{\mathbf{p}}$) since the number of bins that fit well to the experimental data
707   is greater from the first three observables than from the fourth observable alone, thus resulting in
708   lower objective value in the optimization algorithms.

709   For the bilevel optimization methods, we perform the outlier detection technique to see if the
710   fourth observable will be removed. For the robust optimization method, we expect that the optimal
711   weights should be [1,1,1,0], or equivalently, [0.3333, 0.3333, 0.3333, 0] after normalization.

712   Table 11 shows that all proposed methods can recognize that the fourth observable should not
713   be involved in the optimization, and all methods can find the optimal parameter tune $\overline{\mathbf{p}}$. The
714   table also summarizes the comparison metric results obtained with all proposed methods, and the

Table 10: Optimal parameter values obtained with all methods using rational approximation when no filtering (88 observables used), observable-filtering (3 observables were filtered out), and bin-filtering (7 bins were filtered out) was applied. The parameter values on the boundaries of the parameter space are indicated in bold.

	ID	Parameter name	Default	Meanscore	Medianscore	Portfolio	Robust opt	Equal-weights
All observables	1	KT_0	1.00	0.888	0.789	0.919	0.909	0.872
	2	ALPHA_G	1.25	**0.626**	1.500	**0.626**	1.874	**0.626**
	3	ALPHA_L	2.50	**3.749**	1.890	**3.749**	1.252	**3.749**
	4	BETA_L	0.10	**0.150**	**0.050**	0.087	0.150	**0.150**
	5	GAMMA_L	0.50	0.274	0.339	**0.750**	0.683	0.293
	6	ALPHA_H	2.50	3.400	2.897	**1.251**	2.841	3.440
	7	BETA_H	0.75	0.827	0.536	0.783	0.540	0.795
	8	GAMMA_H	0.10	0.148	**0.050**	0.082	0.150	**0.150**
	9	STRANGE_FRACTION	0.50	0.517	0.498	0.583	0.508	0.546
	10	BARYON_FRACTION	0.18	0.100	0.175	0.106	0.136	**0.090**
	11	P_QS_by_P_QQ_norm	0.48	**0.720**	0.419	0.572	0.613	**0.720**
	12	P_SS_by_P_QQ_norm	0.02	**0.010**	0.015	**0.030**	0.030	**0.010**
	13	P_QQ1_by_P_QQ0	1.00	**1.499**	1.206	0.948	1.190	**1.499**
		Euclidean distance from the default solution		1.513	0.984	1.244	1.289	1.531
Observable-filtered	1	KT_0	1.00	0.867	0.744	0.952	0.876	0.886
	2	ALPHA_G	1.25	0.775	**0.626**	**0.626**	0.626	0.957
	3	ALPHA_L	2.50	**3.749**	1.252	**3.749**	1.252	2.424
	4	BETA_L	0.10	0.109	**0.050**	**0.050**	0.150	0.113
	5	GAMMA_L	0.50	**0.250**	0.437	0.413	0.750	0.460
	6	ALPHA_H	2.50	3.053	2.318	**1.251**	2.826	3.132
	7	BETA_H	0.75	0.827	0.625	0.750	0.375	0.969
	8	GAMMA_H	0.10	**0.050**	0.134	0.094	0.050	0.131
	9	STRANGE_FRACTION	0.50	0.479	0.580	0.651	0.506	0.511
	10	BARYON_FRACTION	0.18	**0.270**	0.137	**0.090**	0.137	0.180
	11	P_QS_by_P_QQ_norm	0.48	**0.720**	0.469	0.495	0.470	0.601
	12	P_SS_by_P_QQ_norm	0.02	**0.010**	**0.030**	**0.030**	**0.030**	0.019
	13	P_QQ1_by_P_QQ0	1.00	**0.500**	**1.499**	**1.499**	1.499	0.958
		Euclidean distance from the default solution		1.408	1.249	1.372	1.446	0.637
Bin-filtered	1	KT_0	1.00	0.895	0.821	0.948	0.820	0.899
	2	ALPHA_G	1.25	0.893	1.483	**0.626**	1.874	**0.626**
	3	ALPHA_L	2.50	**3.749**	2.334	2.567	3.749	**3.749**
	4	BETA_L	0.10	0.050	**0.150**	0.074	0.050	0.067
	5	GAMMA_L	0.50	0.390	**0.250**	**0.750**	0.250	0.454
	6	ALPHA_H	2.50	**1.251**	3.670	**1.251**	1.969	**1.251**
	7	BETA_H	0.75	0.715	0.534	0.739	1.125	0.715
	8	GAMMA_H	0.10	0.119	0.142	0.105	0.050	0.089
	9	STRANGE_FRACTION	0.50	0.556	0.542	0.570	0.531	0.559
	10	BARYON_FRACTION	0.18	0.122	0.120	0.124	0.138	0.124
	11	P_QS_by_P_QQ_norm	0.48	0.595	**0.720**	0.492	0.497	0.577
	12	P_SS_by_P_QQ_norm	0.02	**0.030**	0.030	**0.030**	0.030	**0.030**
	13	P_QQ1_by_P_QQ0	1.00	**1.499**	**1.499**	**1.499**	1.499	**1.499**
		Euclidean distance from the default solution		1.266	1.377	1.201	1.462	1.242

715 results show that the meanscore method performs the best under the Weighted χ^2 metric, and the
716 medianscore method performs the best under the A- and D-optimality criteria.

Table 11: Results for the closure test. Shown are the optimal weights obtained with each method, the optimal parameters, and the outcomes for our performance metrics.

	Bilevel-meanscore	Bilevel-medscore	Bilevel-portfolio	Robust optimization
Weights				
Observable 1	0.8060	0.5485	0.2550	0.3333
Observable 2	0.0070	0.3100	0.3663	0.3333
Observable 3	0.1870	0.1415	0.3787	0.3333
Observable 4	0	0	0	0
Parameters				
p_0	-0.7778	-0.7780	-0.7775	-0.7781
p_1	0.2726	0.2729	0.2728	0.2731
Performance metrics (lower numbers are better, best results are in bold)				
Weighted χ^2	**0.5866**	0.7631	0.9867	1.0023
A-optimality	3.21E-06	**2.25E-06**	2.74E-06	2.58E-06
log-D-optimality	-29.6887	**-30.0576**	-29.8999	-29.9521

4.9 A note on computation times

718 The bilevel optimization approaches are run on a 4-core, 32 GB RAM machine running at [Reviewer
719 comment l:] 2.60 GHz. For the results of robust optimization, 100 values for μ are used, each run
720 on a single thread on a server with 64 Intel Xeon Gold CPU cores running at 2.30 GHz. There are
721 two threads per core, but each run of robust optimization is done on a single thread. Additionally,
722 this server is equipped with 1.5TB DDR4 2666 MHz of memory. A simple comparison to find the
723 best μ takes one minute. ~~The all-weights-equal approach is run on a 4-core, 32 GB RAM machine~~
724 ~~running at 1.1 GHz.~~ Note that in our numerical experiments we were not primarily concerned with
725 architecture-dependent run times, but rather to ensure that our codes for automated optimization
726 can be executed on different architectures. [Reviewer comment l:] Although not identical, the
727 technical specifications of the computers we used in the numerical experiments are similar enough to
728 provide us with a rough guide on the computational demand of the different optimization methods.
729 The time taken by all the tuning approaches for unfiltered (*All data*) as well as for bin-filtered and
730 observable-filtered A14 data is given in Table 12. In the unfiltered data case, the bilevel optimization

approaches take approximately 14.5 hours and each run (i.e., one μ) of robust optimization takes an average of about 0.8 hours. Since all 100 values of μ were run in parallel, the total time to complete all 100 runs of robust optimization is approximately two hours. In comparison, campaigns to tune weights by hand takes many weeks or months. Given our results, we can see that the automated weight adjustment by optimization is significantly faster than hand-tuning. The all-weights-equal approach took less than 10 minutes, but it leads to inferior results.

The observable filtering method requires a single-tune to obtain the χ^2 values per observable which takes 1647 seconds (0.45 hours) for all observables in the A14 dataset, which is followed by applying the Z-score method to filter out outliers (see Section 3.1) and this takes about 10 seconds. Once the single-tune to obtain the χ^2 values per observable is performed, the bin filtering takes an additional 300 seconds for the A14 dataset. Thus, the total pre-processing time required for observable filtering is 1657 seconds (0.46 hours) and for bin-filtering is 1947 seconds (0.54 hours).

From Table 12, we observe that the time taken to tune parameters in the observable-filtered and bin-filtered data case is significantly smaller than for the unfiltered data case. For the bilevel optimization approaches, the time required per iteration for the observable- and bin-filtered cases is 6% and 55% less, respectively, and for each run of robust optimization, it is 9% and 36% less, respectively. Also, the overhead of performing observable and bin filtering is small compared to the time it takes to tune parameters. Since the results from Section 4.6.5 show that the bins filtered by bin and observable filtering do not add significant information to the tune, we can claim that using filtered data provides a significant improvement in compute-time performance for tuning parameters.

Table 12: CPU time (in seconds) and time per iteration (in seconds) taken by all approaches when using all, the observable-filtered, and the bin-filtered A14 data. The robust optimization approach converges after 69, 105, and 83 iterations, respectively. The bilevel-medianscore, -meanscore, and -portfolio approaches are all run for 1000 iterations.

Method	All data		Bin filtered		Observable filtered	
	CPU time	Time per iteration	CPU time	Time per iteration	CPU time	Time per iteration
Robust optimization	3035	44	2989	28	3327	40
Bilevel-medianscore	52326	52	23600	24	49057	49
Bilevel-meanscore	52169	52	23600	24	49018	49
Bilevel-portfolio	52366	52	23609	24	49084	49

5   Eigentunes

We use the eigentune approach to calculate confidence intervals for the optimal parameters. We note that the A- and D-optimality criteria provide the size of confidence ellipsoid around the optimal parameters. Here, we expand this information by scanning generator parameters along the principal axes of this ellipsoid. Details of this method are described in [5] and a similar approach is used in estimating the uncertainties of predictions from the parton distribution functions [57]. The interval defines a boundary beyond which the value of the objective function is larger than the objective function value at the minimum by a criterion. The criterion is normally chosen to be the number of degrees of freedom n, which is defined as the total number of bins of all observables minus the number of generator parameters, d, i.e., $n = \sum_{\mathcal{O} \in \mathcal{S}_{\mathcal{O}}} |\mathcal{O}| - d$. However, to properly take into account the weights assigned to observables, we use the scaled effective sample size as the criteria, which is calculated as follows:

$$n = \gamma \times \left(\frac{(\sum_i w_i)^2}{\sum_i w_i^2} - d \right)$$

The weights are normalized so that the sum of weights associated with all observables equals one. γ is iteratively tuned and chosen to be 0.01. The interval would represent the uncertainties of the parameters should the objective function follow a χ^2 distribution. Smaller intervals associated with the tuned parameters indicate that the parameters are better constrained by the experimental data.

Given the non-linearity of the objective function and parameter correlations, a reliable approach to find the 68% confidence interval is to evaluate the objective function for all possible parameter values. However, this poses a computational challenge. Instead, we project the multidimensional parameter space into two directions defined by the eigenvectors $u_{1,2}$ associated with the largest and smallest eigenvalues of the covariance matrix of the parameters, which are calculated using the inverse of Eq. (16). Then we find an offset α such that the sum of all χ^2 satisfies

$$\chi^2(\mathbf{p}'_{1,2}) = \chi^2(\mathbf{p}^*) + n \tag{17}$$

where $\mathbf{p}'_{1,2} = \mathbf{p}^* \pm u_{1,2} \times \alpha$. For each eigenvector, we obtain two vectors $\mathbf{p}'$ from Eq. (17). Finally, the procedure results in a matrix of sizes of 4 times d. Each column represents a generator parameter; the minimum and maximum in each column are used to define the eigentune as shown in Tables 13 and 14 for the A14 and the SHERPA dataset, respectively, using the rational approximation. The same surrogate model is used for all methods. It is possible that the determined intervals go beyond the predefined parameter range. In this case, the MC predictions are extrapolated by the surrogate model. When the lower part of the interval goes negative, we force the value to be zero.

⁷⁸¹ For the A14 data, different optimization methods result in similar intervals for all parame-
⁷⁸² ters.[5] The beam remnants (e.g. `BeamRemnants:reconnectRange`) and space-like showering pa-
⁷⁸³ rameters (e.g. `SpaceShower:pT0Ref`) are better constrained; their intervals are within 1% of
⁷⁸⁴ their optimized parameters. However, the strong coupling parameter in hard scattering processes
⁷⁸⁵ (`SigmaProcess:alphaSvalue`) and time-like showering (`TimeShower:alphaSvalue`) are less con-
⁷⁸⁶ strained.

⁷⁸⁷ For the SHERPA data, different optimization methods produce quite different intervals. Overall,
⁷⁸⁸ the bilevel-meanscore method results in relatively small intervals for all parameters. The heavy
⁷⁸⁹ quark fragmentation parameters (e.g. `ALPHA_H`) are well-constrained thanks to the B-hadron frag-
⁷⁹⁰ mentation measurements, but the light quark fragmentation parameters are not.

Table 13: Eigentune results for the A14 data using the rational approximation for different opti-
mization methods.

Parameters	Expert		Bilevel-meanscore		Bilevel-mediansocre		Bilevel-portfolio		Robust optimization	
	min	max	min	max	min	max	min	max	min	max
`SigmaProcess:alphaSvalue`	0.075	0.193	0.079	0.192	0.079	0.190	0.074	0.195	0.085	0.183
`BeamRemnants:primordialKThard`	1.903	1.906	1.805	1.910	1.674	1.769	1.744	1.850	1.876	1.892
`SpaceShower:pT0Ref`	1.636	1.653	1.516	1.547	1.142	1.228	1.298	1.344	1.586	1.591
`SpaceShower:pTmaxFudge`	0.905	0.912	1.012	1.016	1.069	1.096	1.037	1.046	1.025	1.026
`SpaceShower:pTdampFudge`	1.044	1.048	1.064	1.076	1.082	1.086	1.058	1.064	1.078	1.091
`SpaceShower:alphaSvalue`	0.121	0.124	0.125	0.131	0.127	0.130	0.124	0.133	0.123	0.129
`TimeShower:alphaSvalue`	0.043	0.197	0.044	0.192	0.039	0.213	0.030	0.213	0.051	0.198
`MultipartonInteractions:pT0Ref`	1.665	2.543	1.649	2.562	1.780	1.979	1.160	2.829	1.461	2.528
`MultipartonInteractions:alphaSvalue`	0.068	0.177	0.072	0.161	0.115	0.121	0.062	0.186	0.094	0.151
`BeamRemnants:reconnectRange`	1.788	1.795	2.065	2.105	1.912	1.915	1.972	2.000	2.589	2.618

⁷⁹¹ The eigentune results serve as a good platform for comparing our automated optimization algo-
⁷⁹² rithms, but it requires manual adjustment of the criteria n and the exploitation of all eigenvectors
⁷⁹³ to produce a realistic uncertainty band. We tried to generate new events with the eigentunes based
⁷⁹⁴ on the robust optimization outcomes as shown in Table 13 using the PYTHIA8 generator configured
⁷⁹⁵ closely to the one used in the A14 tune. The uncertainty band was too large to be practically used.
⁷⁹⁶ To find a reasonable uncertainty band, we performed the eigentune for all ten eigenvectors sepa-
⁷⁹⁷ rately and concluded the strong coupling constant affects most observables. Therefore, we manually
⁷⁹⁸ adjust the strong coupling values and with an uncertainty of 5% on the strong coupling constant
⁷⁹⁹ we produced a reasonable uncertainty band. Figure 7 shows two exemplary distributions with the
⁸⁰⁰ uncertainty band (blue and red lines) included.

---

[5]See Table 15 for a description of the physics parameters.

Table 14: Eigentune results for the SHERPA data using the rational approximation for different optimization methods. Parameters with negative values are set to zero.

Parameters	Bilevel-meanscore		Bilevel-mediansocre		Bilevel-portfolio		Robust optimization	
	min	max	min	max	min	max	min	max
KT_0	0.815	0.970	0.688	0.957	0.524	1.254	0.491	1.273
ALPHA_G	0.438	0.792	1.325	1.604	0.571	0.691	1.597	2.115
ALPHA_L	3.683	3.824	1.309	2.863	3.525	3.939	0.291	2.088
BETA_L	0	0.460	0.043	0.062	0	0.440	0	0.387
GAMMA_L	0.175	0.362	0.330	0.352	0.688	0.823	0.220	1.087
ALPHA_H	3.245	3.537	2.843	2.988	1.200	1.311	2.289	3.475
BETA_H	0.747	0.898	0.484	0.585	0.623	0.972	0.350	0.759
GAMMA_H	0.059	0.249	0	0.080	0.013	0.133	0	0.469
STRANGE_FRACTION	0.496	0.556	0.395	0.595	0.415	0.706	0.440	0.567
BARYON_FRACTION	0	0.459	0.129	0.218	0.018	0.170	0	0.342
P_QS_by_P_QQ_norm	0.552	0.809	0.319	0.524	0.552	0.588	0.594	0.629
P_SS_by_P_QQ_norm	0.	0.031	0.	0.103	0	0.081	0	0.068
P_QQ1_by_P_QQ0	1.492	1.512	1.202	1.210	0.945	0.952	1.167	1.210
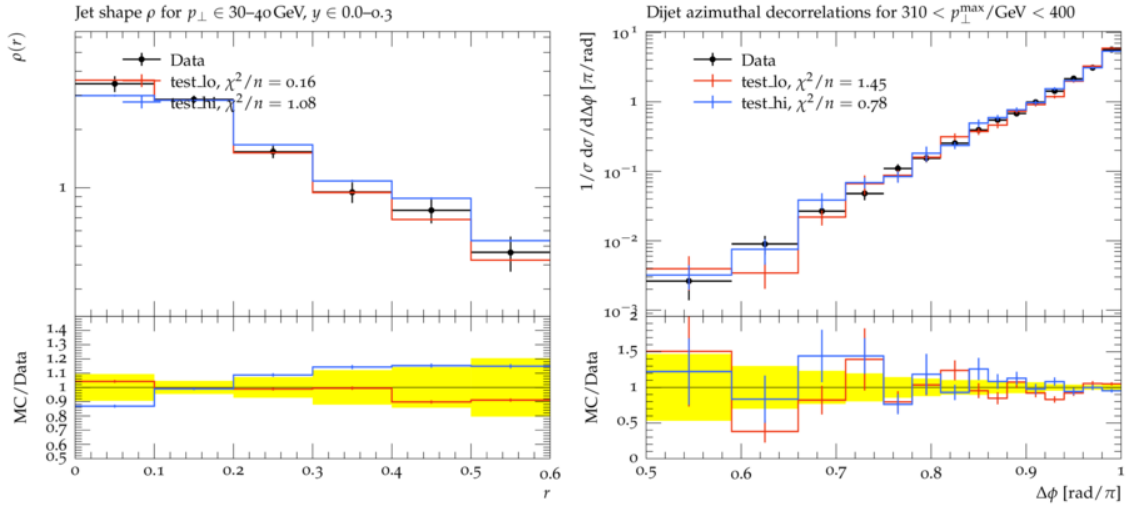
Figure 7: Two exemplary distributions with uncertainty band included. The upper band is in blue and lower band in red. The bottom panel shows the ratio of MC predictions over the data where the yellow band shows the uncertainties associated with the data. Left: jet shape ρ as a function of the distance to the jet axis r; Right: the differential cross section of dijet events as a function of the azimuth angle differences between the two jets $\Delta\phi$.

6 Discussion

The results presented in the previous sections demonstrate that automated tuning methods can produce better fits of the generator predictions to data. Several figures of merit for comparing different tunes were considered. The automation of the process means that tuning can be performed in less time and with less subjective bias. In this section, we discuss the physics impact of various tuning results.

6.1 Implications of our results on physics

Physics event generators are imperfect tools. They contain a mixture of solid physics predictions, approximations, and *ad hoc* models. The approximations and models are expected to be incomplete, and thus are unlikely to describe the full range of observables accessible by the experiment. Despite this fact, for a certain choice of parameters, a model may be able to describe parts of the data. This agreement would be accidental and would likely compromise predictions of this model for different parts of the data. The weighting of data by an expert is a primitive attempt to force the model to agree with data in a region of interest to the physicist – which, most of the time, corresponds to a region where a model should be applied. It is equivalent to adding a large systematic uncertainty to the data that is de-emphasized by the weighting.

Here, we address whether the automated methods accomplish this weighting of data without explicit input from the physicist. First, we should state our expectations for a tune to the A14 dataset. The features of the expert tune were previously discussed in [3, Section. 2.2.1]. The A14 data is all of interest to the physicist, but some of those observables are expected *a priori* to be described better by the event generator than others. The parton shower and hadronization model are expected to describe well *Tracked jet properties* and *Jet shapes*. The description of jets is essential for all hadron collider analyses and is the *raison d'être* for event generators. $t\bar{t}$ *jet shapes* emphasize the final state parton shower, and is critical to be described well when making precision predictions that are sensitive to the top quark mass. *Dijet decorr* and p_T^Z observables provide constraints on initial state parton shower and intrinsic transverse momentum parameters free from most other parameters, and are generically important to be described well. Additional properties, such as the number of jets produced in di-jet or Z events or the production of jets at extreme angles, are beyond the scope of the PYTHIA predictions. *Track-jet UE* and *Jet UE* observables are sensitive to PYTHIA's multi-parton-interaction model, which describes most of the particles produced in a high-energy collision. The addition of *Multijets* observables is biasing the parton shower to describe a next-to-leading order observable, while the leading-logarithm parton shower includes only an approximation

833 to the full result. Experience shows that this biasing provides a globally better description of many
834 observables of interest to the physicist with little effort and without significantly impacting other
835 predictions. This feature was built into the *Expert* tune by applying a large weight to this dataset.
836 Finally, adding the $t\bar{t}$ *gap* category is asking for the description of an exclusive observable, which
837 has very strong requirements in its construction, whereas the PYTHIA prediction here is valid for
838 more inclusive observables. Including this data in the tune is a very specific physics requirement
839 that may be beyond the scope of the PYTHIA approximations.

6.2   Observables with improved descriptions

841 Examples of observable predictions with a lower $\chi_{\mathcal{O}}^2$ value than the *expert* tune are displayed in
842 Figures 8a-8c. These reflect an improvement in a class of observables and are indicative of all the
843 comparisons between predictions and data.

844   All of our methods produce a better description of the data than the expert tune for the category
845 *Jet shapes*, though the expert prediction is mainly differing in only the first bin. This observable
846 is expected to be described well, in general, since it lies in a physics regime compatible with the
847 PYTHIA approximations.

848   The predictions for the p_T^Z and *Dijet decorr* categories are also improved. We note that the
849 weights found for these analyses are not substantially different than for the expert tune, but that
850 other categories have their weights reduced (see Table 7 for reference). This implies some tension
851 between these observables and the *Multijets* category (to be discussed below).

852   The comparisons between predictions and data shown in our figures are based on runs of the
853 MC event generator for the parameter values derived using the surrogate model. Before continuing,
854 we should comment on the differences in Figure 5 (and in Figure 16 in Section 8.9 of the online
855 supplement) between the surrogate model (RA) and explicit runs of the event generator (MC)
856 at the output tuned parameters. The surrogate model would be unreliable if the output tune
857 parameters were outside or near the boundary of the parameter range used to derive the inputs for
858 the surrogate. A comparison of the parameter values relative to the expert tune and Figure 17 shows
859 the distribution of parameter values normalized to the sampling range: $r_{\text{param}} = \frac{\mathbf{P}-\mathbf{P}_{\min}}{\mathbf{P}_{\max}-\mathbf{P}_{\min}}$. All
860 of the central values for the parameters are well within the sampling range. Only the parameters
861 `SpaceShower:pTdampFudge` and `BeamRemnants:reconnectRange` come near the boundaries. For
862 the former, the minimum sampling value was 1.0, and the tuning results only indicate that this
863 parameter should be near 1.0. For the latter, the maximum sampling value was chosen quite large
864 so that all results appear to be close to the minimum value.

865   Furthermore, the most noticeable differences between the RA surrogate predictions and MC

(a) *Jet shapes [39]*

(b) p_T^Z *[42]*

(c) *Dijet decorr [40]*
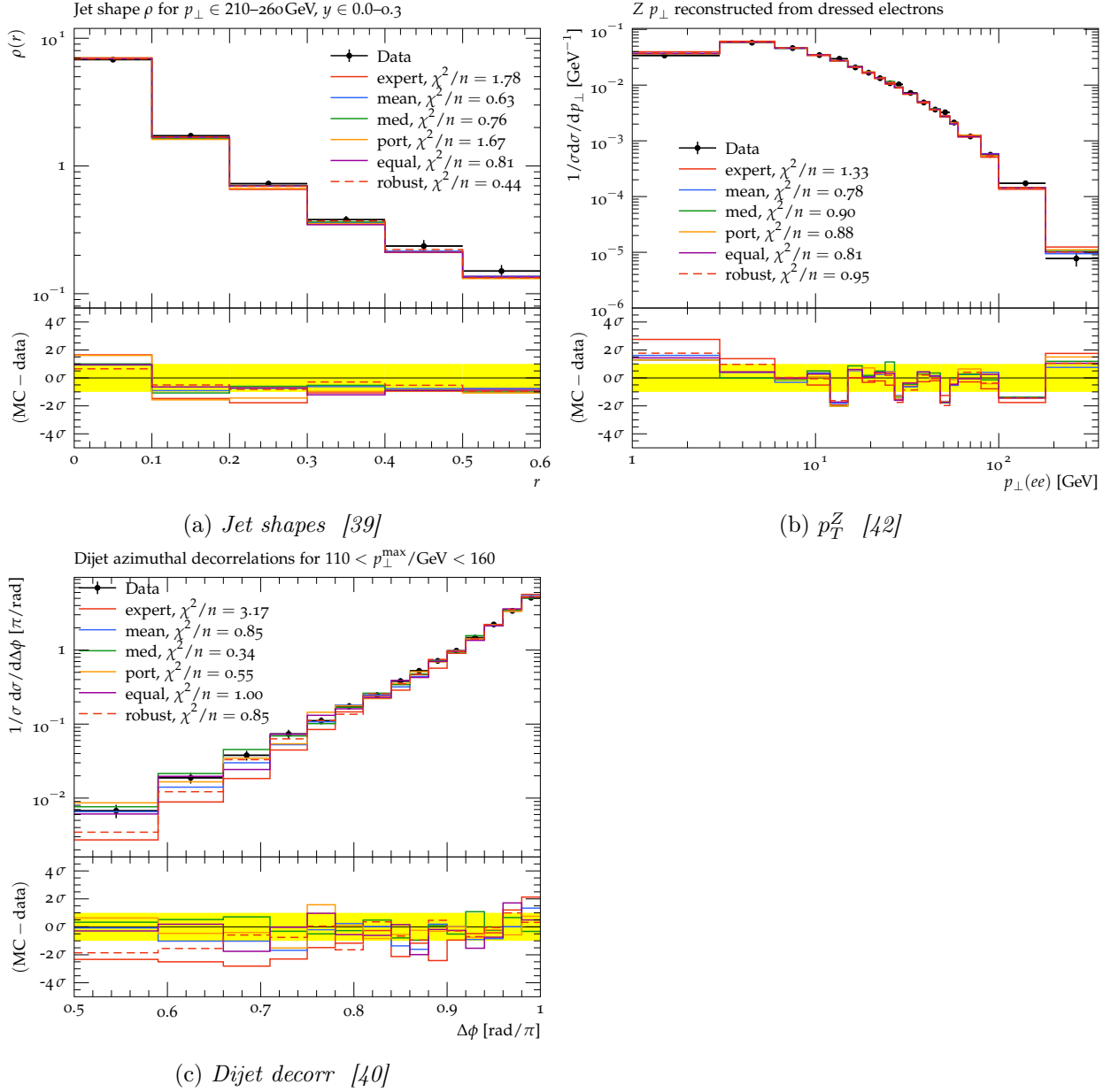
Figure 8: Examples of A14 observables and their $\chi_{\mathcal{O}}^2$ values for which the automated tuning leads to better fits than the expert's hand tuning.

866 occur for rather small values of the variance between the data and predictions. These values have
867 a negligible impact on the full χ^2, and are within the expected range of validity of the surrogate
868 model.

6.3   Observables with worse descriptions

870 The predictions for *Track jet properties* and *Substructure* are not significantly improved, but also
871 not degraded. Most of the observables in these categories were designed to tune and test the
872 multi-parton interaction model, and thus it is no surprise that they are described well.

873   Two categories stand out as being better described by the expert tune. These are the *Mul-*
874 *tijets* and $t\bar{t}$ *gap* categories that were given a particularly large weight in the expert tune. Some
875 examples can be seen in Figure 9a-9c. It is no surprise that these categories are not described as
876 well as the expert tune. It is surprising that the parameters sensitive to this observable, namely
877 `TimeShower:alphaSvalue` and `SpaceShower:alphaSvalue` are actually somewhat larger than the
878 expert tune values, see Table 6. Larger values for these parameters should mean forcing the predic-
879 tion to look *more* like a higher-order calculation. Clearly, other data, such as *Dijet decorr* and p_T^Z
880 prefer larger values for these parameters than the *Multijets* category alone.

881   Without the expert input, our automated methods do not emphasize these observables. The
882 PYTHIA predictions for *Multijets* and $t\bar{t}$ processes are based on calculations that could be made
883 more accurate (by performing matched or merged calculations based on external input – see [58]),
884 but only at the expense of breaking the universality of the tune. The expert weighting used the
885 flexibility of the PYTHIA model to imitate these more accurate calculations and force agreement with
886 the data. The A14 tune was meant to be applied to physics predictions from the internal PYTHIA
887 model for which the corrections were not readily available or easily applicable. However, if the goal
888 is to provide a tune that can be used even in association with process-dependent corrections, then
889 those provided in this study are more appropriate.

6.4   Results for SHERPA tuning

891 Some of the results of the SHERPA tuning are shown in Figure 10. In general, all of the parameter
892 selection methods applied here yield an improved global $\chi^2_{\mathcal{O}}$ over the default values. The param-
893 eters varied in this tuning exercise are all related to the formation of physical particles. This is
894 a phenomenon that occurs at a low-energy scale and cannot be described realistically (currently,
895 at least) from theory. The model employed in SHERPA is a cluster model that fissions colorless
896 blobs of energy into particles using a parameterized probability distribution. Despite the fact that
897 hadronization occurs at a low-energy scale, it has an impact on observables that are used to test

(a) *Multijets [41]*

(b) $t\bar{t}$ *gap [45]*

(c) *Track jet UE [38]*
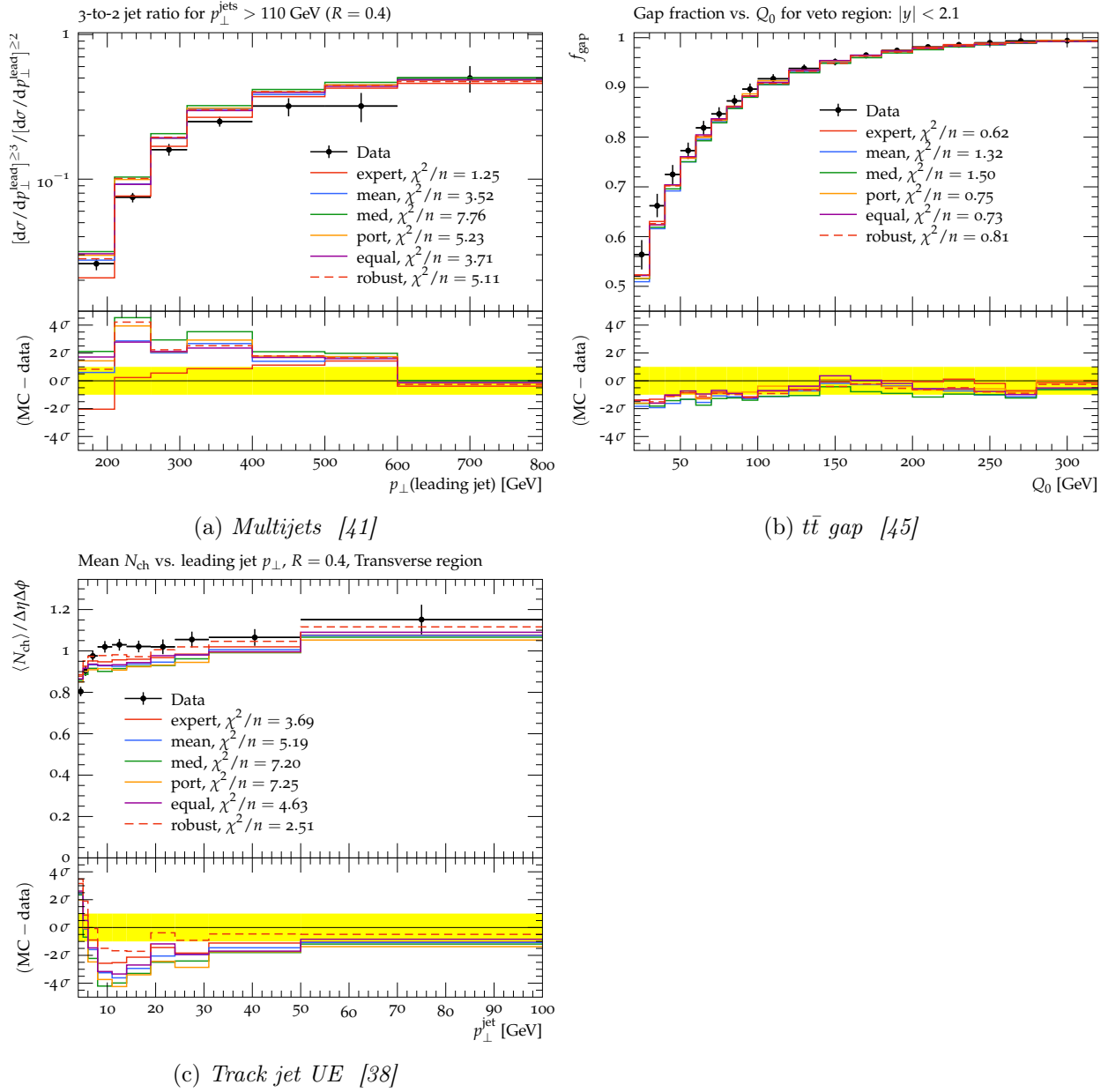
Figure 9: Examples of A14 observables and their $\chi^2_{\mathcal{O}}$ values for which the automated tuning approach performs worse than the expert's hand tuning.
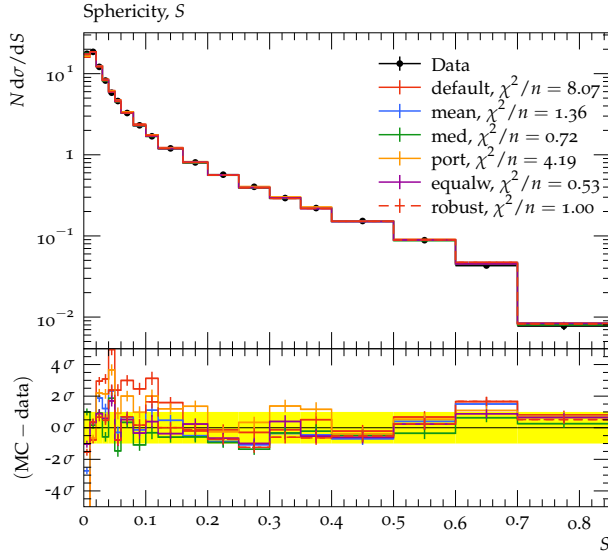
(a) *Jet shapes [53]*
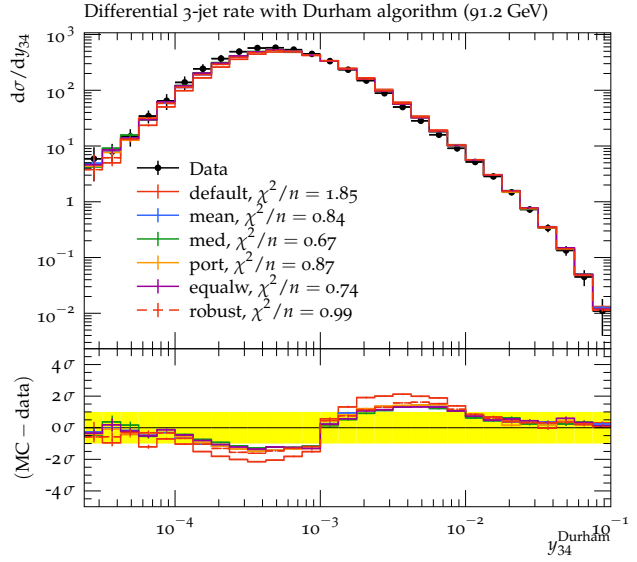
(b) *Jet rates [52]*
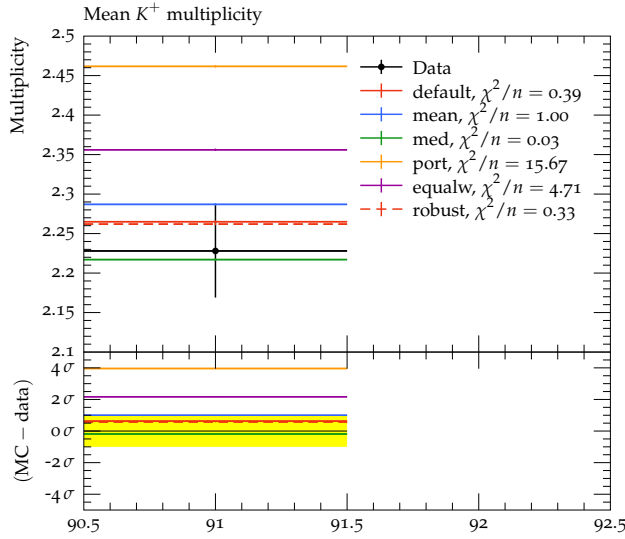
(c) *Particle count [55]*
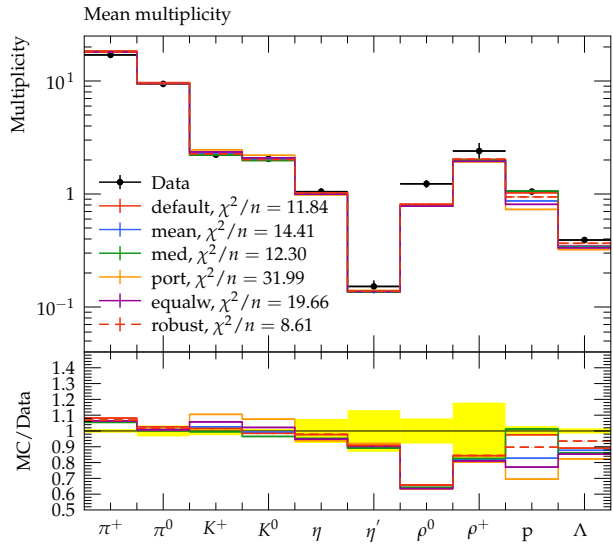
(d) *Several particle counts side-by-side [55]*

Figure 10: Examples of histogram plots of the $\chi^2_{\mathcal{O}}$ values for the SHERPA tune.

perturbative predictions at relatively high-energy scales. For these observables, it is impossible to entirely disentangle the perturbative prediction from the non-perturbative hadronization model prediction. Figures 10a-10b show comparisons of our tunes to the default, demonstrating a significant improvement in most cases. Figure 10c shows mixed results for the production of one particular species of particle. Figure 10d is an example of an inclusive observable that counts the number of particles produced without any direct reference to their energy or position in the detector.

All of these results are for a certain precision of perturbation theory. There are both technical and mathematical reasons to truncate perturbation theory in a certain order. These calculations were based on the lowest order perturbation theory with an improved parton shower approximation to simulate additional perturbative effects. The lowest order prediction produces 2 jets using exact perturbation theory and any additional jets using the parton shower approximation. Figure 10b is an observable that counts the number of 3-jet events as a function of the jet definition. While our results are improved over the default, this indicates higher-order perturbative calculations might improve the description even more (e.g., 3 jets calculated in exact perturbation theory and 4 or more jets from the parton shower approximation).

Table 10 shows the parameters values for the various tunes. The simplest comparison is between the default values and "All-weights-equal." The all-weights-equal method yields the tune that would result if only the data considered in this study were used. One result is that several of the parameters take on the extremum of the values considered here. Without any additional direction to choose the range for our parameter scan, we chose 1/2 of the default value to define our sampling window.

One surprising result is that the parameter `P_QQ1_by_P_QQ0`, which represents the ratio of spin-1 to spin-0 diquarks, is driven to a value > 1. While there is no obvious reason that the cluster model breaks down, spin-1 diquark production is usually expected to be suppressed. The fact that the parameter `BARYON_FRACTION` is driven to its minimal value compensates for this large value.

While the type of large scale parameter tuning we have in mind here can only be performed practically using surrogate models, the fact that some tuned parameters are pushed to the boundaries suggests another direction of algorithmic development. In particular, we would like our algorithm to have the capability to recognize a trust region and update the surrogate model with dedicated simulations when necessary.

7   Conclusions

In this paper, we propose several algorithms for automating the weighting of the importance of data used in the tuning process for Monte Carlo event generators. We performed two studies. The first used particle collider data and predictions are from the Large Hadron Collider (LHC) and had an *expert* selection of analysis weights as a benchmark. The second used data and predictions are from the Large Electron-Positron (LEP) Collider and had only the default parameter choices as a reference. The algorithms considered included a bilevel optimization based on several scoring procedures and a single-level robust optimization. We find that our automatic methods produce parameter tunes that are comparable to labor-intensive, by-hand tunes. For the LHC tuning, filtering of hard-to-describe observables can lead to tunes of superior quality by identifying observables or subsets of observables that cannot be described by the event generator. For the LEP tuning, many of the tuned parameters were driven to the extremum of our sampling range, suggesting that the current models are missing some important physics. We note here that the goal of the filtering approaches is to only eliminate data in regions where the model is highly unlikely to be explained by data, indicating regions in which the model is not valid. However, it is possible that outliers are identified in regions where the model is in fact valid. Based on our eigentune results, however, this case does not affect the parameter uncertainties. Hence, it is a justifiable approach. The filtering is based on the intuition that the models that are highly unlikely to be explained by data could be removed to (a) get a better estimate of the tune, and (b) prevent the algorithms from going into regions of extrapolation.

First, the results show that the parameter values we found agree with and have the potential to improve the physicists' hand-tuned results. Second, since we automate the weight adjustment for the tune-relevant observables, physicists do not need to hand-tune the weights for observables anymore; we propose several methods for adjusting the weights, so physicists are not involved in the subjective re-weighting anymore. Third, by filtering out and excluding observables and bins, we can save computational time during optimization and improve the parameter values. Fourth, we derived new metrics to easily compare different tunes, and it shows that our methods can perform better than the physicists' hand-tuning approach.

To get the baseline recommendation among the proposed methods, we suggest that the physicist first select a metric to be minimized. Then, from Tables 5 and 9, we see that if the goal is to minimize the weighted χ^2 metric, the robust optimization approach should be chosen. On the other hand, if the goal is to minimize the uncertainty of the estimate, we recommend performing the observable- or bin-filtering first and then using the bilevel-portfolio method.

For the SHERPA data, most of the optimal parameters are on the boundaries of the parameter space, indicating that we might need to change the size of the parameter domain to avoid model extrapolation. One possible solution to this problem is to build an outer loop for moving the center of the parameter search space and apply the trust region method. We leave this to future research.

In this work, we assumed that each bin is completely independent of all the other bins. To consider correlations, we need to solve $\widehat{\mathbf{p}}_{\mathbf{w}} \in \arg\min_{\mathbf{p} \in \Omega} ||\mathcal{F}(\mathbf{p}) - \mathcal{D}||^2_{\boldsymbol{\Gamma}^{-1/2}(\mathbf{p})\mathbf{W}\boldsymbol{\Gamma}^{-1/2}(\mathbf{p})}$, where $\mathcal{F}(\mathbf{p})$ is an aggregate vector of central values of the model prediction obtained using a polynomial or rational approximation, $\mathcal{D}$ is the aggregated vector of data, $\mathbf{W}$ is the weight vector, and $\boldsymbol{\Gamma}(\mathbf{p})$ is the covariance matrix. As we see, the inclusion of the covariance matrix only affects the inner optimization and the methods proposed here for automatic weight adjustment would be unchanged. However, including the covariance matrix has its challenges. Specifically, (a) the information of the correlations among the bins is currently unavailable, (b) since the covariance matrix depends on the parameter values, we would need to approximate it using a kernel function, and (c) solving this optimization problem is non-trivial since it would require the inversion and taking the square root of the covariance kernel for each objective function evaluation. Tackling these issues is outside the scope of this paper and hence, taking into account bin correlations is left as future work.

In this work, we do not address the issue of the gap that may exist between the model and the MC event generator. However, this gap only affects the inner optimization. As a result, the parameter tune obtained from minimizing the weighted χ^2 objective in the inner optimization problem may not yield the same χ^2 value when used in the MC event generator. Another issue is how to select the bounds of the parameter domain Ω. To overcome these issues, we need an approach that queries the MC event generator directly in the inner optimization. This can be achieved by using a derivative-free optimization approach. However, this task is non-trivial since doing this efficiently would require using the correct fidelity of the MC, the number of parameters at which to run the MC, and also deal with other issues that would affect the convergence of such an algorithm. Hence, we leave this work as a future research topic.

Acknowledgements

SM thanks Stefan Hoeche for discussions about our SHERPA results.

Funding information   This work was supported by the U.S. Department of Energy, Office of Science, Advanced Scientific Computing Research, under Contract DE-AC02-06CH11357. Support

for this work was provided through the Scientific Discovery through Advanced Computing (SciDAC) program funded by U.S. Department of Energy, Office of Science, Advanced Scientific Computing Research. This work was also supported by the U.S. Department of Energy through grant DE-FG02-05ER25694, and by Fermi Research Alliance, LLC under Contract No. DE-AC02-07CH11359 with the U.S. Department of Energy, Office of Science, Office of High Energy Physics. This work was supported in part by the U.S. Department of Energy, Office of Science, Office of Advanced Scientific Computing Research and Office of Nuclear Physics, SciDAC program through the FASTMath Institute under Contract No. DE-AC02-05CH11231 at Lawrence Berkeley National Laboratory.

References

[1] A. Buckley *et al.*, *General-purpose event generators for LHC physics*, Phys. Rept. **504**, 145 (2011), doi:10.1016/j.physrep.2011.03.005, `1101.2599`.

[2] P. Skands, S. Carrazza and J. Rojo, *Tuning PYTHIA 8.1: the Monash 2013 Tune*, Eur. Phys. J. **C74**(8), 3024 (2014), doi:10.1140/epjc/s10052-014-3024-y, `1404.5630`.

[3] ATLAS Collaboration, *ATLAS PYTHIA 8 tunes to 7 TeV data*, Tech. Rep. ATL-PHYS-PUB-2014-021, CERN, Geneva (2014).

[4] J. Nocedal and S. Wright, *Numerical Optimization*, Springer New York (1999).

[5] A. Buckley, H. Hoeth, H. Lacker, H. Schulz and J. von Seggern, *Systematic event generator tuning for the LHC*, The European Physical Journal C **65**, 331 (2010), doi:10.1140/epjc/s10052-009-1196-7.

[6] J. Bellm and L. Gellersen, *High dimensional parameter tuning for event generators*, Eur. Phys. J. C **80**(1), 54 (2020), doi:10.1140/epjc/s10052-019-7579-5, `1908.10811`.

[7] P. Ilten, M. Williams and Y. Yang, *Event generator tuning using Bayesian optimization*, JINST **12**(04), P04028 (2017), doi:10.1088/1748-0221/12/04/P04028, `1610.08328`.

[8] Y. Chen and M. Florian, *The nonlinear bilevel programming problem: Formulations, regularity and optimality conditions*, Optimization **32**, 193 (1995).

[9] P. Marcotte and D. L. Zhu, *Exact and inexact penalty methods for the generalized bilevel programming problem*, Mathematical Programming **74**(2), 141 (1996).

[10] J. J. Ye, D. L. Zhu and Q. J. Zhu, *Exact penalization and necessary optimality conditions for generalized bilevel programming problems*, SIAM J. Optimization **7**(2), 481 (1997).

[11] B. Colson, P. Marcotte and G. Savard, *An overview of bilevel optimization*, Annals of operations research **153**(1), 235 (2007).

[12] J. F. Bard, *Practical bilevel optimization: algorithms and applications*, vol. 30, Springer Science & Business Media (2013).

[13] H. Markowitz, *Portfolio selection*, The Journal of Finance **7**, 77 (1952), doi:10.2307/2975974.

[14] T. Gneiting and A. Raftery, *Strictly proper scoring rules, prediction, and estimation*, Journal of the American Statistical Association **102**(477), 359 (2007).

[15] M. Powell, *Advances in Numerical Analysis, vol. 2: wavelets, subdivision algorithms and radial basis functions. Oxford University Press, Oxford, pp. 105-210*, chap. The Theory of Radial Basis Function Approximation in 1990, Oxford University Press, London (1992).

[16] J. Müller and C. Shoemaker, *Influence of ensemble surrogate models and sampling strategy on the solution quality of algorithms for computationally expensive black-box global optimization problems*, Journal of Global Optimization **60**, 123 (2014).

[17] J. Müller and J. Woodbury, *GOSAC: global optimization with surrogate approximation of constraints*, Journal of Global Optimization **doi:10.1007/s10898-017-0496-y** (2017).

[18] D. M. Hawkins, *Identification of outliers*, vol. 11, Springer (1980).

[19] C. Croarkin, P. Tobias, J. Filliben, B. Hembree, W. Guthrie *et al.*, *NIST/SEMATECH e-handbook of statistical methods*, NIST/SEMATECH, July. Available online: http://www. itl. nist. gov/div898/handbook (2006).

[20] G. Upton and I. Cook, *Understanding statistics*, Oxford University Press (1996).

[21] B. Rosner, *Percentage points for a generalized esd many-outlier procedure*, Technometrics **25**(2), 165 (1983).

[22] F. E. Grubbs, *Procedures for detecting outlying observations in samples*, Technometrics **11**(1), 1 (1969).

[23] W. Stefansky, *Rejecting outliers in factorial designs*, Technometrics **14**(2), 469 (1972).

[24] W. Dixon, *Processing data for outliers*, Biometrics **9**(1), 74 (1953).

[25] R. Thompson, *A note on restricted maximum likelihood estimation with an alternative outlier model*, Journal of the Royal Statistical Society: Series B (Methodological) **47**(1), 53 (1985).

[26] C. Dardis, *Peirce's criterion for the rejection of non-normal outliers; defining the range of applicability*, J Stat Softw **10**, 1 (2004).

[27] G. L. Tietjen and R. H. Moore, *Some Grubbs-type statistics for the detection of several outliers*, Technometrics **14**(3), 583 (1972).

[28] W. G. Cochran, *The χ^2 test of goodness of fit*, Ann. Math. Statist. **23**(3), 315 (1952), doi:10.1214/aoms/1177729380.

[29] A. Shapiro, Y. Xie and R. Zhang, *Goodness-of-fit tests on manifolds* (2019), `1909.05229`.

[30] J. Bentley, *Programming pearls: Algorithm design techniques*, Commun. ACM **27**(9), 865–873 (1984), doi:10.1145/358234.381162.

[31] L. Pronzato and A. Pázman, *Design of experiments in nonlinear models*, Lecture notes in statistics **212**, 1 (2013).

[32] S. Körkel, *Numerische Methoden Für Optimale Versuchsplanungsprobleme Bei Nichtlinearen DAE-Modellen*, PhD Thesis, Universität Heidelberg, Heidelberg (2002).

[33] B. Crestel, A. Alexanderian, G. Stadler and O. Ghattas, *A-optimal encoding weights for nonlinear inverse problems, with application to the helmholtz inverse problem*, Inverse problems **33**(7), 074008 (2017).

[34] E. Kuram, B. Ozcelik, M. Bayramoglu, E. Demirbas and B. T. Simsek, *Optimization of cutting fluids and cutting parameters during end milling by using d-optimal design of experiments*, Journal of Cleaner Production **42**, 159 (2013), doi:https://doi.org/10.1016/j.jclepro.2012.11.003.

[35] T. Sjöstrand, S. Ask, J. R. Christiansen, R. Corke, N. Desai, P. Ilten, S. Mrenna, S. Prestel, C. O. Rasmussen and P. Z. Skands, *An introduction to PYTHIA 8.2*, Comput. Phys. Commun. **191**, 159 (2015), doi:10.1016/j.cpc.2015.01.024, `1410.3012`.

[36] A. Buckley, J. Butterworth, D. Grellscheid, H. Hoeth, L. Lonnblad, J. Monk, H. Schulz and F. Siegert, *RIVET user manual*, Comput. Phys. Commun. **184**, 2803 (2013), doi:10.1016/j.cpc.2013.05.021, `1003.0694`.

[37] S. B. Pope, *Algorithms for ellipsoids*, Cornell University Report No. FDA pp. 08–01 (2008).

[38] G. Aad *et al.*, *Properties of jets measured from tracks in proton-proton collisions at center-of-mass energy $\sqrt{s} = 7$ TeV with the ATLAS detector*, Phys. Rev. D **84**, 054001 (2011), doi:10.1103/PhysRevD.84.054001, `1107.3311`.

[39] G. Aad *et al.*, *Study of Jet Shapes in Inclusive Jet Production in pp Collisions at $\sqrt{s} = 7$ TeV using the ATLAS Detector*, Phys. Rev. D **83**, 052003 (2011), doi:10.1103/PhysRevD.83.052003, `1101.0070`.

[40] G. Aad *et al.*, *Measurement of Dijet Azimuthal Decorrelations in pp Collisions at $\sqrt{s} = 7$ TeV*, Phys. Rev. Lett. **106**, 172002 (2011), doi:10.1103/PhysRevLett.106.172002, `1102.2696`.

[41] G. Aad *et al.*, *Measurement of multi-jet cross sections in proton-proton collisions at a 7 TeV center-of-mass energy*, Eur. Phys. J. C **71**, 1763 (2011), doi:10.1140/epjc/s10052-011-1763-6, `1107.2092`.

[42] G. Aad *et al.*, *Measurement of the transverse momentum distribution of $Z/\gamma*$ bosons in proton–proton collisions at $\sqrt{s}$=7 TeV with the ATLAS detector*, Phys. Lett. B **705**, 415 (2011), doi:10.1016/j.physletb.2011.10.018, `1107.2381`.

[43] G. Aad *et al.*, *Measurement of the Z/γ^* boson transverse momentum distribution in pp collisions at $\sqrt{s} = 7$ TeV with the ATLAS detector*, JHEP **09**, 145 (2014), doi:10.1007/JHEP09(2014)145, `1406.3660`.

[44] G. Aad *et al.*, *Jet mass and substructure of inclusive jets in $\sqrt{s} = 7$ TeV pp collisions with the ATLAS experiment*, JHEP **05**, 128 (2012), doi:10.1007/JHEP05(2012)128, `1203.4606`.

[45] G. Aad *et al.*, *Measurement of $t\bar{t}$ production with a veto on additional central jet activity in pp collisions at sqrt(s) = 7 TeV using the ATLAS detector*, Eur. Phys. J. C **72**, 2043 (2012), doi:10.1140/epjc/s10052-012-2043-9, `1203.5015`.

[46] G. Aad *et al.*, *Measurement of jet shapes in top-quark pair events at $\sqrt{s} = 7$ TeV using the ATLAS detector*, Eur. Phys. J. C **73**(12), 2676 (2013), doi:10.1140/epjc/s10052-013-2676-3, `1307.5749`.

[47] G. Aad *et al.*, *Measurements of the pseudorapidity dependence of the total transverse energy in proton-proton collisions at $\sqrt{s} = 7$ TeV with ATLAS*, JHEP **11**, 033 (2012), doi:10.1007/JHEP11(2012)033, `1208.6256`.

[48] G. Aad *et al.*, *Underlying event characteristics and their dependence on jet size of charged-particle jet events in pp collisions at $\sqrt{s} = 7$ TeV with the ATLAS detector*, Phys. Rev. D **86**, 072004 (2012), doi:10.1103/PhysRevD.86.072004, `1208.0563`.

[49] G. Aad *et al.*, *Measurement of the underlying event in jet events from 7 TeV proton-proton collisions with the ATLAS detector*, Eur. Phys. J. C **74**(8), 2965 (2014), doi:10.1140/epjc/s10052-014-2965-5, `1406.0392`.

[50] G. Aad *et al.*, *Measurement of distributions sensitive to the underlying event in inclusive Z-boson production in pp collisions at $\sqrt{s} = 7$ TeV with the ATLAS detector*, Eur. Phys. J. C **74**(12), 3195 (2014), doi:10.1140/epjc/s10052-014-3195-6, `1409.3433`.

[51] E. Bothmann *et al.*, *Event Generation with Sherpa 2.2*, SciPost Phys. **7**(3), 034 (2019), doi:10.21468/SciPostPhys.7.3.034, `1905.09127`.

[52] P. Pfeifenschneider *et al.*, *QCD analyses and determinations of α_s in e^+e^- annihilation at energies between 35-GeV and 189-GeV*, Eur. Phys. J. C **17**, 19 (2000), doi:10.1007/s100520000432, `hep-ex/0001055`.

[53] P. Abreu *et al.*, *Tuning and test of fragmentation models based on identified particles and precision event shape data*, Z. Phys. C **73**, 11 (1996), doi:10.1007/s002880050295.

[54] K. Abe *et al.*, *Measurement of the b quark fragmentation function in Z^0 decays*, Phys. Rev. D **65**, 092006 (2002), doi:10.1103/PhysRevD.66.079905, [Erratum: Phys.Rev.D 66, 079905 (2002)], `hep-ex/0202031`.

[55] C. Amsler *et al.*, *Review of Particle Physics*, Phys. Lett. B **667**, 1 (2008), doi:10.1016/j.physletb.2008.07.018.

[56] C. Forbes, M. Evans, N. Hastings and B. Peacock, *Statistical distributions*, John Wiley & Sons (2011).

[57] J. Pumplin, D. Stump, R. Brock, D. Casey, J. Huston, J. Kalk, H. L. Lai and W. K. Tung, *Uncertainties of predictions from parton distribution functions. 2. The Hessian method*, Phys. Rev. D **65**, 014013 (2001), doi:10.1103/PhysRevD.65.014013, `hep-ph/0101032`.

[58] T. Sjöstrand, *Status and developments of event generators*, PoS **LHCP2016**, 007 (2016), doi:10.22323/1.276.0007, `1608.06425`.

[59] A. Booker, J. Dennis Jr, P. Frank, D. Serafini, V. Torczon and M. Trosset, *A rigorous framework for optimization of expensive functions by surrogates*, Structural Multidisciplinary Optimization **17**, 1 (1999).

[60] M. Powell, *Recent Research at Cambridge on Radial Basis Functions*, New Developments in Approximation Theory, pp. 215-232. Birkhäuser, Basel (1999).

[61] S. Kotz, N. Balakrishnan and N. L. Johnson, *Continuous multivariate distributions, Volume 1: Models and applications*, John Wiley & Sons (2004).

[62] D. M. Blei, A. Y. Ng and M. I. Jordan, *Latent Dirichlet allocation*, the Journal of machine Learning research **3**, 993 (2003).

[63] K. W. Ng, G.-L. Tian and M.-L. Tang, *Dirichlet and related distributions: Theory, methods and applications* (2011).

[64] R. Regis and C. Shoemaker, *A stochastic radial basis function method for the global optimization of expensive functions*, INFORMS Journal on Computing **19**, 497 (2007).

8 Online Supplement

Online supplement for "BROOD: Bilevel and Robust Optimization and Outlier Detection for Efficient Tuning of High-Energy Physics Event Generators".

8.1 Solving the outer problem with derivative-free surrogate optimization

Solving the inner optimization problem can become computationally demanding as it depends on the number of observables involved, the number of bins per observable (and therefore the number of parameters), and the starting guess (and therefore the number of iterations needed). Thus, the goal is to determine the optimal weights $\mathbf{w}^*$ within as few iterations of the outer loop as possible since this number determines how often we have to solve the inner optimization problem. We do not have a full analytic expression of $g(\mathbf{w}, \widehat{\mathbf{p}}_{\mathbf{w}})$ (black box) since computing this value involves solving the inner optimization problem. Thus, also derivatives of $g(\mathbf{w}, \widehat{\mathbf{p}}_{\mathbf{w}})$ are not available. A widely used approach for optimizing computationally expensive black-box functions is to use computationally cheap approximations (surrogates, metamodels) of the expensive function and to use the approximation throughout the optimization to make iterative sampling decisions [59]. Here, we approximate $g(\mathbf{w}, \widehat{\mathbf{p}}_{\mathbf{w}})$ with a radial basis function (RBF) [60], although in general any approximation model could be used. An RBF interpolant is defined as follows:

$$s(\mathbf{w}) = \sum_{i=1}^{n} \gamma_i \phi(\|\mathbf{w} - \mathbf{w}_i\|_2) + q(\mathbf{w}), \tag{18}$$

where $s : \mathbb{R}^{|\mathcal{S}_{\mathcal{O}}|} \mapsto \mathbb{R}$, $\mathbf{w}_i$, $i = 1, \ldots, n$, are the weight vectors for which we have already evaluated the objective function of the outer optimization problem, γ_i are parameters that must be determined, $\phi(\cdot)$ is the radial basis function (here, we choose the cubic, $\phi(r) = r^3$, but other options are possible), $\|\cdot\|_2$ denotes the Euclidean norm, and $q(\cdot)$ is a polynomial tail whose order depends on the choice of ϕ. When using the cubic RBF, the polynomial tail must be at least linear ($q(\mathbf{w}) = \beta_0 + \boldsymbol{\beta}^\top \mathbf{w}$) in order to uniquely determine the RBF parameters ($\gamma_i, i = 1, \ldots, n, \beta_0, \boldsymbol{\beta} = [\beta_1, \ldots, \beta_{|\mathcal{S}_{\mathcal{O}}|}]^\top$). The RBF interpolant $s(\mathbf{w})$ then predicts the value of the objective function at the point $\mathbf{w}$. It is interpolating, and thus the prediction at an already evaluated point $\mathbf{w}_i$ will agree with the observed function value. Using the RBF, we thus have $g(\mathbf{w}, \widehat{\mathbf{p}}_{\mathbf{w}}) = s(\mathbf{w}) + e(\mathbf{w})$, where $e(\mathbf{w})$ denotes the difference between the RBF and the true function value and it is 0 at already evaluated vectors $\mathbf{w}_i$.

The values of the RBF parameters are determined by solving a linear system of equations:

$$\begin{bmatrix} \mathbf{\Phi} & \mathbf{W} \\ \mathbf{W}^\top & \mathbf{0} \end{bmatrix} \begin{bmatrix} \boldsymbol{\gamma} \\ \boldsymbol{\beta'} \end{bmatrix} = \begin{bmatrix} \mathbf{G} \\ \mathbf{0} \end{bmatrix}, \tag{19}$$

where the elements of $\mathbf{\Phi}$ are $\Phi_{\iota\nu} = \phi(\|\mathbf{w}_\iota - \mathbf{w}_\nu\|_2)$, $\iota, \nu = 1 \ldots n$, $\mathbf{0}$ is a matrix with all entries 0 of appropriate dimension, and

$$\mathbf{W} = \begin{bmatrix} \mathbf{w}_1^\top & 1 \\ \vdots & \vdots \\ \mathbf{w}_n^\top & 1 \end{bmatrix} \quad \boldsymbol{\gamma} = \begin{bmatrix} \gamma_1 \\ \gamma_2 \\ \vdots \\ \gamma_n \end{bmatrix} \quad \boldsymbol{\beta'} = \begin{bmatrix} \beta_1 \\ \beta_2 \\ \vdots \\ \beta_{|\mathcal{S}_\mathcal{O}|} \\ \beta_0 \end{bmatrix} \quad \mathbf{G} = \begin{bmatrix} g(\mathbf{w}_1, \widehat{\mathbf{p}}_{\mathbf{w}_1}) \\ g(\mathbf{w}_2, \widehat{\mathbf{p}}_{\mathbf{w}_2}) \\ \vdots \\ g(\mathbf{w}_n, \widehat{\mathbf{p}}_{\mathbf{w}_n}) \end{bmatrix}. \tag{20}$$

The linear system in Eq. (19) has a solution if and only if rank$(\mathbf{W}) = |\mathcal{S}_\mathcal{O}| + 1$ [15]. During the optimization, we use the RBF prediction at unsampled points to determine a new vector $\mathbf{w}$ for which we solve the inner optimization problem. It is important that at this step only weights that sum up to 1 are chosen. The steps of the iterative sampling algorithm are summarized in Algorithm 8.1.

The inputs that must be supplied to the algorithm are the number of points n_0 to be used in the initial experimental design and the maximum number $n_{\max}$ of outer objective function evaluations (i.e., the number of inner optimizations) one is willing to allow. The number n_0 should in our case be at least $|\mathcal{S}_\mathcal{O}| + 1$, since this is the minimum number of points we need to fit the RBF model. $n_{\max}$ should depend on how long the inner optimization takes and the time budget of the user.

When creating the initial experimental design in Step 1, we have to ensure that the constraint (3b) is satisfied. Also, we have the condition that the weights lie in $[0, 1]$ and are uniform in their support. This means that the weights follow the Dirichlet distribution, i.e., the set of points are uniformly distributed over the open standard $(|\mathcal{S}_\mathcal{O}| - 1)$-simplex. To achieve this, we generate an initial design where all weights are drawn from the symmetric Dirichlet distribution, $Dir(\alpha_1 = \alpha_2 = \ldots = \alpha_{|\mathcal{S}_\mathcal{O}|} = 1)$ [61–63].

We evaluate the outer objective function at these points, i.e., we solve the inner optimization problem at each point and we obtain $\mathbf{G}$ in Eq. (20). With the sum-one-scaled initial experimental design, however, the rank of the matrix $\mathbf{W}$ is now only $|\mathcal{S}_\mathcal{O}|$ (and not the required $|\mathcal{S}_\mathcal{O}| + 1$). Thus, we solve the problem as one of dimension $|\mathcal{S}_\mathcal{O}| - 1$, i.e., for fitting the RBF model, we only use the

---

Algorithm 8.1: Derivative-free optimization of the outer equality-constrained optimization problem

---

Input: Number of initial experimental design points n_0; the maximum number of evaluations $n_{\max}$

Output: The best weight vector $\mathbf{w}^*$ and corresponding $\widehat{\mathbf{p}}^*_{\mathbf{w}^*}$

1: Create an initial experimental design with n_0 points; ensure that Eq. (3b) is satisfied for all points;

2: Compute the value of the outer optimization objective function at all points in the initial design;

3: Fit an RBF model to the sample data pairs $\{(\mathbf{w}_i, g(\mathbf{w}_i, \widehat{\mathbf{p}}_{\mathbf{w}_i}))\}_{i=1}^{n_0}$

4: Set $n = n_0$

5: **while** $n < n_{\max}$ **do**

6:     Use the RBF to determine a new point $\mathbf{w}_{\text{new}}$ and ensure that Eq. (3b) is satisfied;

7:     Solve the inner optimization problem for $\mathbf{w}_{\text{new}}$ and obtain $\widehat{\mathbf{p}}_{\mathbf{w}_{\text{new}}}$;

8:     Compute the value of the outer optimization objective function for $(\mathbf{w}_{\text{new}}, \widehat{\mathbf{p}}_{\mathbf{w}_{\text{new}}})$;

9:     Update the RBF model with the new data;

10:     $n \leftarrow n + 1$;

11: **end while**

12: **return** the best parameter values $(\mathbf{w}^*, \widehat{\mathbf{p}}^*_{\mathbf{w}^*})$;

---

first $|\mathcal{S}_\mathcal{O}| - 1$ values of each sample point (the "reduced" sample points). Thus, we use

$$
\boldsymbol{W} = \begin{bmatrix} w_{1,1} & w_{1,2} & \cdots & w_{1,|\mathcal{S}_\mathcal{O}|-1} & 1 \\ w_{2,1} & w_{2,2} & \cdots & w_{2,|\mathcal{S}_\mathcal{O}|-1} & 1 \\ \vdots & \vdots & \vdots & \vdots & \vdots \\ w_{n,1} & w_{n,2} & \cdots & w_{n,|\mathcal{S}_\mathcal{O}|-1} & 1 \end{bmatrix} \tag{21}
$$

and the coefficient vector for the polynomial tail thus becomes $[\beta_1, \ldots, \beta_{|\mathcal{S}_\mathcal{O}|-1}, \beta_0]^\top$. The vector $\boldsymbol{\gamma}$ and the matrix $\boldsymbol{G}$ do not change. The elements of $\boldsymbol{\Phi}$ are computed from the $(|\mathcal{S}_\mathcal{O}| - 1)$-dimensional sample vectors. Note, however, that when we evaluate the objective function in Eq. (3a), we always evaluate it for the full-dimensional vectors, as we can simply compute $w_{j,|\mathcal{S}_\mathcal{O}|} = 1 - \sum_{i=1}^{|\mathcal{S}_\mathcal{O}|-1} w_i$ for each $j = 1, \ldots, n$.

In the iterative sampling procedure (Steps 5-11), we use the RBF model to determine a new vector $\mathbf{w}_{\text{new}}$ at which we will do the next evaluation of Eq. (3a). Since we do not know whether the objective function is multimodal, we have to balance local and global search steps, i.e., we have to balance our sample point selection such that we select points with low predicted function values but also points that are far away from already evaluated points. Moreover, the new sample point must satisfy Eq. (3b). In order to do so, we generate a large set of candidate points from the Dirichlet distribution. We use the RBF to predict the function values at the candidate points. Since the RBF is defined over the $(|\mathcal{S}_\mathcal{O}| - 1)$-dimensional space, we use only the first $|\mathcal{S}_\mathcal{O}| - 1$ parameter values of each candidate point. We denote the $(|\mathcal{S}_\mathcal{O}| - 1)$-dimensional candidate points by $\mathbf{x}_1, \ldots, \mathbf{x}_{N_{\text{cand}}}$, where we choose N_{cand} large (for example, $500|\mathcal{S}_\mathcal{O}|$). For each candidate point, we use the RBF to predict its function value using (18) and we obtain $s(\mathbf{x}_k), k = 1, \ldots, N_{\text{cand}}$. We scale these values to [0,1] according to

$$
V_s(\mathbf{x}_k) = \frac{s(\mathbf{x}_k) - s_{\min}}{s_{\max} - s_{\min}}, k = 1, \ldots, N_{\text{cand}}, \tag{22}
$$

where

$$
s_{\min} = \min\{s(\mathbf{x}_k), k = 1, \ldots, N_{\text{cand}}\} \text{ and } s_{\max} = \max\{s(\mathbf{x}_k), k = 1, \ldots, N_{\text{cand}}\}. \tag{23}
$$

We also compute the distances $d(\mathbf{x}_k, S)$ of each candidate point to the set of already evaluated points S (in the $(|\mathcal{S}_\mathcal{O}| - 1)$-dimensional Euclidean space), and we scale these distances to [0,1] according to

$$
V_d(\mathbf{x}_k) = \frac{d_{\max} - d(\mathbf{x}_k)}{d_{\max} - d_{\min}}, k = 1, \ldots, N_{\text{cand}}, \tag{24}
$$

where

$$
d_{\min} = \min\{d(\mathbf{x}_k, S), k = 1, \ldots, N_{\text{cand}}\} \text{ and } d_{\max} = \max\{d(\mathbf{x}_k, S), k = 1, \ldots, N_{\text{cand}}\}. \tag{25}
$$

The ideal new sample point $\mathbf{w}_{\text{new}}$ will have a large distance to the set of already evaluated points S and a low predicted objective function value. Using the two criteria defined above, we compute a weighted sum of both (following [64])

$$V(\mathbf{x}_k) = \nu V_s(\mathbf{x}_k) + (1 - \nu)V_d(\mathbf{x}_k), k = 1, \ldots, N_{\text{cand}}, \tag{26}$$

where $\nu \in [0, 1]$ is a parameter that determines how much emphasis we put on either criterion. If ν is large, it means we put most emphasis on V_s, and we favor candidate points that have low predicted objective function values. This also means that the search is more local as low function values are usually predicted around the best point found so far. If ν is small, we put more emphasis on V_d and we favor points that are far away from the set of already evaluated points, and thus the search is more global. By varying the weights ν between different values in [0,1], we can achieve a repeated transition between local and global search, and therefore we can avoid becoming stuck in a local optimum. The candidate point with the lowest V value will become the new sample point $\mathbf{w}_{\text{new}}$. We evaluate the objective function (inner optimization) at the new point (augmented with the missing parameter value), and given the new data, we update the RBF model. The algorithm iterates until the maximum number of function evaluations n_{max} has been reached.

8.2 Polynomial-time algorithm for filtering bins by hypothesis testing

In this section, we describe the polynomial-time algorithm to solve the problem of finding the largest contiguous subset of bins $\mathcal{B} \subset \mathcal{O}$ to be kept for tuning, i.e., finding the largest contiguous subset of bins $\mathcal{B} \subset \mathcal{O}$ such that $\chi^2_{\mathcal{B}} \leq \chi^2_{c,\mathcal{B}}$, where $\chi^2_{c,\mathcal{B}}$ is the critical value for bins in $\mathcal{B}$. This algorithm is described in Algorithm 8.2 and it is based on the maximum subarray problem [30].

In this algorithm, we first find the critical value for each bin in line 1 as described in Section 3.2. The degree of the freedom is given by $\rho_{\mathcal{B}} = |\mathcal{B}| - d$ and since $\rho_{\mathcal{B}}$ cannot be negative, the critical values for only the bin index $b > d$ is calculated in line 1. Then the χ^2 test statistic is computed for each bin in $\mathcal{O}$ in lines 2-3. Then, while iterating through the bins in $\mathcal{O}$, in lines 6, we check whether the current bin b can be added to $\mathcal{B}$ and if so, we update the counters and add the current bin b to the end of $\mathcal{B}$ (via e) in lines 7-10. If the current bin b cannot be added to $\mathcal{B}$, then in lines 12-13 we shift the start s of $\mathcal{B}$ (through τ) such that the start is now at the bin index where the condition in line 6 could be satisfied in future iterations. Finally, in lines 14-19, we perform a sanity check to make sure that $\mathcal{B}$ contains the set of bins that yield the lowest $\chi^2_{\mathcal{B}}$ test statistic.

Algorithm 8.2: Algorithm to find bins $\mathcal{B}$ in observable $\mathcal{O}$ to keep for tuning

Input : $f_b, \mathcal{R}_b, \Delta f_b, \Delta \mathcal{R}_b, \forall b \in \mathcal{O}$; significance level α

Output: start index s and end index e of bins, i.e., $\mathcal{B} = \{s, \ldots, e\}$ to keep in $\mathcal{O}$

1 Calculate the critical values for each bin:

$$k_b = \begin{cases} \chi^2_{c,b} = f(\rho_b, \alpha), & \text{if } b > d \\ \infty, & \text{otherwise} \end{cases}, \quad \forall b \in \{1, 2, \ldots, |\mathcal{O}|\}, \mathbf{p} \in \Omega \subset \mathbb{R}^d$$

2 Find $\mathbf{p}^*$ by minimizing $\chi^2_{\mathcal{O}}$ in Eq. (12)

3 Calculate the test statistic values for each bin:

$\chi^2_b(\mathbf{p}^*) = \frac{(f_b(\mathbf{p}^*) - \mathcal{R}_b)^2}{\Delta f_b(\mathbf{p}^*)^2 + \Delta \mathcal{R}_b^2}, \quad \forall b \in \{1, 2, \ldots, |\mathcal{O}|\}$

4 Initialize $\Sigma \leftarrow 0, \widehat{b} \leftarrow 0, s \leftarrow 0, e \leftarrow 0, \tau \leftarrow 0$

5 for $b \in \{1, 2, \ldots, |\mathcal{O}|\}$ **do**

6   **if** $\Sigma + \chi^2_b \le k_{\widehat{b}+1}$ **then**

7 $\Sigma \leftarrow \Sigma + \chi^2_b$

8 $\widehat{b} \leftarrow \widehat{b} + 1$

9 $s \leftarrow \tau$

10 $e \leftarrow b$

11   **else if** $\Sigma \ne 0$ **then**

12 $\Sigma \leftarrow \Sigma - \chi^2_{b-\widehat{b}} + \chi^2_b$

13 $\tau \leftarrow b - \widehat{b} + 1$

14 if $s > 0$ *and* $\chi^2_{s-1} < \chi^2_e$ **then**

15 $e \leftarrow e - 1$

16 $s \leftarrow s - 1$

17 else if $e < |\mathcal{O}|$ *and* $\chi^2_s > \chi^2_{e+1}$ **then**

18 $e \leftarrow e + 1$

19 $s \leftarrow s + 1$

20 return $\mathcal{B} = \{s, \ldots, e\}$.

8.3 A14 and SHERPA physics parameters

The A14 tunable physics parameters, their definitions and tuning ranges are shown in Table 15. The SHERPA parameters, their definitions and tuning ranges are shown in Table 16.

Table 15: PYTHIA physics parameters used in the A14 tune, their definitions, and tuning ranges (min, max). More details of the parameters can be found in the on-line PYTHIA manual: `pythia.org/latest-manual/Welcome.html`

Parameter	Description	min	max
`SigmaProcess:alphaSvalue`	Strong coupling parameter α_S, at the scale $Q^2 = M_Z^2$, used to calculate QCD cross sections	0.12	0.15
`BeamRemnants:primordialKThard`	Hard process scale dependence of the primordial $k_\perp$ added to hard scattering subsystems.	1.5	2.0
`SpaceShower:pT0Ref`	Regulator of the $p_T \to 0$ divergence of the initial state (ISR) parton shower kernels	0.75	2.5
`SpaceShower:pTmaxFudge`	Factor to modify the starting ISR evolution scale	0.5	1.5
`SpaceShower:pTdampFudge`	Factor to dampen the ISR evolution scale	1.0	1.5
`SpaceShower:alphaSvalue`	Similar to `SigmaProcess:alphaSvalue`, but for ISR	0.10	0.15
`TimeShower:alphaSvalue`	Similar to `SigmaProcess:alphaSvalue`, but for final state (FSR) parton showers	0.10	0.15
`MultipartonInteractions:pT0Ref`	Similar to `SpaceShower:pT0Ref`, but used in the multiparton interaction (MPI) model	1.5	3.0
`MultipartonInteractions:alphaSvalue`	Similar to `SigmaProcess:alphaSvalue`, but for MPI	0.10	0.15
`BeamRemnants:reconnectRange`	Sets probability for color reconnections between lower and higher p_T systems	1.0	10.0

8.4 Selection of the best hyperparameter in robust optimization

In order to find the best value for μ in the robust optimization, we first build for each run (each μ) a cumulative density curve of the number of observables for which $\frac{\chi_\mathcal{O}^2(\mathbf{p}^*,\mathbf{w})}{|\mathcal{O}|} \leq \tau$, where $\mathbf{p}^*$ is the optimal parameter obtained from the robust optimization run, $\mathbf{w} = \mathbf{1}$, $\tau \in \mathbb{R}^+$ and $\mathcal{O} \in \mathcal{S}_\mathcal{O}$. Then, we construct the "ideal" cumulative density curve, for which $\mathbf{p}^*$ in $\frac{\chi_\mathcal{O}^2(\mathbf{p}^*,\mathbf{w})}{|\mathcal{O}|} \leq \tau$ is obtained by optimizing for each observable $\mathcal{O}$ separately. An example plot showing the cumulative density curve from the ideal case to some of the robust optimization runs is shown in Figure 11.

Then, the area between the cumulative density curve for each robust optimization run and the ideal cumulative density curve is computed. For the A14 dataset and all runs completed for robust optimization, the area between the curve is given in Table 17 (smaller values are better). Finally,

Table 16: SHERPA physics parameters, their definitions and tuning ranges (min, max).

Parameters	Definition	min	max
KT_0	generic parameter for non-perturbative transverse momentum	0.5	1.5
ALPHA_G	gluon fragmentation	0.62	1.88
ALPHA_L	light quark fragmentation z power	1.25	3.75
BETA_L	light quark fragmentation $1 - z$ power	0.05	0.15
GAMMA_L	light quark fragmentation exp power	0.25	0.75
ALPHA_H	heavy quark fragmentation z power	1.25	3.75
BETA_H	heavy quark fragmentation $1 - z$ power	0.375	1.125
GAMMA_H	heavy quark fragmentation exp power	0.05	0.15
STRANGE_FRACTION	suppression of s quarks	0.25	0.75
BARYON_FRACTION	suppression of baryons	0.09	0.27
P_QS_by_P_QQ_norm	fraction of di-quarks with one strange quark	0.24	0.72
P_SS_by_P_QQ_norm	fraction of di-quarks with two strange quarks	0.01	0.03
P_QQ1_by_P_QQ0	fraction of di-quarks with spin-1 to spin-0	0.5	1.5

for completeness, the best values of μ found for both the A14 and SHERPA datasets are given in Table 18.

8.5   Outlier observables in the A14 dataset

There are 12 outlier observables using the cubic polynomial approximation and 9 outlier observables using the rational approximation in the A14 dataset.

Cubic Polynomial Model	Rational Approximation Model
/ATLAS_2011_I919017/d01-x02-y02	/ATLAS_2011_I919017/d01-x02-y02
/ATLAS_2011_I919017/d01-x02-y03	/ATLAS_2011_I919017/d01-x04-y04
/ATLAS_2011_I919017/d01-x03-y02	/ATLAS_2011_I919017/d02-x04-y03
/ATLAS_2011_I919017/d01-x03-y07	/ATLAS_2011_I919017/d02-x04-y04
/ATLAS_2011_I919017/d01-x04-y07	/ATLAS_2011_I919017/d02-x04-y05
/ATLAS_2011_I919017/d01-x04-y08	/ATLAS_2011_I919017/d02-x04-y09
/ATLAS_2011_I919017/d01-x04-y09	/ATLAS_2011_I919017/d02-x04-y10
/ATLAS_2011_I919017/d02-x04-y04	/ATLAS_2011_I919017/d02-x04-y14
/ATLAS_2011_I919017/d02-x04-y10	/ATLAS_2011_I919017/d02-x04-y15
/ATLAS_2011_I919017/d02-x04-y13	
/ATLAS_2011_I919017/d02-x04-y14	

```
/ATLAS_2011_I919017/d02-x04-y15
```

8.6   Outlier observables in the SHERPA dataset

There are 2 outlier observables using the cubic polynomial approximation and 3 outlier observables using the rational approximation in the SHERPA dataset.

Cubic Polynomial Model	Rational Approximation Model
/DELPHI_1996_S3430090/d07-x01-y01	/DELPHI_1996_S3430090/d02-x01-y01
/DELPHI_1996_S3430090/d08-x01-y01	/DELPHI_1996_S3430090/d07-x01-y01
	/DELPHI_1996_S3430090/d08-x01-y01

8.7   Bin filtered data for A14 dataset

In Table 21, we give the names of the A14 observables from which bins have been filtered, the number of bins filtered out, critical χ^2 value, and χ^2 test statistic before and after filtering the bins.

8.8   Bin filtered data for SHERPA dataset

In Table 22, we give the names of the SHERPA observables from which bins have been filtered, the number of bins filtered out, critical χ^2 value, and χ^2 test statistic before and after filtering the bins.

8.9   Complete results from filtering out observables and bins

In Figures 12 and 13, the cumulative distribution plots for parameters obtained after bin filtering and observable filtering for the A14 data are presented. In Figures 14 and 15, the cumulative distribution plots for parameters obtained after bin filtering and observable filtering for the SHERPA data are presented. From these figures, we observe that there is no significant difference in the number of bins within the 1 σ variance level between the optimal parameters $\mathbf{p}_a^*$ obtained when all bins were used for tuning and the optimal parameters $\mathbf{p}_b^*$ and $\mathbf{p}_o^*$ obtained when only the bin filtered and observable filtered bins are used for tuning, respectively. There is some disagreement in the cumulative distribution of bins when the variance level is less than 10^{-1}. But this is not significant since the number of these bins is small and all of them have small levels of variance. Additionally, to get $\mathbf{p}_a^*$, the filtered bins were used. So we see that for variance levels less than 10^{-1}, $\mathbf{p}_a^*$ performs better on the filtered data (solid blue line) than $\mathbf{p}_b^*$ or $\mathbf{p}_o^*$ (dashed blue line). However, for variance levels beyond 10^{-1}, this difference is negligible. This means that filtering the

Table 17: Area between ideal cumulative density curve and the cumulative density curves of the robust optimization runs for various hyperparameters μ for the A14 full dataset (smaller values are better). The data are organized in ascending order of the area between the curves.

rank	μ	Area	rank	μ	Area	rank	μ	Area	rank	μ	Area
1	80	7.51e+02	26	79	1.05e+03	51	24	1.32e+03	76	38	1.66e+03
2	78	7.93e+02	27	81	1.12e+03	52	35	1.32e+03	77	29	1.72e+03
3	76	7.95e+02	28	71	1.13e+03	53	93	1.35e+03	78	51	1.72e+03
4	77	8.15e+02	29	95	1.14e+03	54	89	1.39e+03	79	49	1.73e+03
5	73	8.53e+02	30	10	1.15e+03	55	45	1.40e+03	80	57	1.73e+03
6	70	8.91e+02	31	11	1.17e+03	56	42	1.41e+03	81	50	1.74e+03
7	90	8.96e+02	32	12	1.17e+03	57	41	1.43e+03	82	43	1.74e+03
8	26	9.09e+02	33	18	1.18e+03	58	68	1.43e+03	83	44	1.76e+03
9	88	9.11e+02	34	3	1.19e+03	59	67	1.44e+03	84	55	1.79e+03
10	74	9.14e+02	35	21	1.19e+03	60	46	1.44e+03	85	47	1.87e+03
11	86	9.42e+02	36	20	1.19e+03	61	39	1.46e+03	86	60	1.93e+03
12	72	9.43e+02	37	16	1.19e+03	62	30	1.48e+03	87	37	1.94e+03
13	27	9.44e+02	38	69	1.20e+03	63	63	1.48e+03	88	59	1.95e+03
14	83	9.47e+02	39	22	1.20e+03	64	40	1.51e+03	89	33	1.96e+03
15	75	9.53e+02	40	23	1.21e+03	65	64	1.52e+03	90	54	1.97e+03
16	87	9.59e+02	41	19	1.21e+03	66	28	1.55e+03	91	58	1.99e+03
17	8	9.61e+02	42	13	1.22e+03	67	61	1.56e+03	92	53	2.08e+03
18	82	9.72e+02	43	25	1.23e+03	68	98	1.56e+03	93	94	2.13e+03
19	2	9.77e+02	44	97	1.24e+03	69	62	1.58e+03	94	56	2.14e+03
20	84	9.80e+02	45	7	1.25e+03	70	66	1.58e+03	95	52	2.23e+03
21	5	9.90e+02	46	15	1.27e+03	71	32	1.58e+03	96	99	2.74e+03
22	85	9.99e+02	47	17	1.28e+03	72	48	1.59e+03	97	36	3.00e+03
23	1	1.01e+03	48	14	1.29e+03	73	31	1.60e+03	98	34	3.02e+03
24	9	1.03e+03	49	92	1.30e+03	74	65	1.61e+03	99	91	3.05e+03
25	6	1.04e+03	50	4	1.31e+03	75	96	1.64e+03	100	100	3.89e+03
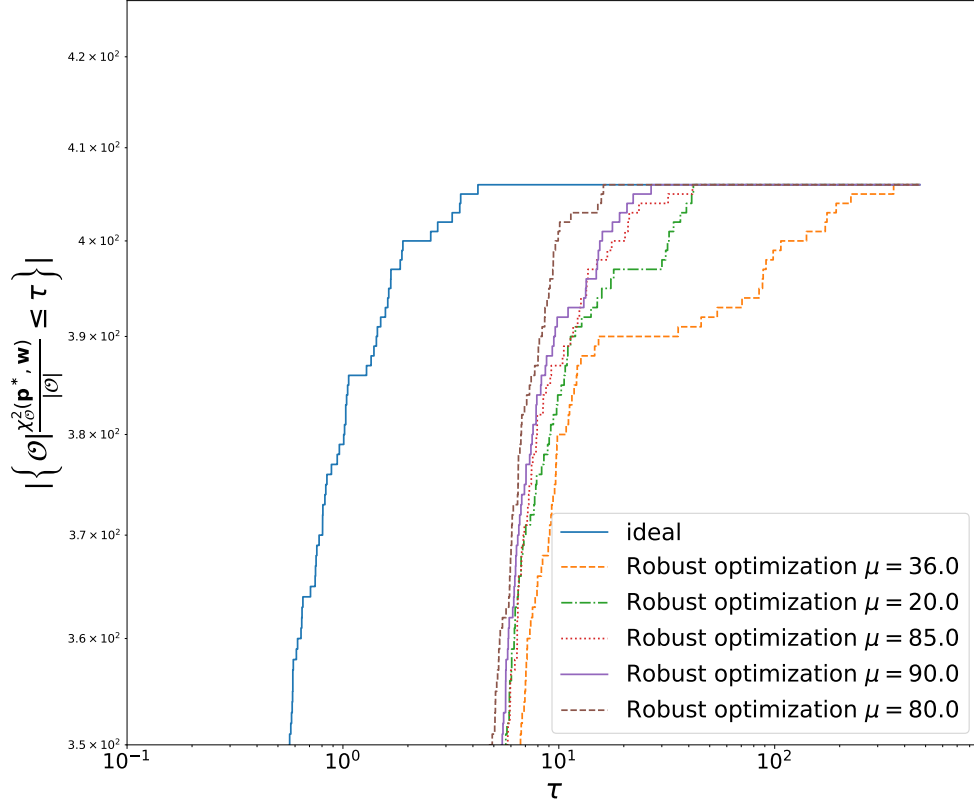
Figure 11: Ideal cumulative density curve and the cumulative density curves of robust optimization runs with selected hyperparameter values μ for the A14 dataset.

Table 18: Best μ obtained for A14 and SHERPA datasets when unfiltered (*All data*), bin filtered and observable filtered data are used for parameter tuning.

Dataset	All data	Bin filtered	Observable filtered
A14	80	76	80
SHERPA	82	71	73

bins or observables does not deteriorate the variance of the bins for levels greater than 10^{-1}. To summarize, we conclude that the MC generator cannot explain very well the data of the bins that were removed by filtering. Hence, removing these bins from the tuning process does not reduce the information required to achieve a good tune as the performance for bins with moderate and high variance in the filtered case is very similar to the case when all the bins are included.
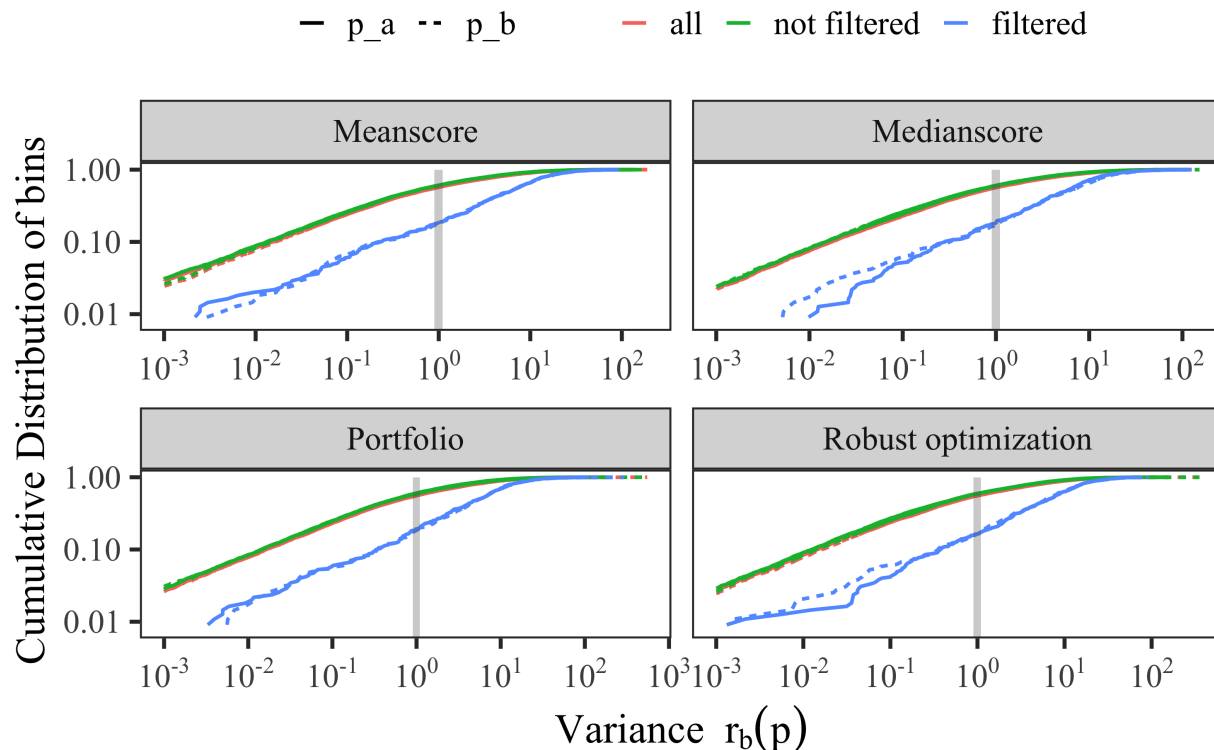
Figure 12: Cumulative distribution of bins for the A14 dataset at different bands of variance levels using different approaches. Results are shown using the parameters $\mathbf{p}_a^*$ obtained using all bins during optimization, and the parameters $\mathbf{p}_b^*$ obtained when only the bin filtered bins are used during optimization.

8.10 Comparison of the rational approximation with the MC generator

We compare the cumulative distribution of bins at different bands of variance levels computed using the rational approximation (RA) model as $r_b(\mathbf{p}) = \frac{(f_b(\mathbf{p}) - \mathcal{R}_b)^2}{\Delta f_b(\mathbf{p})^2 + \Delta \mathcal{R}_b^2}$ and the MC generator model as $\widetilde{r_b(\mathbf{p})} = \frac{(\mathrm{MC}_b(\mathbf{p}) - \mathcal{R}_b)^2}{\Delta \mathrm{MC}_b(\mathbf{p})^2 + \Delta \mathcal{R}_b^2}$, where $\mathbf{p}$ are the parameters obtained from the different tuning approaches. In Figure 5, we showed the plot of this comparison for bins in each category of the A14 dataset using the parameters from three approaches. For completeness, in Figure 16, we show the plot of this comparison for the remaining three approaches.

We observe in Figure 16 that around the variance boundary, except for in the *Track-jet UE* and *Multijets* categories, there is no significant difference in performance between $r_b(\mathbf{p})$ and $\widetilde{r_b(\mathbf{p})}$ for
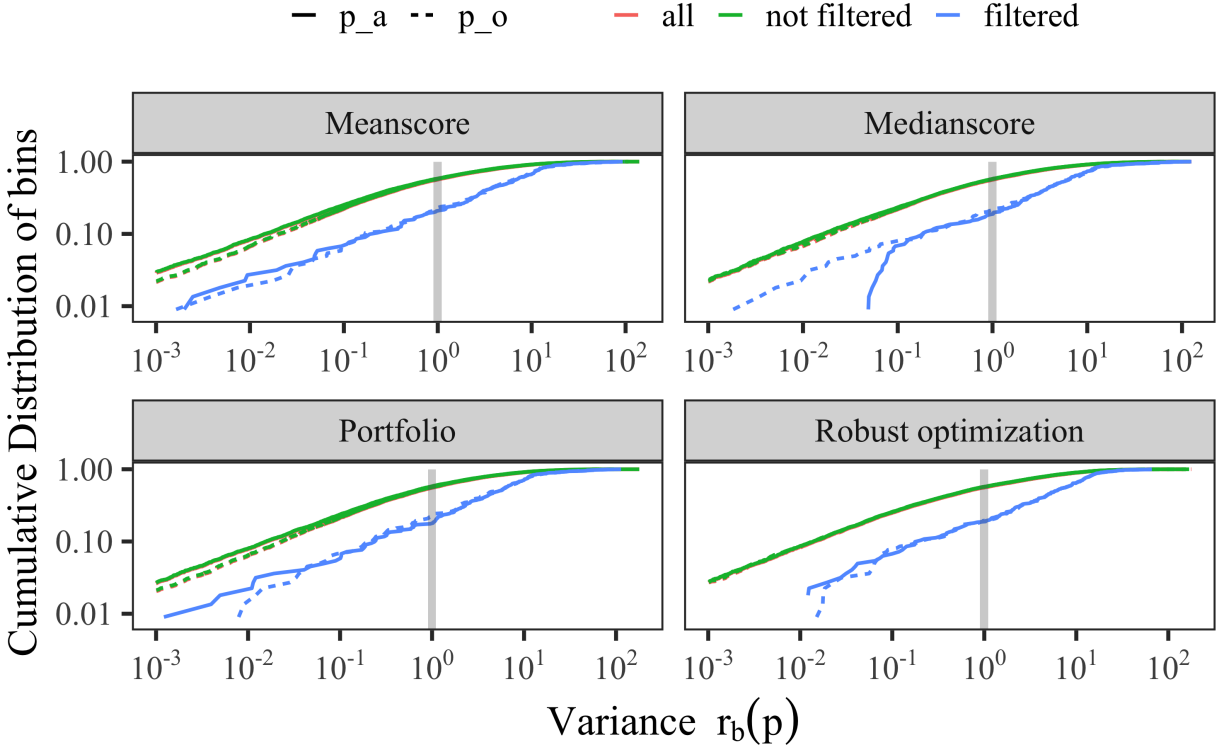
Figure 13: Same as Figure 12, but using observable filtering.

each approach. In the case of *Track-jet UE* and *Multijets* categories, the number of bins that lie within the variance boundary is quite low compared to other categories. This suggests that many bins in these categories cannot be explained well by either the MC generator or the approximation for the optimal tuning parameters reported by the approaches. Additionally, we observe in these categories that the approximations are not able to capture the MC generator perfectly.

8.11 Optimal parameter values for the A14 dataset with the rational approximation

To better visually compare the different solutions obtained with our optimization methods, we show the [0,1]-scaled optimal parameter values in Figure 17.
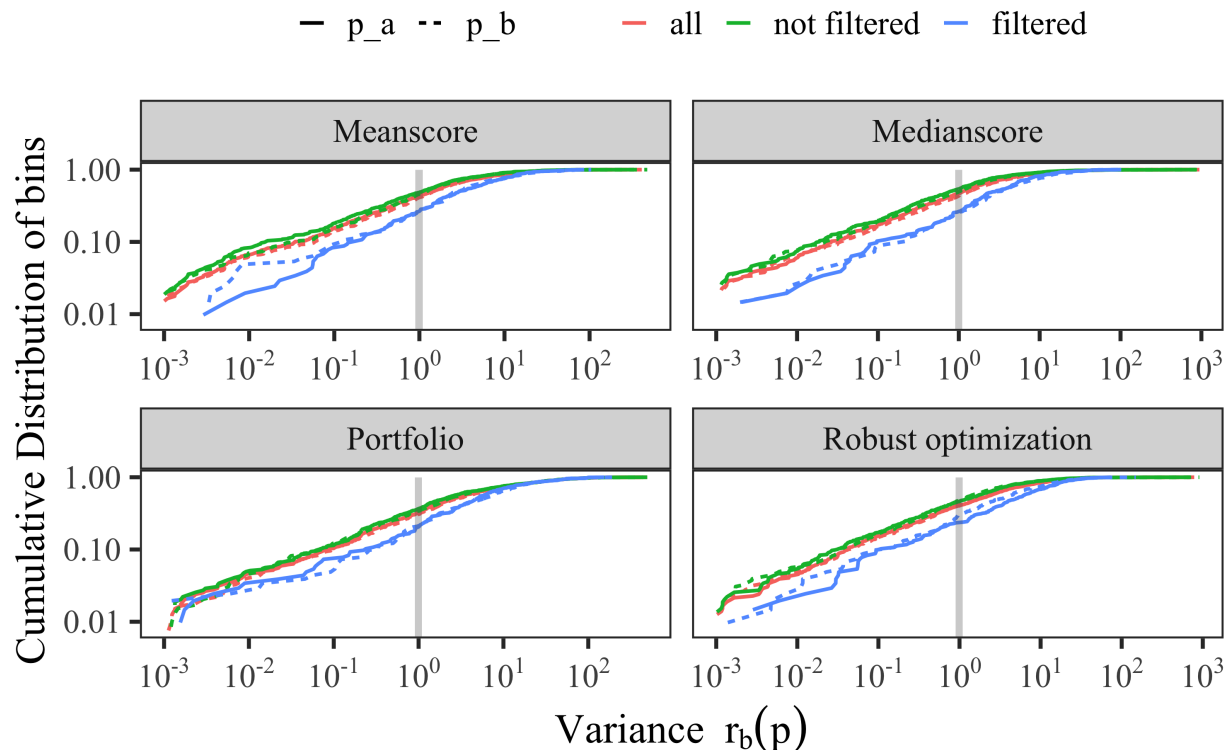
Figure 14: Same as Figure 12 , but for the SHERPA dataset.

8.12 Results for using the cubic polynomial to approximate the MC simulation

In the main paper, we showed the numerical results when using a rational approximation of the MC simulation during tuning. In the A14 publication [3], a cubic polynomial was used. Thus, in this section, we present the results obtained with our optimization methods when using a cubic polynomial instead of a rational approximation.

8.12.1 Comparison metric outcomes for the A14 dataset using the cubic polynomial approximation

Table 23 shows the comparison metrics we introduced in the main paper in Section 4.2 when using the cubic polynomial approximation for the full data, the observable-filtered data, and the bin-filtered data, respectively. We see that for all three cases and most criteria (except for the D-optimality in the observable-filtered case), our automated methods for adjusting the observable weights perform
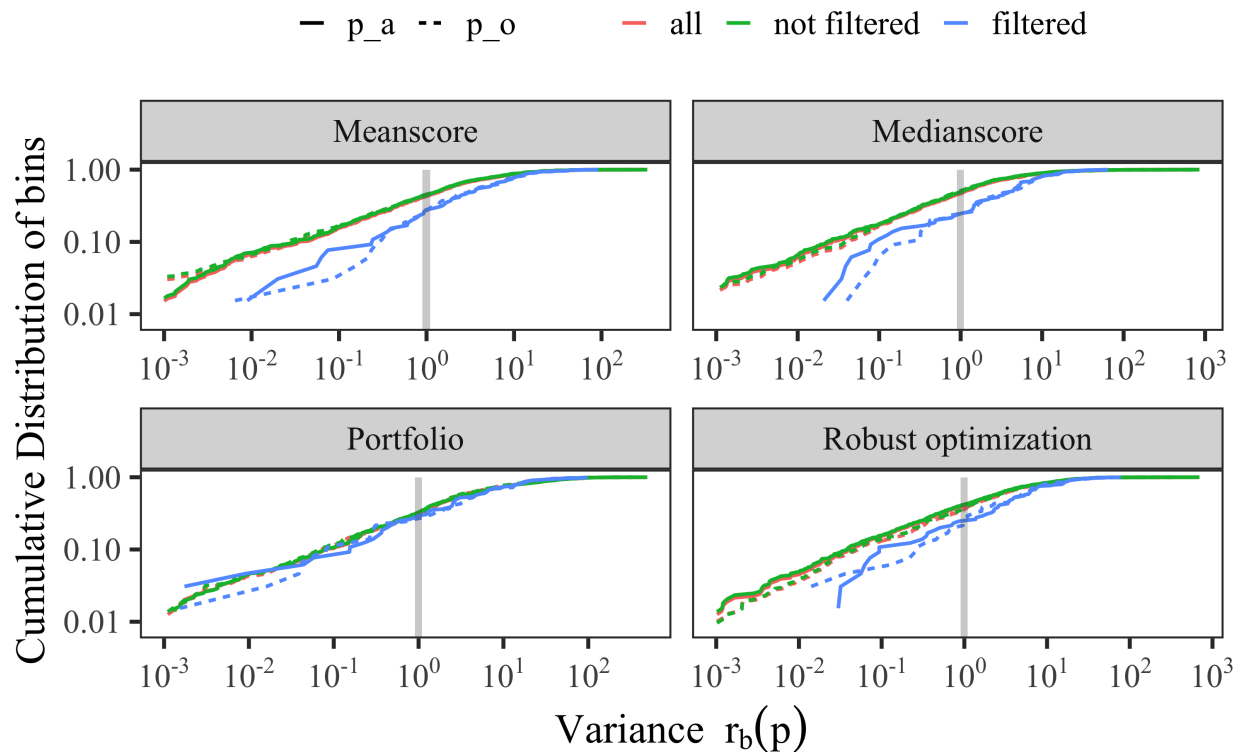
Figure 15: Same as Figure 14, but using observable filtering.

better than the expert solution (i.e., using the parameters published in [3]).

8.12.2 Optimal parameter values for the A14 dataset using the cubic polynomial approximation

Table 24 shows the optimal values for the tuned parameters obtained by all methods for the A14 dataset when using all observables in the tune. For Bilevel-meanscore, -medianscore and -portfolio, we repeated the experiments three times using different random number seeds and we report the best results among the three trials based on their respective objective functions. From these results, we can see that the Bilevel-medianscore method leads to a solution that is closest to the expert's solution.

To better visually compare the different solutions obtained with our methods, we show the [0,1]-scaled optimal values in Figure 17. We can see that there are differences between the optimal
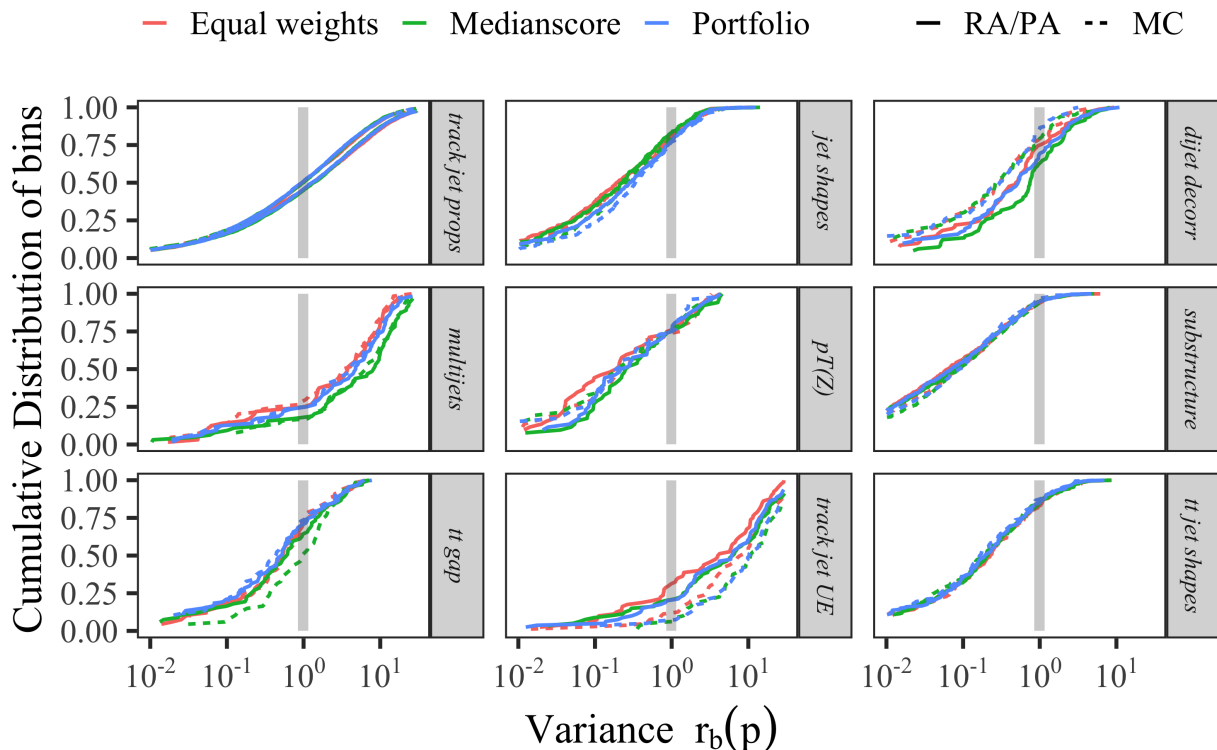
Figure 16: Cumulative distribution of bins in each category of the A14 dataset at different bands of variance levels computed with the rational approximation (RA) given by, $r_b(\mathbf{p}) = \frac{(f_b(\mathbf{p}) - \mathcal{R}_b)^2}{\Delta f_b(\mathbf{p})^2 + \Delta \mathcal{R}_b^2}$ and the MC simulation given by $\widetilde{r_b(\mathbf{p})} = \frac{(\mathrm{MC}_b(\mathbf{p}) - \mathcal{R}_b)^2}{\Delta \mathrm{MC}_b(\mathbf{p})^2 + \Delta \mathcal{R}_b^2}$

parameters obtained with the different methods, in particular, the results of the robust optimization method tend to be further away from the expert's solution for parameters 1, 2, 3, 7, 8, 9 and 10. The results of the portfolio optimization differ from the expert tune in particular for parameters 1, 2, 3, 4 and 7. The mean- and medianscore results are very similar to each other as well as to the expert's solution.

We conducted a similar analysis on the observable- and bin-filtered data. Table 25 shows the optimal parameter values that we obtain with the automated optimization methods after filtering out the 12 observables that the model cannot explain (see also Section 3.1). The expert solution is the same as before and based on all observables. We include it for easier comparison. With only a
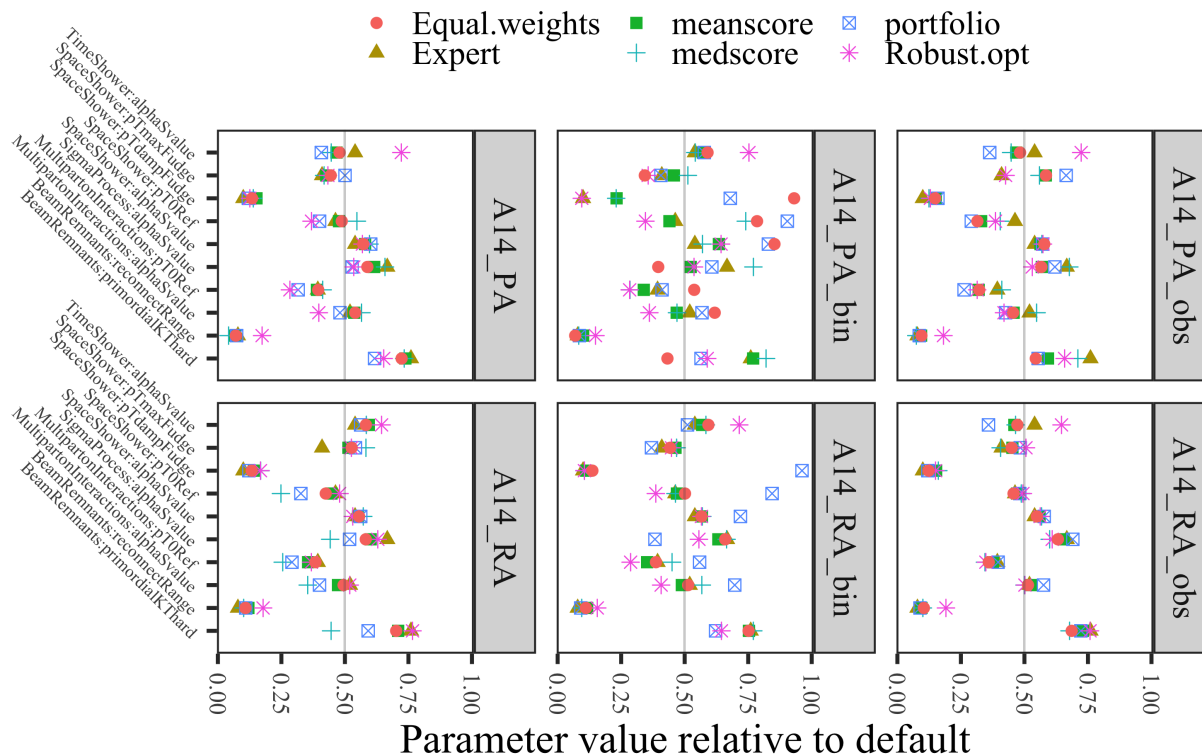
Figure 17: Optimal parameter values for the A14 dataset obtained when using all, bin-filtered (_bin) and observable-filtered (_obs) data in the optimization and the polynomial approximation (PA) and rational approximation (RA). Values are normalized to [0,1].

few exceptions, all parameters obtained with the automated optimizations change (as compared to using the full dataset). Figure 17 shows the optimal parameter values obtained with each method scaled to [0,1]. In comparison to when using the full dataset, we see that the results of the robust optimization now agree better with the expert's tune for parameters 3, 4, and 8, but less agreement is achieved for parameter 10. Of the three bilevel methods, the medianscore objective function leads to optimal parameters that are most similar to the expert tune.

In Table 26 and Figure 17 we show the optimal parameter values obtained with our methods after applying the bin-filtering approach described in Section 3.2 in the main document. In comparison to our results that do not use any filtering, we can see a much larger disagreement in the optimal parameters for all methods. In fact, all methods yield optimal parameters that are significantly further away from the expert's solution, except for parameters 7 and 10. The Euclidean distance

between the optimal parameters obtained by our proposed methods and the expert solution shows that the bilevel-medianscore method leads to the most similar parameter values while all the other methods lead to very different tunes.

8.12.3 Comparison of optimal weights for the A14 dataset with cubic polynomial approximation

In Table 27 we present the optimal weights assigned to each observable group by each method following the presentation style in [3]. The weights reported for our method are averages of the weights over all observables that belong to the same group. We scaled the weights such that they are on equal footing (all add up to 4580).

The largest differences between the expert-adjusted values and the values determined by our methods are for *Multijets*, $t\bar{t}$ *gap* and *Jet UE*, while for the remaining groups, the values are very similar. These results, together with our analysis above let us conclude that an automated method for adjusting the weights of observables for tuning parameters is a viable approach and can lead to better results than hand-tuning.

8.12.4 Optimal parameter values for the SHERPA dataset with rational approximation

For a better visual comparison of the different solutions obtained with our methods, we show the [0,1]-scaled optimal values in Figure 18. Compared to the results for the A14 dataset, we see that there are significant differences between the optimal parameters obtained with the different methods.

8.12.5 Optimal parameter values for the SHERPA dataset with the cubic polynomial approximation

The physics parameters $\mathbf{p}$ and their optimization ranges are shown in Table 16. Tables 28, 29 and 30 shows the optimal values for the physics parameters obtained by all methods when no filtering was applied before optimization, after using outlier detection to remove observables from the optimization, and after using the bin-filtering approach that excludes individual bins from the optimization, respectively. For an illustrative comparison, we show the [0,1]-scaled optimal parameter values in Figure 18. The default values lie right in the middle of the parameter range.
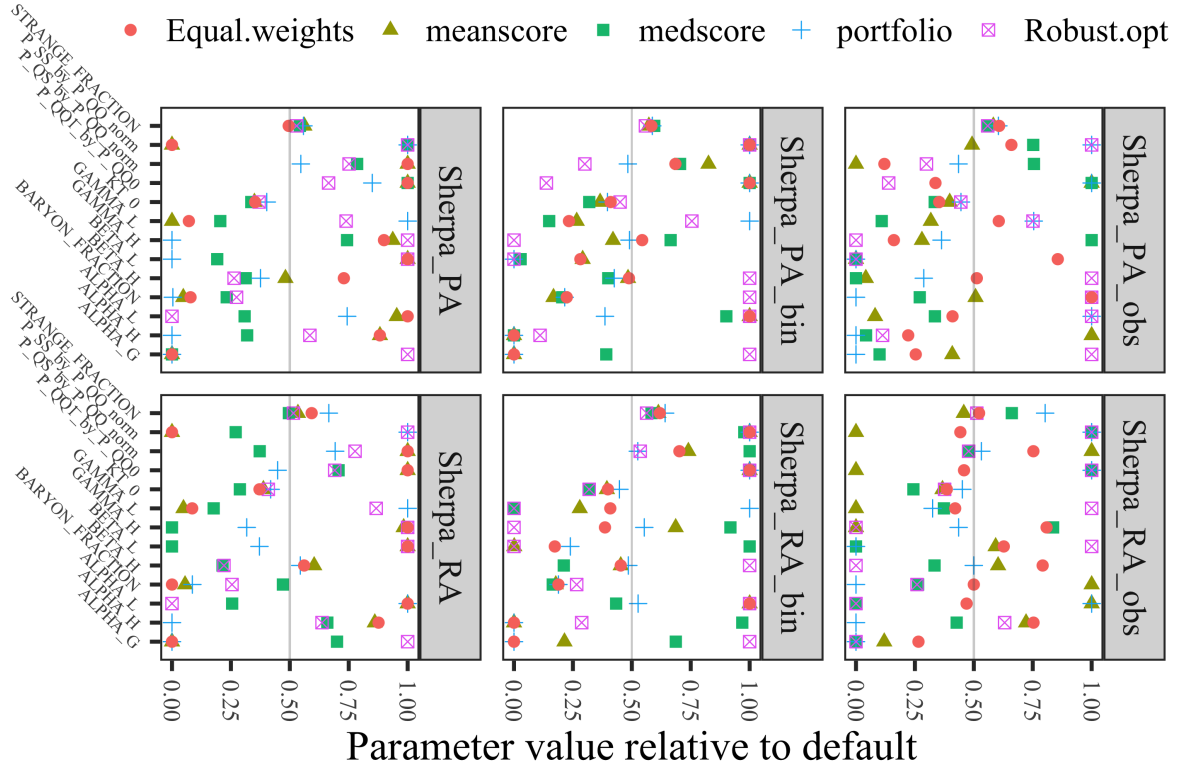
Figure 18: Comparison of the optimal parameter values for SHERPA obtained with the different optimization methods when no, observable, and bin data filtering was applied and the *rational* and polynomial approximation was used. Values are normalized to [0,1].

8.12.6 Comparison metric outcomes for the SHERPA dataset with the cubic polynomial approximation

Table 31 shows the comparison metrics of our experiments when using the cubic polynomial approximation for the full data, the observable-filtered data, and the bin-filtered data, respectively. Smaller numbers indicate better performance. The smallest number of each metric is bold for better visualization.

Based on these results, we can see that the all-weights-equal method (i.e. not adjusting any weights) has the best performance for the full dataset under the A- and D-optimality. The bilevel-portfolio method performs best under the A- and D-optimality for both the observable- and bin-filtered datasets. The robust optimization method performs best in all three cases under the

1380 Weighted χ^2 criterion.

8.13 Weights assigned by different fitting methods

1382 Figure 19 shows the weights per observable obtained from the tune to Sherpa using the methods described in this paper.
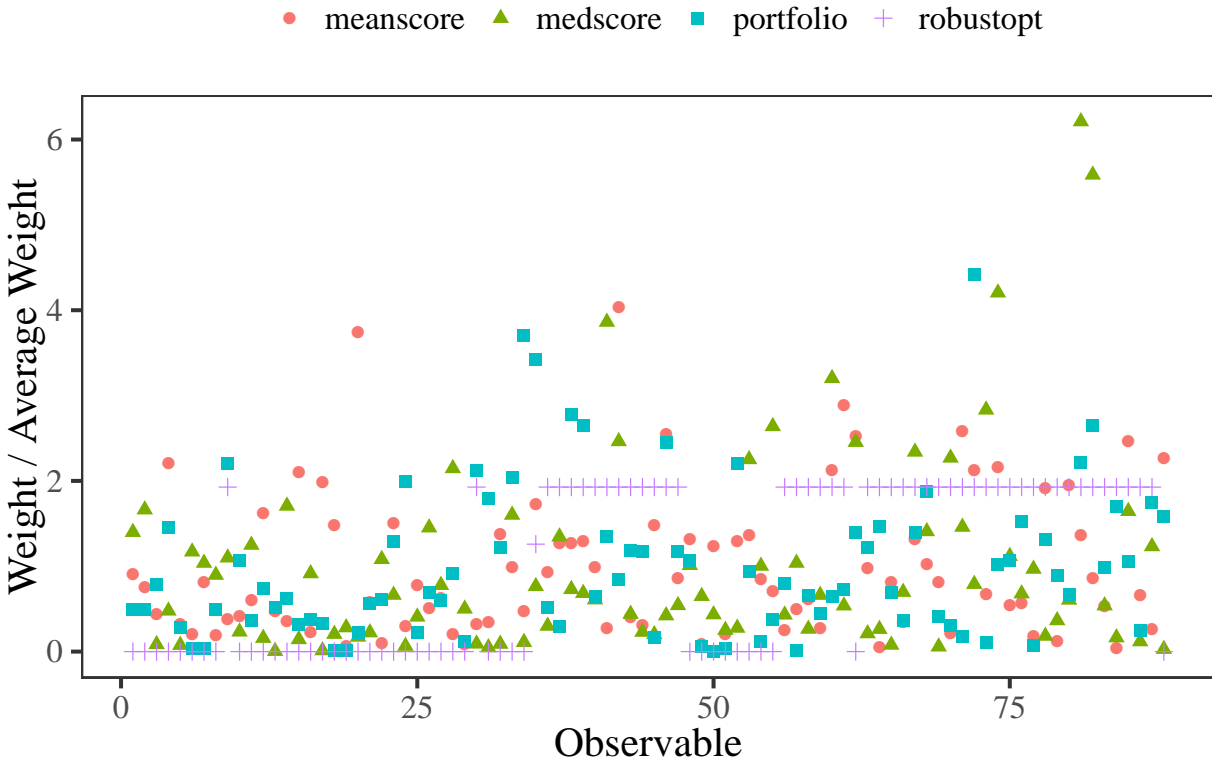
Figure 19: Distribution of weights assigned to observables for the different fitting methods described in the paper. Observables to the left are based on kinematic properties of events, while those to the right are particle multiplicities.

1383

8.14 Coefficients of the approximation function of the toy model

1385 In Table 32, we give the coefficients of the approximation $f_b(\mathbf{p})$ for each bin b, which is a linear
1386 function of the form $\mathbf{a}^T\mathbf{p} + c$ of the toy model from the closure test described in Section 4.8.

1387 ## 8.15 Eigentunes for the results obtained with the cubic polynomial approxima-
1388   tion

1389 Tables 33 and 34 shows the eigentune results for the A14 and SHERPA datasets, respectively, when
1390 using the cubic polynomial approximation.

1391 ## 8.16 Generator settings for PYTHIA and SHERPA

1392 Typical run card for A14 studies using PYTHIAv8.186.

```
Tune:pp = 14
Tune:ee = 7

PDF:useLHAPDF = on
PDF:LHAPDFset = NNPDF23_lo_as_0130_qed
PDF:LHAPDFmember = 0
PDF:extrapolateLHAPDF = off

! 3) Beam parameter settings. Values below agree with default ones.
Beams:idA = 2212                        ! first beam, p = 2212, pbar = -2212
Beams:idB = 2212                        ! second beam, p = 2212, pbar = -2212
Beams:eCM = 7000.              ! CM energy of collision

# uncomment for QCD
PhaseSpace:pTHatMin = 10.0
HardQCD:all = on
PhaseSpace:bias2Selection = on
PhaseSpace:bias2SelectionRef = 10.0
# uncomment for t-tbar
#Top:qqbar2ttbar = on
#Top:gg2ttbar = on
#SpaceShower:pTmaxMatch = 2
#SpaceShower:pTmaxFudge = 1
#SpaceShower:pTdampMatch = 1
# uncomment for Z
#WeakSingleBoson:ffbar2gmZ = On
#23:onMode = off
#23:onIfAny = 11 13 15 5 4 3
#SpaceShower:pTmaxMatch = 2
```

```
#SpaceShower:pTmaxFudge = 1
#SpaceShower:pTdampMatch = 1

# Example set of tuning parameters
SigmaProcess:alphaSvalue                 0.1343
BeamRemnants:primordialKThard             1.711
SpaceShower:pT0Ref                        1.823
SpaceShower:pTmaxFudge                    1.047
SpaceShower:pTdampFudge                   1.492
SpaceShower:alphaSvalue                   0.1302
TimeShower:alphaSvalue                    0.1166
MultipartonInteractions:pT0Ref           2.953
MultipartonInteractions:alphaSvalue      0.127
BeamRemnants:reconnectRange               4.747

ParticleDecays:limitTau0 = on
ParticleDecays:tau0Max = 10
```

We used these settings to reproduce the original results when necessary and to make full predictions for parameters selected using the surrogate function. Some of the original data using in the A14 study was private at that time and was only made public later. In a relatively small number of cases, the public data was in a different form than that used for the original study, so we were unable to reproduce those predictions.

Typical run card for SHERPA studies using v3.0.0.

```
# general settings

SHOWER_GENERATOR: CSS
ANALYSIS: Rivet
FRAGMENTATION: Ahadic
INTEGRATION_ERROR: 0.02

# model parameters

ALPHAS(MZ): 0.1188
ORDER_ALPHAS: 2

# collider setup
```

```
BEAMS: [11, -11]
BEAM_ENERGIES: 45.6

# hadronization parameters
AHADIC:
 KT_0  : 0.9088969039427998
 ALPHA_G  : 1.8736652396525728
 ALPHA_L  : 1.2518697247467987
 BETA_L  : 0.14989272155179253
 GAMMA_L  : 0.6832145156132761
 ALPHA_H  : 2.840868263919124
 BETA_H  : 0.5404054759080933
 GAMMA_H  : 0.14984034099619253
 STRANGE_FRACTION  : 0.5075082631730515
 BARYON_FRACTION  : 0.1357479921139296
 P_QS_by_P_QQ_norm  : 0.612797404412154
 P_SS_by_P_QQ_norm  : 0.029994467832440565
 P_QQ1_by_P_QQ0  : 1.1896505751927051

PARTICLE_DATA:
  4: {Massive: true}
  5: {Massive: true}

PARTICLE_CONTAINER:
  1098: {Name: C, Flavours: [4, -4]}
  1099: {Name: B, Flavours: [5, -5]}

PROCESSES:
- 11 -11 -> 93 93:
    Order: {QCD: 0, EW: 2}
- 11 -11 -> 4 -4:
    Order: {QCD: 0, EW: 2}
- 11 -11 -> 5 -5:
    Order: {QCD: 0, EW: 2}

RIVET:
  ANALYSES:
      - SLD_2002_S4869273
      - DELPHI_1996_S3430090
```

- `JADE_OPAL_2000_S4300807`
- `PDG_HADRON_MULTIPLICITIES`

1399 We used these settings to reproduce the data for our surrogate function and to make full predictions
1400 for parameters selected using the surrogate function.

Table 21: Bin filtering of A14 data: Shown are the observables from which bins were removed and the number of bins removed. We also show the critical χ^2 values and the χ^2 test statistic before and after bin filtering. If all the bins were removed from the observable then the number of bins removed is shown in bold font and the χ^2 test statistic before and after bin filtering is the same.

Observable Name	No. of filtered bins	$\chi^2_{c,\mathcal{B}}$	$\chi^2_{\mathcal{B}}$ before filtering bins	$\chi^2_{\mathcal{B}}$ after filtering bins
/ATLAS_2011_I919017/d01-x02-y04	**11**	3.84	9.77	9.77
/ATLAS_2011_I919017/d01-x02-y05	**13**	7.81	13.51	13.51
/ATLAS_2011_I919017/d01-x02-y13	**11**	3.84	9.43	9.43
/ATLAS_2011_I919017/d01-x02-y18	**11**	3.84	6.20	6.20
/ATLAS_2011_I919017/d01-x03-y01	11	21.03	24.00	3.57
/ATLAS_2011_I919017/d01-x03-y02	4	21.03	48.57	19.72
/ATLAS_2011_I919017/d01-x03-y03	2	25.00	28.99	24.72
/ATLAS_2011_I919017/d01-x03-y04	2	32.67	35.36	32.19
/ATLAS_2011_I919017/d01-x03-y06	10	26.30	59.81	26.13
/ATLAS_2011_I919017/d01-x03-y07	7	25.00	58.78	23.91
/ATLAS_2011_I919017/d01-x03-y08	5	28.87	36.98	28.27
/ATLAS_2011_I919017/d01-x03-y09	6	35.17	41.10	35.10
/ATLAS_2011_I919017/d01-x03-y12	3	23.68	31.51	21.33
/ATLAS_2011_I919017/d01-x03-y13	15	31.41	58.77	26.18
/ATLAS_2011_I919017/d01-x03-y14	12	33.92	69.51	32.38
/ATLAS_2011_I919017/d01-x03-y17	3	23.68	30.48	22.60
/ATLAS_2011_I919017/d01-x03-y18	1	30.14	30.65	26.75
/ATLAS_2011_I919017/d01-x03-y19	12	33.92	43.45	6.13
/ATLAS_2011_I919017/d01-x04-y03	**22**	21.03	45.11	45.11
/ATLAS_2011_I919017/d01-x04-y04	**21**	19.68	93.99	93.99
/ATLAS_2011_I919017/d01-x04-y05	4	16.92	22.81	16.74
/ATLAS_2011_I919017/d01-x04-y08	**22**	21.03	65.21	65.21
/ATLAS_2011_I919017/d01-x04-y09	**22**	21.03	71.99	71.99
/ATLAS_2011_I919017/d01-x04-y10	2	18.31	25.18	18.27
/ATLAS_2011_I919017/d01-x04-y13	12	22.36	49.09	2.36
/ATLAS_2011_I919017/d01-x04-y14	**24**	23.68	71.30	71.30
/ATLAS_2011_I919017/d01-x04-y15	4	21.03	27.53	20.80
/ATLAS_2011_I919017/d01-x04-y18	2	23.68	23.77	22.57
/ATLAS_2011_I919017/d01-x04-y19	8	22.36	36.75	16.78
/ATLAS_2011_I919017/d01-x04-y25	3	26.30	29.14	24.98
/ATLAS_2011_I919017/d02-x02-y05	1	11.07	13.84	9.87
/ATLAS_2011_I919017/d02-x02-y09	1	9.49	12.32	8.52
/ATLAS_2011_I919017/d02-x02-y14	1	9.49	12.19	9.18
/ATLAS_2011_I919017/d02-x03-y02	15	30.14	40.31	7.63
/ATLAS_2011_I919017/d02-x03-y06	3	31.41	36.64	28.59
/ATLAS_2011_I919017/d02-x03-y07	4	31.41	55.51	29.12
/ATLAS_2011_I919017/d02-x03-y12	7	31.41	45.41	30.04
/ATLAS_2011_I919017/d02-x03-y17	1	30.14	30.64	28.11
/ATLAS_2011_I919017/d02-x04-y03	10	26.30	46.87	19.20
/ATLAS_2011_I919017/d02-x04-y04	**25**	25.00	136.83	136.83
/ATLAS_2011_I919017/d02-x04-y05	**28**	28.87	74.75	74.75
/ATLAS_2011_I919017/d02-x04-y08	16	27.59	82.23	25.29
/ATLAS_2011_I919017/d02-x04-y09	**27**	27.59	156.13	156.13
/ATLAS_2011_I919017/d02-x04-y10	**30**	31.41	126.00	126.00
/ATLAS_2011_I919017/d02-x04-y13	14	26.30	71.23	23.47
/ATLAS_2011_I919017/d02-x04-y14	**27**	27.59	103.20	103.20
/ATLAS_2011_I919017/d02-x04-y15	9	28.87	70.47	26.49
/ATLAS_2011_I919017/d02-x04-y18	3	26.30	32.01	25.80
/ATLAS_2011_I919017/d02-x04-y19	13	28.87	67.53	23.91
/ATLAS_2011_I919017/d02-x04-y20	10	28.87	57.69	28.31
/ATLAS_2011_I919017/d02-x04-y24	10	28.87	43.46	28.24
/ATLAS_2011_I919017/d02-x04-y25	3	31.41	39.98	28.20
/ATLAS_2011_ZPT/d02-x01-y01	1	14.07	15.77	14.06
/ATLAS_2011_ZPT/d02-x02-y02	2	14.07	16.94	13.93
/ATLAS_2011_ZPT/d03-x01-y01	1	14.07	15.32	13.85
/ATLAS_2013_JETUE/d08-x01-y03	1	12.59	19.97	11.51

Table 22: Bin filtering of SHERPA data: Shown are the observables from which bins were removed and the number of bins removed. We also show the critical χ^2 values and the χ^2 test statistic before and after bin filtering. If all the bins were removed from the observable then the number of bins removed is shown in bold font and the χ^2 test statistic before and after bin filtering is the same.

Observable Name	No. of filtered bins	$\chi^2_{c,\mathcal{B}}$	$\chi^2_{\mathcal{B}}$ before filtering bins	$\chi^2_{\mathcal{B}}$ after filtering bins
/DELPHI_1996_S3430090/d02-x01-y01	**17**	9.49	35.19	35.19
/DELPHI_1996_S3430090/d04-x01-y01	**17**	9.49	24.89	24.89
/DELPHI_1996_S3430090/d06-x01-y01	**21**	15.51	41.59	41.59
/DELPHI_1996_S3430090/d07-x01-y01	**22**	16.92	83.91	83.91
/DELPHI_1996_S3430090/d08-x01-y01	**26**	22.36	80.11	80.11
/DELPHI_1996_S3430090/d10-x01-y01	2	11.07	15.90	10.59
/DELPHI_1996_S3430090/d11-x01-y01	**20**	14.07	94.30	94.30
/DELPHI_1996_S3430090/d16-x01-y01	**14**	3.84	17.63	17.63
/DELPHI_1996_S3430090/d18-x01-y01	**23**	18.31	101.31	101.31
/DELPHI_1996_S3430090/d19-x01-y01	**21**	15.51	59.12	59.12
/DELPHI_1996_S3430090/d20-x01-y01	**16**	7.81	20.48	20.48
/DELPHI_1996_S3430090/d33-x01-y01	5	52.19	75.18	50.31

Table 23: A14 results with the *full dataset*, *observable-filtered dataset* and *bin-filtered dataset* when using the *cubic polynomial* approximation, calculated on the reduced dataset. Lower numbers are better. The best results are in bold. In each dataset, W-χ^2 refers to the Weighted χ^2 metric, A-o refers to the A-opt metric, and l-D-o refers to the log D-opt metric.

Data	full dataset			observable-filtered dataset			bin-filtered dataset		
Method	W-χ^2	A-o	l-D-o	W-χ^2	A-o	l-D-o	W-χ^2	A-o	l-D-o
Bilevel-meanscore	0.1290	0.5358	-66.0364	0.1079	0.8082	-61.9210	0.0778	1.0199	-60.6441
Bilevel-medscore	0.1645	**0.4114**	**-70.0545**	0.1702	**0.4955**	-66.6920	0.1085	0.7208	-67.4322
Bilevel-portfolio	0.1900	0.6590	-63.0378	0.1764	0.7408	-61.3839	0.0738	**0.4231**	**-69.4117**
Expert tune	0.1306	0.5466	-68.6511	0.0799	0.5542	**-68.6748**	0.0456	0.8985	-63.5606
All-weights-equal	0.1034	0.5553	-65.6099	0.0857	0.6769	-63.6881	**0.0379**	0.7390	-63.8424
Robust optimization	**0.0697**	0.9749	-66.7931	**0.0829**	1.0574	-66.3665	0.0642	0.9559	-64.8659

Table 24: Optimal parameter values for the A14 dataset obtained when using all observables in the optimization and the *cubic polynomial* approximation.

ID	Parameter name	Expert	Bil.-meanscore	Bil.-medianscore	Bil.-portfolio	Robust opt	All-weights-equal
1	SigmaProcess:alphaSvalue	0.143	0.139	0.141	0.140	0.136	0.138
2	BeamRemnants:primordialKThard	1.904	1.867	1.884	1.866	1.826	1.862
3	SpaceShower:pT0Ref	1.643	1.632	1.735	1.651	1.395	1.603
4	SpaceShower:pTmaxFudge	0.908	0.939	0.904	0.988	0.933	0.944
5	SpaceShower:pTdampFudge	1.046	1.079	1.069	1.047	1.063	1.067
6	SpaceShower:alphaSvalue	0.123	0.129	0.130	0.130	0.128	0.129
7	TimeShower:alphaSvalue	0.128	0.123	0.124	0.121	0.136	0.124
8	MultipartonInteractions:pT0Ref	2.149	2.083	2.065	2.039	1.925	2.092
9	MultipartonInteractions:alphaSvalue	0.128	0.127	0.127	0.126	0.120	0.127
10	BeamRemnants:reconnectRange	1.792	1.531	1.405	1.591	2.567	1.636
	Euclidean distance from the expert solution		0.246	0.235	0.428	0.451	0.259

Table 25: Optimal parameter values for A14 when using the *cubic polynomial* approximation with all methods after outlier detection to filter out observables that cannot be approximated well by the model.

ID	Parameter name	Expert	Bilevel-meanscore	Bilevel-medianscore	Bilevel-portfolio	Robust opt	All-weights-equal
1	SigmaProcess:alphaSvalue	0.143	0.136	0.141	0.137	0.136	0.137
2	BeamRemnants:primordialKThard	1.904	1.793	1.853	1.754	1.829	1.772
3	SpaceShower:pT0Ref	1.643	1.329	1.369	1.218	1.425	1.301
4	SpaceShower:pTmaxFudge	0.908	1.079	1.088	1.223	0.926	1.085
5	SpaceShower:pTdampFudge	1.046	1.069	1.053	1.101	1.065	1.074
6	SpaceShower:alphaSvalue	0.123	0.129	0.128	0.129	0.129	0.129
7	TimeShower:alphaSvalue	0.128	0.124	0.123	0.116	0.136	0.124
8	MultipartonInteractions:pT0Ref	2.149	1.971	2.098	1.870	1.971	1.983
9	MultipartonInteractions:alphaSvalue	0.128	0.122	0.126	0.120	0.121	0.123
10	BeamRemnants:reconnectRange	1.792	1.812	1.614	1.714	2.632	1.851
	Euclidean distance from the expert solution		0.447	0.279	0.553	0.432	0.480

Table 26: Optimal parameter values obtained for A14 with the *cubic polynomial* approximation with all methods after using the bin-filtering approach that excludes individual bins from the optimization.

ID	Parameter name	Expert	Bilevel-meanscore	Bilevel-medianscore	Bilevel-portfolio	Robust opt	All-weights-equal
1	SigmaProcess:alphaSvalue	0.143	0.141	0.143	0.136	0.136	0.132
2	BeamRemnants:primordialKThard	1.904	1.919	1.918	1.575	1.794	1.716
3	SpaceShower:pT0Ref	1.643	1.802	2.284	2.300	1.355	2.123
4	SpaceShower:pTmaxFudge	0.908	0.968	1.014	0.920	0.856	0.843
5	SpaceShower:pTdampFudge	1.046	1.071	1.147	1.442	1.047	1.465
6	SpaceShower:alphaSvalue	0.123	0.130	0.130	0.144	0.132	0.143
7	TimeShower:alphaSvalue	0.128	0.129	0.127	0.131	0.138	0.130
8	MultipartonInteractions:pT0Ref	2.149	2.059	1.800	2.228	1.925	2.306
9	MultipartonInteractions:alphaSvalue	0.128	0.126	0.120	0.131	0.118	0.131
10	BeamRemnants:reconnectRange	1.792	1.860	1.922	1.807	2.340	1.622
	Euclidean distance from the expert solution		0.376	0.354	0.848	0.525	1.111

Table 27: Comparison of the optimal weights obtained by each method using the *cubic polynomial* approximation. The observable grouping corresponds to the same grouping used in [3].

	expert	Bilevel-meanscore	Bilevel-medianscore	Bilevel-portfolio	robustopt
Track jet properties					
Charged jet multiplicity (50 distributions)	10	10.74	14.98	10.64	19.38
Charged jet z (50 distributions)	10	11.29	8.66	13.71	0.00
Charged jet p_T^{rel} (50 distributions)	10	11.20	10.39	10.99	0.00
Charged jet $\rho_{ch}(r)$ (50 distributions)	10	11.57	10.58	12.55	0.00
Jet shapes					
Jet shape ρ (59 distributions)	10	11.57	11.06	10.20	19.38
Dijet decorr					
Decorrelation $\Delta\phi$ (Fit range: $\Delta\phi > 0.75$) (9 distributions)	20	12.39	8.37	9.39	15.07
Multijets					
3-to-2 jet ratios (8 distributions)	100	12.99	27.19	5.88	19.38
p_T^Z (Fit range: $p_T^Z < 50\text{GeV}$)					
Z-boson p_T (20 distributions)	10	12.78	14.53	6.71	19.38
Substructure					
Jet mass, $\sqrt{d_{12}}, \sqrt{d_{23}}, \tau_{21}, \tau_{23}$ (36 distributions)	5	10.55	9.91	9.74	15.61
$t\bar{t}$ gap					
Gap fraction vs Q_0, Q_{sum} for $|y| < 0.8$	100	0.18	2.10	3.88	19.38
Gap fraction vs Q_0, Q_{sum} for $0.8 < |y| < 1.5$	80	0.75	9.52	5.71	19.38
Gap fraction vs Q_0, Q_{sum} for $1.5 < |y| < 2.1$	40	7.93	8.31	39.20	19.38
Gap fraction vs Q_0, Q_{sum} for $|y| < 2.1$	10	18.19	13.43	11.05	19.38
Track-jet UE					
Transverse region N_{ch} profiles (5 distributions)	10	15.87	13.45	13.53	19.38
Transverse region mean p_T profiles for $R = 0.2, 0.4, 0.6$ (3 distributions)	10	7.56	11.72	10.30	19.38
$t\bar{t}$ jet shapes					
Jet shapes $\rho(r), \psi(r)$ (20 distributions)	5	10.86	10.91	12.25	10.66
Jet UE					
Transverse, trans-max, trans-min sum p_T incl. profiles (3 distributions)	20	12.76	22.51	9.65	19.38
Transverse, trans-max, trans-min N_{ch} incl. profiles (3 distributions)	20	15.57	9.65	6.01	19.38
Transverse sum E_T incl. profiles (2 distributions)	20	12.71	12.75	25.03	3.73
Transverse sum $ET/\text{sum } p_T$ ratio incl., excl. profiles (2 distributions)	5	7.53	18.29	28.35	19.38
Transverse mean p_T incl. profiles (2 distributions)	10	7.65	7.45	13.34	19.38
Transverse, trans-max, trans-min sum p_T incl. distributions (15 distributions)	1	9.39	5.50	11.04	19.38
Transverse, trans-max, trans-min sum N_{ch} incl. distributions (15 distributions)	1	11.92	9.85	14.52	19.38

Table 28: Optimal parameter values for the SHERPA dataset obtained with all methods using the *cubic polynomial* approximation when no filtering was applied before optimization (88 observables).

ID	Parameter name	Default	Bilevel-meanscore	Bilevel-medscore	Bilevel-portfolio	Robust opt	All-weights-equal
1	KT_0	1.00	0.850	0.837	0.903	0.870	0.853
2	ALPHA_G	1.25	0.626	0.626	0.626	1.874	0.626
3	ALPHA_L	2.50	3.634	2.022	3.108	1.252	3.749
4	BETA_L	0.10	0.150	0.069	0.050	0.150	0.150
5	GAMMA_L	0.50	0.250	0.353	0.750	0.619	0.286
6	ALPHA_H	2.50	3.455	2.047	1.251	2.712	3.454
7	BETA_H	0.75	0.736	0.610	0.657	0.573	0.922
8	GAMMA_H	0.10	0.144	0.124	0.050	0.150	0.140
9	STRANGE_FRACTION	0.50	0.531	0.521	0.529	0.514	0.497
10	BARYON_FRACTION	0.18	0.099	0.132	0.091	0.139	0.104
11	P_QS_by_P_QQ_norm	0.48	0.720	0.617	0.502	0.601	0.720
12	P_SS_by_P_QQ_norm	0.02	0.010	0.030	0.030	0.030	0.010
13	P_QQ1_by_P_QQ0	1.00	1.499	1.499	1.349	1.164	1.499
	Euclidean distance from the default solution		1.508	1.130	1.400	1.236	1.497

Table 29: Optimal parameter values for the SHERPA dataset obtained with all methods using the *cubic polynomial* approximation after using outlier detection to remove observables from the optimization (3 observables removed).

ID	Parameter name	Default	Bilevel-meanscore	Bilevel-medscore	Bilevel-portfolio	Robust opt	All-weights-equal
1	KT_0	1.00	0.898	0.834	0.946	0.945	0.853
2	ALPHA_G	1.25	1.136	0.751	0.626	1.874	0.942
3	ALPHA_L	2.50	1.454	2.088	3.749	3.749	2.275
4	BETA_L	0.10	0.050	0.050	0.050	0.050	0.136
5	GAMMA_L	0.50	0.409	0.305	0.627	0.626	0.553
6	ALPHA_H	2.50	3.748	1.358	1.251	1.533	1.804
7	BETA_H	0.75	0.406	0.375	0.591	1.125	0.760
8	GAMMA_H	0.10	0.078	0.150	0.086	0.050	0.066
9	STRANGE_FRACTION	0.50	0.541	0.528	0.552	0.529	0.553
10	BARYON_FRACTION	0.18	0.181	0.139	0.090	0.270	0.270
11	P_QS_by_P_QQ_norm	0.48	0.240	0.602	0.449	0.384	0.298
12	P_SS_by_P_QQ_norm	0.02	0.020	0.025	0.030	0.030	0.023
13	P_QQ1_by_P_QQ0	1.00	1.499	1.499	1.499	0.639	0.837
	Euclidean distance from the default solution		1.222	1.327	1.378	1.463	0.937

Table 30: Optimal parameter values for the SHERPA dataset obtained with all methods using the *cubic polynomial* approximation after using the bin-filtering approach that excludes individual bins from the optimization (204 bins out of 5246 total bins were removed).

ID	Parameter name	Default	Bilevel-meanscore	Bilevel-medscore	Bilevel-portfolio	Robust opt	All-weights-equal
1	KT_0	1.00	0.866	0.820	0.897	0.950	0.911
2	ALPHA_G	1.25	0.626	1.114	0.626	1.874	0.626
3	ALPHA_L	2.50	3.749	3.502	2.216	3.749	3.749
4	BETA_L	0.10	0.079	0.053	0.050	0.050	0.078
5	GAMMA_L	0.50	0.383	0.325	0.750	0.627	0.367
6	ALPHA_H	2.50	1.251	1.251	1.251	1.527	1.251
7	BETA_H	0.75	0.738	0.675	0.694	1.125	0.741
8	GAMMA_H	0.10	0.092	0.116	0.099	0.050	0.104
9	STRANGE_FRACTION	0.50	0.536	0.547	0.543	0.529	0.541
10	BARYON_FRACTION	0.18	0.120	0.127	0.129	0.270	0.130
11	P_QS_by_P_QQ_norm	0.48	0.636	0.578	0.472	0.384	0.569
12	P_SS_by_P_QQ_norm	0.02	0.030	0.030	0.030	0.030	0.030
13	P_QQ1_by_P_QQ0	1.00	1.499	1.499	1.499	0.637	1.499
	Euclidean distance from the default solution		1.263	1.215	1.272	1.464	1.224

Table 31: Results for the comparison metrics for the full, observable-filtered and bin-filtered SHERPA dataset using the *cubic polynomial* approximation, calculated on the reduced dataset. The best results are in bold. In each dataset, W-χ^2 refers to the Weighted χ^2 metric, A-o refers to the A-opt metric, and l-D-o refers to the log D-opt metric. Note that we do not have an expert solution for this dataset.

Data	full dataset			observable-filtered dataset			bin-filtered dataset		
Method	W-χ^2	A-o	l-D-o	W-χ^2	A-o	l-D-o	W-χ^2	A-o	l-D-o
Bilevel-meanscore	0.1777	9.0959	-39.9863	0.4740	14.3374	-35.2608	0.2526	17.5098	-32.5916
Bilevel-medscore	0.2370	13.3943	-37.1420	0.4786	13.6299	-36.6594	0.1147	15.1990	**-36.2567**
Bilevel-portfolio	0.3409	8.7863	-39.6956	0.2139	**10.4481**	**-36.8254**	0.2255	15.5833	-34.9095
All-weights-equal	0.2305	**6.8732**	**-42.0678**	0.3922	28.9575	-27.9246	0.1571	**13.5814**	-34.7914
Robust optimization	**0.0507**	56.9168	-21.9561	**0.0093**	94.7811	-23.5723	**0.0856**	77.0710	-26.2532

Table 32: Coefficients of the approximation $f_b(\mathbf{p})$ for each bin b, which is a linear function of the form $\mathbf{a}^T\mathbf{p} + c$ of the toy model from the closure test described in Section 4.8.

Observable	Bin	$\mathbf{a}^T$	c
	Bin 1	(8.21, 8.22)	17.65
	Bin 2	(8.13, 5.23)	18.96
Observable 1	Bin 3	(9.53, 5.54)	18.37
	Bin 4	(8.08, 6.41)	17.61
	Bin 5	(8.80, 8.75)	17.07
	Bin 1	(6.01, 9.71)	15.63
	Bin 2	(6.16, 7.12)	16.71
Observable 2	Bin 3	(7.96, 9.10)	17.18
	Bin 4	(6.54, 8.98)	16.74
	Bin 5	(8.95, 9.42)	18.93
	Bin 1	(9.13, 7.66)	18.23
	Bin 2	(7.79, 7.86)	18.07
Observable 3	Bin 3	(7.94, 9.14)	13.81
	Bin 4	(7.16, 9.07)	16.15
	Bin 5	(9.61, 7.97)	17.49
	Bin 1	(8.21, 8.22)	14.40
	Bin 2	(8.13, 5.23)	16.98
Observable 4	Bin 3	(9.53, 5.54)	10.89
	Bin 4	(8.08, 6.41)	19.48
	Bin 5	(8.80, 8.75)	16.50

Table 33: Eigentune results for the A14 dataset using the optimal physics parameters $\mathbf{p}^*$ obtained with the different optimization methods when using the *cubic polynomial* approximation.

Parameters	Expert		Bilevel-meanscore		Bilevel-medianscore		Bilevel-portfolio		Robust optimization	
	min	max	min	max	min	max	min	max	min	max
SigmaProcess:alphaSvalue	0.072	0.196	0.071	0.197	0.079	0.190	0.076	0.191	0.079	0.187
BeamRemnants:primordialKThard	1.899	1.904	1.849	1.888	1.877	1.894	1.855	1.881	1.764	1.895
SpaceShower:pT0Ref	1.616	1.633	1.622	1.640	1.733	1.737	1.631	1.667	1.377	1.411
SpaceShower:pTmaxFudge	0.904	0.914	0.938	0.940	0.884	0.923	0.986	0.990	0.932	0.935
SpaceShower:pTdampFudge	1.039	1.047	1.059	1.102	1.053	1.085	1.045	1.049	1.061	1.064
SpaceShower:alphaSvalue	0.116	0.128	0.128	0.130	0.118	0.141	0.129	0.131	0.128	0.129
TimeShower:alphaSvalue	0.076	0.199	0.034	0.223	0.046	0.205	0.083	0.145	0.042	0.198
MultipartonInteractions:pT0Ref	1.749	2.666	1.533	2.707	1.536	2.621	1.989	2.116	1.866	1.965
MultipartonInteractions:alphaSvalue	0.045	0.186	0.095	0.154	0.114	0.140	0.044	0.180	0.100	0.133
BeamRemnants:reconnectRange	1.719	1.719	1.523	1.541	1.390	1.420	1.589	1.595	2.565	2.568

Table 34: Eigentune results for the SHERPA dataset using the optimal physics parameters $\mathbf{p}^*$ obtained with the different optimization methods when using the *cubic polynomial* approximation.

Parameters	Bilevel-meanscore		Bilevel-medianscore		Bilevel-portfolio		Robust optimization	
	min	max	min	max	min	max	min	max
KT_0	0.572	1.845	0.818	0.884	0.798	1.002	0.350	1.021
ALPHA_G	0.113	0.769	0.472	0.690	0.612	0.639	1.288	2.044
ALPHA_L	3.468	4.227	1.956	2.181	2.917	3.309	0	1.697
BETA_L	0	0.255	0	0.487	0	0.305	0	0.233
GAMMA_L	0.064	0.915	0.226	0.405	0.746	0.755	0.328	1.625
ALPHA_H	2.981	3.587	2.000	2.162	1.235	1.268	2.427	2.898
BETA_H	0.662	0.771	0.582	0.677	0.637	0.675	0	0.741
GAMMA_H	0.045	0.190	0.070	0.255	0	0.134	0	0.652
STRANGE_FRACTION	0.068	0.749	0.446	0.655	0.501	0.558	0.413	0.546
BARYON_FRACTION	0	0.335	0.117	0.166	0	0.186	0.030	0.516
P_QS_by_P_QQ_norm	0.669	0.828	0.576	0.715	0.458	0.549	0.537	0.619
P_SS_by_P_QQ_norm	0	0.087	0	0.105	0	0.076	0	0.050
P_QQ1_by_P_QQ0	1.496	1.508	1.498	1.500	1.348	1.349	1.153	1.200